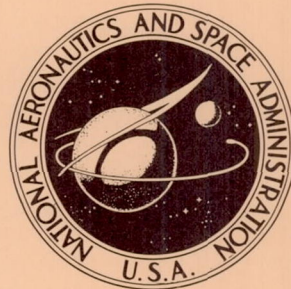


NASA TECHNICAL NOTE

NASA TN D-5129



NASA TN D-5129

CASE FILE
COPY

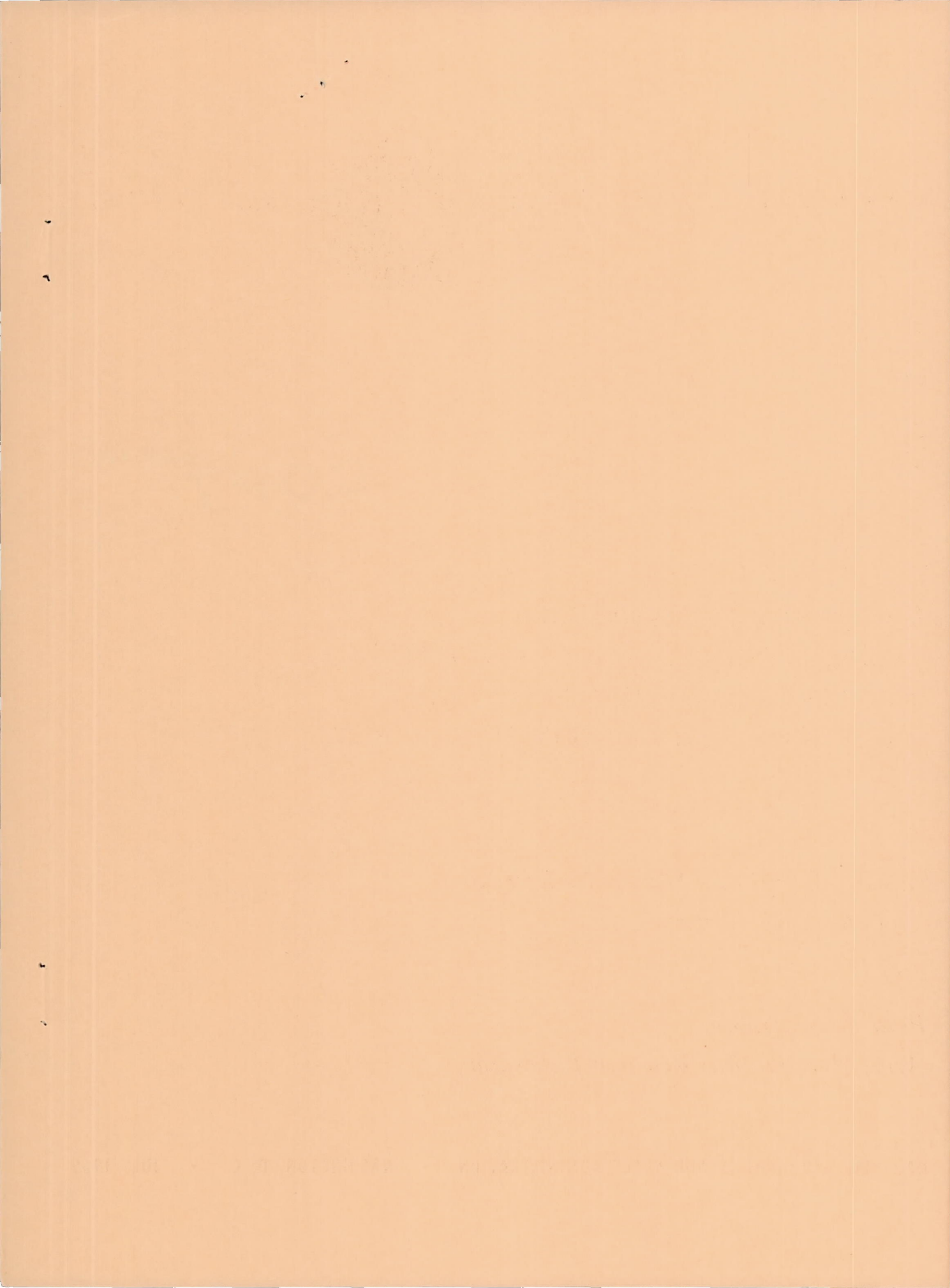
INVESTIGATION OF
A 0.3-SCALE JET-TRANSPORT
MODEL HAVING A JET-AUGMENTED
BOUNDARY-LAYER-CONTROL FLAP
WITH DIRECT-LIFT CONTROL CAPABILITY

by

Kiyoshi Aoyagi and Stanley O. Dickinson
Ames Research Center

and

Paul T. Soderman
Army Aeronautical Research Laboratory



INVESTIGATION OF A 0.3-SCALE JET-TRANSPORT MODEL
HAVING A JET-AUGMENTED BOUNDARY-LAYER-CONTROL
FLAP WITH DIRECT-LIFT CONTROL CAPABILITY

By Kiyoshi Aoyagi and Stanley O. Dickinson

Ames Research Center
Moffett Field, Calif.

and

Paul T. Soderman
Army Aeronautical Research Laboratory

NATIONAL AERONAUTICS AND SPACE ADMINISTRATION

For sale by the Clearinghouse for Federal Scientific and Technical Information
Springfield, Virginia 22151 - CFSTI price \$3.00



INVESTIGATION OF A 0.3-SCALE JET-TRANSPORT MODEL
HAVING A JET-AUGMENTED BOUNDARY-LAYER-CONTROL
FLAP WITH DIRECT-LIFT CONTROL CAPABILITY

By Kiyoshi Aoyagi and Stanley O. Dickinson
Ames Research Center

and

Paul T. Soderman
Army Aeronautical Research Laboratory

SUMMARY

An investigation has been conducted to define a trailing-edge flap system for a large-scale subsonic jet transport model that would provide high lift at low-thrust-to-weight ratios (0.05 to 0.10) and direct-lift control. The model had a 35° swept wing of aspect ratio 6.43 and four pod-mounted engines under the wing. The flap system was externally jet-augmented from the exhaust of the inboard jet engines. The flap system consisted of a main flap with blowing boundary-layer control and a small auxiliary flap for providing direct-lift control. Results were obtained with three boundary-layer-control arrangements and two different auxiliary flap chords at several main and auxiliary flap deflections. Three-component longitudinal data and descent capabilities of the model with the resultant flap system are presented.

The results of descent performance computations indicate that the resultant flap system is capable of providing ± 0.2 g incremental acceleration normal to the flight path at an approach speed of 117 knots (1 g flight wing loading = 53 psf) or a 4° change in flight-path angle with a thrust-to-weight ratio of 0.05.

INTRODUCTION

Several methods of increasing lift in order to improve the low-speed takeoff and landing performance of subsonic jet transport aircraft have been investigated and reported in references 1, 2, and 3. Reference 1 also reported the problem of engine noise during the landing approach of an airplane that had blowing boundary-layer-control trailing-edge flaps and suggested a lower engine thrust level and steeper approach paths as possible solutions to the noise problem. These solutions, however, require a highly effective flap system and improved airplane control to permit the increase in descent angle without compromising safety. The use of an external jet-augmented flap with direct-lift control, similar to that reported in reference 3, is one possibility for meeting these requirements. A wind-tunnel, a flight simulator, and a flight test were therefore used to determine the

degree to which such a flap system would permit the descent angle to be increased and the noise reduced during the landing approach.

The airplane selected for the flight phase of this investigation was representative of current turbofan-powered transports. The purpose of the wind-tunnel investigation was to develop a highly effective flap system for this airplane. The flap was designed to achieve high lift effectiveness at low-thrust-to-weight ratios (0.05 to 0.10) by means of boundary-layer control and external jet augmentation. The external jet augmentation was obtained from inboard jet-engine exhaust impinging on the flap lower surface. The flap system consisted of a main flap with boundary-layer control and an auxiliary flap attached to the main flap. Results were obtained with three boundary-layer-control jet-augmentation arrangements and with two different auxiliary flap chords. Descent capabilities of the resultant flap system are also presented. Nearly all of the data were obtained at a Reynolds number of 3.0×10^6 , based on a mean aerodynamic chord of 5.22 feet and a dynamic pressure of 10 pounds per square foot.

NOTATION

a_n	incremental acceleration normal to flight path, $\frac{\Delta C_L}{C_{L_{\text{trim}}}} \text{aux}$
b	wing span, ft
BLC	boundary-layer control
c	wing chord measured parallel to the plane of symmetry, ft
\bar{c}	mean aerodynamic chord of basic wing, $\frac{2}{S} \int_0^{b/2} c^2 dy$, ft
C_D	drag coefficient, $\frac{\text{drag}}{q_\infty S}$
$\Delta C_{D_{\text{aux}}}$	drag-coefficient increment due to auxiliary flap deflection
C_L	lift coefficient, $\frac{\text{lift}}{q_\infty S}$
$\Delta C_{L_{\text{aux}}}$	lift-coefficient increment due to auxiliary flap deflection
C_m	pitching-moment coefficient about 0.38 \bar{c} , $\frac{\text{pitching moment}}{q_\infty S \bar{c}}$
$\Delta C_{m_{\text{aux}}}$	pitching-moment coefficient increment due to auxiliary flap deflection

C_T	inboard engine gross thrust coefficient, <u>gross thrust of inboard engines</u>
	$q_{\infty} S$
C_{μ}	momentum coefficient, $\frac{wV_j}{gq_{\infty} S}$
g	acceleration of gravity, 32.2 ft/sec ²
i_t	horizontal-tail incidence angle, deg
q_{∞}	free-stream dynamic pressure, lb/sq ft
R	Reynolds number
S	wing area, sq ft
$\frac{T}{W}$	net thrust-to-weight ratio
V	equivalent airspeed, knots
V_j	jet velocity assuming isentropic expansion, ft/sec
V_S	1 g stall speed, knots
V_{∞}	free-stream air velocity, ft/sec
w	weight rate of flow, lb/sec
W	airplane gross weight, lb
WCP	wing chord plane
y	spanwise distance perpendicular to the plane of symmetry, ft
α	angle of attack of fuselage, deg
δ_e	horizontal-tail elevator deflection, deg
$\delta_{f_{aux}}$	trailing-edge auxiliary flap deflection, measured normal to the hinge line, deg
δ_{f_m}	trailing-edge main flap deflection, measured normal to the hinge line, deg
δ_s	slat deflection, measured perpendicular to the leading edge, deg
δ_{sp}	wing spoiler deflection, measured perpendicular to the hinge line, deg

γ	flight-path angle, deg
η	wing semispan station, $\frac{y}{b/2}$

Subscripts

OB	outboard
u	uncorrected

MODEL AND APPARATUS

Figure 1 is a photograph of the model in the 40- by 80-foot wind tunnel. Pertinent dimensions of the model are given in figure 2(a). The model was equipped with four T-58-6A engines modified to operate as conventional jet engines.

Wing

The basic wing had a quarter-chord sweep of 35° , an aspect ratio of 6.46, a dihedral of 6° , and an incidence of 2° . The airfoil section had an NACA 65-012 thickness distribution at the root tapering linearly to an NACA 65-009 thickness distribution at the tip. A 230 mean line was used at each section. The wing trailing-edge sweep varied from 27.8° to 22.0° inboard of the 0.67 wing semispan station and from 22.0° to 9.0° inboard of the 0.37 wing semispan station with the addition of chord extensions to the wing (see fig. 2(a)).

Leading-Edge Slats

The slats extended the full span of the wing with breaks at each side of the nacelle pylons and were deflected 35° with respect to the wing chord plane, as shown in figure 2(b). Slat chord tapered linearly from $0.20c$ at the root to $0.18c$ at the tip. The slats were attached to the wing leading edge throughout the investigation.

Trailing-Edge Flap System

A typical cross section of the flap is shown in figure 2(c). Flap geometry and ordinates are based on the wing planform as shown in the figure. The flap segments were rotated to match the model wing trailing-edge sweep angles.

Flap details.- The flap system was composed of the main flap and the auxiliary flap. Both flaps extended from 0.11 to 0.67 of the wing semispan with breaks at 0.11, 0.29, 0.37, 0.53, and 0.67 of the semispan. Total flap

chord (main plus auxiliary flap chord) was 0.18, 0.22, and 0.28 of the local wing chord at 0.11, 0.37, and 0.67 of the semispan, respectively. The normal chord of the auxiliary flap was 0.33 of the total flap chord. During the investigation, a chord extension was added to the auxiliary flap (fig. 2(c)) and this modified version will be referred to as an extended chord auxiliary flap. The average auxiliary flap chord with the extension was 0.42 of the total flap chord.

Boundary-layer control.- Boundary-layer control (BLC) over the main trailing-edge flap was provided by a shroud-mounted, fixed blowing nozzle that spanned the full extent of the flap (fig. 2(d)). Air for BLC was bled from the compressors of T-58-6A engines. Bleed air from the outboard engine was ducted to the wing plenum chamber which distributed the flow to either the inboard ($\eta = 0.11$ to 0.38) or outboard nozzle ($\eta = 0.38$ to 0.70) by valves located in the duct between the plenum and the nozzle. Bleed air from the inboard engine was ducted directly to the inboard nozzle. Calibrated flow-measuring stations were located in each duct connected to the engine bleed ports. Each station contained a total pressure probe, a static orifice, and a thermocouple. Nozzle jet velocity was obtained from a total pressure probe and a thermocouple located ahead of the nozzle.

Main and auxiliary flap arrangements.- When the main flaps were deflected, the flap segments could be arranged relative to the trailing edge of the fixed blowing nozzle with or without a gap as shown in figure 2(e). With no gap, the flap upper surface was approximately tangent to the nozzle centerline. The main flap was tested with three BLC arrangements (fig. 2(e)). Arrangement A had BLC over the entire flap span and had no flap gap. Arrangement B had BLC from 0.11 to 0.37 wing semispan and a 0.01c flap gap from 0.37 to 0.67 semispan. Arrangement C had a 0.01c flap gap from 0.29 to 0.53 of semispan and BLC between 0.11 to 0.29 and 0.53 to 0.67 wing semispan. Flap deflection was measured normal to its pivot line and relative to the wing chord plane.

The normal-chord auxiliary flap was investigated with all three BLC arrangements. This flap was deflected so that it had a constant 0.01c gap below and in line with the main flap pivot line and relative to the main flap chord line.

The extended chord auxiliary flap was investigated only with BLC arrangement A. This flap was deflected from a fixed hinge point relative to the main flap (fig. 2(f)). The deflection was measured normal to its pivot line and relative to the main flap chord line. In order to turn the air more effectively between the gap of the main and auxiliary flaps, an extension plate was attached directly to the main flap upper surface over the full span of the flap (fig. 2(f)). This plate was used only with the extended chord auxiliary flap and was removed when the flap was tested with negative deflections (up position) because of the interference between the flap and plate.

Wing Spoilers

Spoilers were located between 0.14 and 0.37 of the wing semispan and from 0.41 to 0.68 of the wing semispan as shown in figure 2(g). The inboard and

and outboard section had constant chords of 0.85 and 0.93 foot, respectively. The trailing edge of the spoilers at each section was located 0.17 foot ahead of the blowing nozzle trailing edge. Both sections were deflected together during the investigation. Deflection was measured perpendicular to the hinge line.

Fuselage

The fuselage had a constant 4-foot diameter except at the nose and tail. The nose section had elliptical outlines with circular cross sections that decreased from 4 feet to a smaller diameter. The tail section tapered from a 4-foot circular section to a small elliptical section.

Tail

The horizontal and vertical tails, which were on the model throughout the investigation, are described in figure 2(a). The vertical tail rudder was fixed at 0° , the horizontal tail was set at -5° incidence, and the elevator was set at 0° . A 0.15-chord inverted leading-edge slat was mounted along the full extent of the horizontal tail and was deflected -35° .

Engines

T-58-6A engines, modified to operate as conventional jet engines, were located at 0.41 and 0.71 of the wing semispan. All four engines provided the high pressure air for boundary-layer control, but the inboard engines also provided external jet augmentation on the trailing-edge flap system. The outboard engines were operated only to provide high pressure air for BLC.

A jet exhaust ejector behind the conventional tailpipe of each engine (fig. 2(e) and (f)) simulated the exhaust wake of a fan jet engine. Ejectors of 0.91 and 1.42 feet diameter were used behind the inboard engines during the investigation. Both ejectors had the same length of 2.36 feet and a faired leading-edge radius of 0.08 foot. The smaller diameter ejector was used when main flap arrangement A, B, or C was tested with the normal chord auxiliary flap. The larger one was used when flap arrangement A was tested with the extended chord auxiliary flap. The smaller ejector was mounted behind the outboard engines throughout the investigation.

A jet exhaust deflector was located behind the inboard engine ejector and pivoted about the ejector centerline (fig. 2(e) and (f)). The deflector had a constant chord of 1.17 feet and extended the diameter of either ejector. It was deflected 15° throughout most of the investigations.

CORRECTIONS

The lift, drag, and pitching-moment coefficient data were corrected for the effects of operating the outboard engines. The corrections were obtained while the outboard engine thrust and model angle of attack were varied and the inboard engines were not operating. The dynamic pressure was 10 pounds per square foot. The data were also corrected for strut tares and wind-tunnel-wall effects. The tunnel-wall corrections were as follows:

$$\alpha = \alpha_u + 0.461 C_L$$

$$C_D_{(measured)} = C_{Du} + 0.0080 C_L^2$$

$$C_m = C_{mu} + 0.0111 C_L$$

Since the minimum measured drag coefficient of the model with flaps up was higher than that of the KC 135A airplane (ref. 4) with flaps up and gear down (airplane geometrically similar to that used in flight test), the drag coefficients were further corrected as follows:

$$C_D = C_{D(measured)} - 0.030 \text{ (normal chord auxiliary flap)}$$

$$C_D = C_{D(measured)} - 0.033 \text{ (extended chord auxiliary flap)}$$

TESTING AND PROCEDURE

Model forces and moments were measured in most cases through an angle-of-attack range of -4° to $+20^\circ$. Pitching-moment data were computed about a moment center of $0.38c$ to give a static margin of approximately 0.05. All tests except those to show Reynolds number effect were conducted at a Reynolds number of 3.0×10^6 , based on a mean aerodynamic chord of 5.22 feet and a dynamic pressure of 10 pounds per square foot.

Tests With Constant C_μ and Varying Angle of Attack

Variables tested were main flap deflection, auxiliary flap deflection, wing spoiler deflection, and inboard engine gross thrust coefficient. Thrust coefficients were based on calibration of the inboard engine static thrust variation with engine tailpipe total pressure. This calibration was obtained with both the jet exhaust deflector and the flap undeflected. Thrust coefficients were held constant at 0, 0.06, 0.13, and 0.29 during the investigation.

BLC arrangement A was tested with the main flap deflected 30°, 40°, and 50° with the extended chord auxiliary flap, and deflected 30° with the normal chord auxiliary flap. The C_{μ} was adequate to maintain attached flow over the flap except at 50° with zero inboard engine thrust coefficient. For this case, C_{μ} was limited to 0.022 since air for BLC was supplied only by the outboard engines. Auxiliary flap deflections ranged from -25° to +50° with the extended chord and from 0° to 30° with the normal chord.

BLC arrangements B and C were tested with a deflection of 30° at a C_{μ} of 0.014. In addition, arrangement C was tested at a deflection of 40° with BLC and at a deflection of 30° without BLC. Only the normal chord auxiliary flap was tested with these flap arrangements. The flap deflection ranged from 0° to 30°.

Tests With Varying C_{μ} at 0° Angle of Attack

Momentum coefficient was varied with inboard engine gross thrust coefficient and dynamic pressure constant. The variation of lift coefficient with C_{μ} was obtained with each of the flap arrangements and deflections tested.

RESULTS

The figures presenting three-component longitudinal force and moment data and the variation of lift coefficient with momentum coefficient are listed in table I along with the configurations and variables tested. All of the data shown have been corrected for the effects of the outboard engine operation as discussed previously in the section entitled, "Corrections." Three-component longitudinal force and moment data are presented in figures 3 through 12, and the variation of lift coefficient with momentum coefficient is shown in figures 13 through 15.

Figures 16 through 30 are summary plots of the data in figures 5 through 15. The effect of several BLC arrangements on lift coefficient, trimmed $C_{L_{max}}$, lift increment due to auxiliary flap deflection, and momentum coefficient required for BLC is shown in figures 16 through 19, respectively. The effect of auxiliary flap deflections on drag coefficient, trimmed maximum lift, and pitching-moment coefficient is shown in figures 20, 21, and 22, respectively. The effect of varying the inboard span auxiliary flap deflection on pitching moment is presented in figure 23. The untrimmed lift increments due to auxiliary flap deflection at 0° angle of attack are shown in figures 24 through 30.

Figure 31 shows the longitudinal characteristics of the model at T/W of 0.05 and 0.10 used in calculating flight-path control capability with the extended chord auxiliary flap. The variations of incremental normal acceleration, flight-path angles, and approach speed with auxiliary flap deflection are shown in figures 32, 33, and 34, respectively.

DISCUSSION

The prime objective of this investigation was to develop an effective boundary-layer-control flap system having minimum C_L requirement for attached flow and to provide direct lift control by external jet augmentation on an auxiliary flap at low-thrust-to-weight ratio (0.05 to 0.10). Jet augmentation was attained by jet exhaust impingement of the flap lower surface from the inboard engines. Three boundary-layer-control arrangements were investigated initially with the normal chord auxiliary flap. Total lift coefficient at 0° angle of attack, maximum lift coefficient, lift increment due to auxiliary flap deflection, and boundary-layer-control requirement are summarized in figures 16 through 19. Boundary-layer-control flap arrangements B and C had no large advantages over BLC arrangement A in terms of increased lift or reduced BLC requirements. In addition, the effectiveness of the auxiliary flap was marginal for developing the lift increments desired for direct-lift control. Therefore, the chord of the auxiliary flap was increased, and BLC arrangement A (which required the least modification to the airplane used in the flight studies) was selected for further investigation. The following discussion will be based mainly on the results of this flap system with the extended chord auxiliary flap.

Effect of Auxiliary Flap Deflection on the Longitudinal Characteristics of the Model

Auxiliary flap deflections increased lift coefficient but did not affect the lift-curve slopes at the linear portion of the curve, as shown in figures 5 through 7. Drag coefficient also increased with auxiliary flap deflections, as shown in these figures and summarized in figure 20. Maximum trimmed lift coefficient increased to an auxiliary flap deflection of 30° when the main flap was deflected 30° or 40° and to 15° when the main flap was deflected 50° (see fig. 21). Maximum lift coefficients at the thrust coefficients tested were attained at a main flap deflection of 30°. The highest value of 2.54 was attained at a thrust coefficient of 0.29. In most cases, angles of attack at maximum lift coefficient decreased 2° to 4° with auxiliary flap deflections.

In general, deflecting the auxiliary flap did not affect static margin but did cause a nose-down pitching moment (figs. 5-7). The variation of pitching moment with auxiliary flap deflection is summarized in figure 22. One method of reducing moment changes due to the auxiliary flap was to vary only the deflection of the inboard span auxiliary flap (0.11 to 0.37 of the wing semispan) while the outboard span was deflected 15°. This arrangement caused essentially no variation of pitching moment (fig. 23). However, when the inboard span flap was deflected more than 15°, the lift coefficients attained with this arrangement were less than those with the full-span auxiliary flap at a constant deflection. For example, lift coefficients were reduced 6 percent ($C_T = 0.06$) to 8 percent ($C_T = 0.29$) of that obtained with the full-span auxiliary flap deflected 30°.

Variation of Untrimmed Auxiliary Flap Lift Increment at 0° Angle of Attack

The lift increment due to auxiliary flap deflection is shown in figure 24 for the main flap deflected 30°, 40°, and 50° and with BLC. Without external jet augmentation ($C_T = 0$) on the flap system, the incremental lift was nearly the same for both the 30° and 40° flap deflections and varied almost linearly with deflections from -25° to +30°. With the main flap deflected 50°, the increase in lift increment due to auxiliary flap deflection was small.

External jet augmentation increased auxiliary flap effectiveness by a factor of 3 for a C_T of 0.29. The variation of lift with auxiliary flap deflection was linear up to 30° with the main flaps deflected 30° or 40°, and lift increased with auxiliary flap deflection up to 50°. With the main flap deflected 50°, this variation was the same as that obtained with a lower main flap deflection to 15° auxiliary flap deflection. Lift effectiveness above 15° was less than that obtained with a lower main flap deflection.

Effect of jet engine exhaust deflector.- The effect of the engine exhaust deflector on the auxiliary flap lift increment is shown in figures 25 and 26 for main flap deflections of 30° and 50°, respectively. With the main flap deflected 30°, lift effectiveness increased substantially with auxiliary flap deflection above 15° and with the deflector. Benefits from the deflector were reduced at a main flap deflection of 50°, probably because of the trailing-edge flap being more directly in the path of the jet exhaust.

Effect of auxiliary flap chord.- The effect of flap chord on the lift increment due to auxiliary flap deflection and on total lift coefficient is shown in figure 27. Results with the normal chord auxiliary flap were obtained from figure 10 and were corrected to a C_u of 0.014 in order to make them comparable with the extended chord flap data. The lift increment due to auxiliary flap deflection was approximately the same with either flap chord. However, higher total lift coefficients were obtained with the extended chord flap. Lift coefficient increased approximately 10 and 8 percent at auxiliary flap deflections of 0° and 30°, respectively. These values agree closely with the 7 percent increase obtained from the theory of reference 5 when the averaged flap-chord ratio is increased from 0.23 (main flap plus normal chord auxiliary flap) to 0.26 (main flap plus extended chord flap).

Effect of momentum coefficient.- The effect of blowing BLC over the main flap on the lift effectiveness of the auxiliary flap was small (fig. 28). However, the total lift coefficient increased significantly over the range of auxiliary flap deflections tested (fig. 29).

Figures 13 through 15 show that the variation of lift coefficient with momentum coefficient was unaffected by external jet augmentation on the flap system.

Effect of symmetrically deflected wing spoilers with auxiliary flap deflection.- Figure 30 shows the variation of lift coefficient with gross thrust coefficient with and without spoilers. Despite the flow separation caused by the spoilers, significant increases were achieved by increasing

thrust coefficient. Spoilers deflected 5° and 10° over the range of thrust coefficients tested reduced the lift increment due to auxiliary flap deflection approximately 0.08.

Estimated Flight-Path Control During Descent With Extended Chord Auxiliary Flap

Figure 31 shows the longitudinal characteristics of the model at $T/W = 0.05$ and 0.10 used in the computations. The curves in the figure were obtained by interpolation of the data in figures 5 through 7 and figure 12. The effects of the outboard engine thrust are not included in the computations.

The calculated incremental accelerations normal to the flight path $[a_n = (\Delta C_{Laux}/C_{Ltrim})]$ due to the extended chord auxiliary flap deflection are shown in figure 32 and are based on the angle of attack and C_{Ltrim} values tabulated below. These values were selected at approximately midpoint of the available C_L range at $1.3 V_s$ (1 g flight) because of the auxiliary flap deflection shown in figure 31. Because of this method of selecting C_{Ltrim} values, a_n does not become zero at 0° auxiliary flap deflection.

δ_f_m , deg	T/W = 0.05			T/W = 0.10		
	α , deg	C_{Ltrim}	W/S = 53 psf approach speed $1.3 V_s$, k	α , deg	C_{Ltrim}	W/S = 53 psf approach speed $1.3 V_s$, k
30	4	1.14	117.0	5	1.28	110.5
40	3	1.14	117.0	3	1.20	113.8
50	2	1.20	114.0	2	1.30	109.5
30 with $\delta_f_{aux,OB} = 15^\circ$	4	1.14	117.0	5	1.25	111.8

Flight studies (refs. 6 and 7) have indicated that ± 0.2 g is a reasonable margin for maneuvering during the landing approach. This criterion is met when the main flap deflected 30° or 40° at $T/W = 0.05$ and the deflection is constant over the full extent of the auxiliary flap. With the main flap deflected 50°, incremental normal accelerations are -0.13 g and +0.19 g. At $T/W = 0.10$ the incremental normal acceleration of ± 0.2 g is achieved with any of the main flap deflections, and the variation of normal acceleration with auxiliary flap deflection is essentially linear. Deflecting only the inboard span auxiliary flap reduced incremental normal acceleration 36 to 44 percent of that obtained with full-span deflection at $T/W = 0.05$ and 0.10, respectively.

The variation of steady-state flight-path angle¹ with auxiliary flap deflection (1 g flight) at constant angle of attack is shown in figure 33. A normal 3° descent angle can be achieved with a main flap deflection of 30° for T/W = 0.10. For steeper approaches, higher main flap deflections and/or lower thrust-to-weight ratios would be required. Flight-path angle changes of 4.4° and 5.9° at T/W = 0.05 and 0.10, respectively, are feasible if the auxiliary flap is deflected from -10° to +50° at a main flap deflection of 30°. When only the inboard span auxiliary flap deflection was varied, the flight-path angle changed 2°.

Figure 34 shows the variation of steady-state approach speed (1 g flight, W/S = 53 psf) with auxiliary flap deflection at the corresponding flight-path angle shown in figure 33. Approach speeds close to 1.3 V_s (1 g flight) are indicated by tick marks in the figure.

CONCLUDING REMARKS

The trailing-edge flap system consisting of a main flap with full-span, blowing boundary-layer control and an extended chord auxiliary flap with external flow jet augmentation was found to be an effective high-lift device at low-thrust-to-weight ratios (0.05 to 0.10). The flap system also provided a method of direct-lift control by deflecting the auxiliary flap.

At each main flap deflection tested, this flap system increased lift coefficient and C_{Lmax} significantly compared to the system without external flow jet augmentation. A maximum trimmed lift coefficient of 2.54 was attained with the main flap deflected 30° at a thrust coefficient of 0.29. Performance computations indicate that by deflecting the auxiliary flap with the main flap deflected 30° and T/W = 0.05, this flap system could provide 0.2 g incremental normal acceleration at an approach speed of 117 knots (1 g flight, W/S = 53 psf) or a 4° change in flight-path angle at approach speeds (1 g flight) from 133 to 108 knots.

Ames Research Center

National Aeronautics and Space Administration

Moffett Field, Calif., 94035 April 3, 1969

721-01-00-14-00-21

¹The equation for computing flight-path angle is:

$$-\sin \gamma = \frac{D}{W} - \frac{T}{W} + \frac{dV/dt}{g} \quad (\text{minus sign for descending flight})$$

Assume 1 g flight and dV/dt = 0. L ≈ W

$$-\sin \gamma = \frac{C_D}{C_L}$$

$$\left. \begin{array}{l} C_L q_\infty S = W \\ C_D q_\infty S = D - T \end{array} \right\} (\text{Fig. 31})$$

T = inboard engines net thrust (outboard engine thrusts equal zero)

REFERENCES

1. Schade, Robert O.; and Crane, Harold L.: Low-Speed Flight Investigation of a Jet Transport With a Powered-Lift Boundary-Layer Control System. AGARD Rep. 503, June 1965.
2. Deckert, Wallace H.; Koenig, David G.; and Weiberg, James A.: A Summary of Recent Large-Scale Research on High-Lift Devices. NASA SP-116, 1966, pp. 63-79.
3. Kirk, Jerry V.; Hickey, David H.; and Aoyagi, Kiyoshi: Large-Scale Wind-Tunnel Investigation of a Model With an External Jet-Augmented Flap. NASA TN D-4278, 1967.
4. Hickey, David H.; and Aoyagi, Kiyoshi: Large-Scale Wind-Tunnel Tests and Evaluation of the Low-Speed Performance of a 35° Sweptback Wing Jet Transport Model Equipped With a Blowing Boundary-Layer-Control Flap and Leading-Edge Slat. NASA TN D-333, 1960.
5. De Young, John: Theoretical Symmetric Span Loading Due to Flap Deflection for Wings of Arbitrary Plan Form at Subsonic Speeds. NACA Rep. 1071, 1952.
6. Drinkwater, Fred J., III: Operational Technique for Transition of Several Types of V/STOL Aircraft. NASA TN D-774, 1961.
7. Staff of the Langley Research Center: Determination of Flight Characteristics of Supersonic Transports During the Landing Approach With a Large Jet Transport In-Flight Simulator. NASA TN D-3971, 1967.

TABLE I.- LONGITUDINAL CHARACTERISTICS OF THE MODEL

Figure	Main flap arrangement	δf_m , deg	Aux. flap chord	δf_{aux} , deg	C_T	C_μ	α_u , deg	δ_d , deg	δ_{sp} , deg	Remarks
3	---	0	Normal Extended	0	0	0	0 to 20 -4 to 24	0	Off	Plain wing
4	---		Normal				-8 to 32			Reynolds number effect
5(a)	A	30	Extended	0	0	0.013	-4 to 20	15		Auxiliary flap effect
5(b)				.06			-4 to 22			
5(c)				.13						
5(d)				.29						
5(e)					0	0.014	-4 to 20			
5(f)					.06					
6(a)	40			15	0	0.013	-4 to 20			
6(b)				.06						
6(c)				.13						
6(d)				.29						
		30	0	0.014						
			.06							
			.13							
			.29							
			40	0	0.013					
				.06						
				.13						
				.29						
				50	0	0.014				
					.06					
					.13					
					.29					
				0	0	0.021	-4 to 16			
					.06					
					.13					
					.29					
				-25	0	0.022	-4 to 18			
					.06					
					.13					
					.29					
				30	0	0.021	-4 to 18			
					.06					
					.13					
					.29					
				40	0		-4 to 20			
					.06					
					.13					
					.29					

TABLE I.- LONGITUDINAL CHARACTERISTICS OF THE MODEL - Continued

Figure	Main flap arrangement	δ_{f_m} , deg	Aux. flap chord	$\delta_{f_{aux}}$, deg	C_T	C_μ	α_u , deg	δ_d , deg	δ_{sp} , deg	Remarks	
7(a)	A	50	Extended	0	0 .06 .06 .13 .29	0.022 .022 .031 .031 .032	-4 to 18	15	Off	Auxiliary flap effect	
7(b)				-25	0 .06 .06 .13 .29	0.024 .024 .032 .032 .034	-4 to 20				
7(c)				-10	0 .06 .06 .13 .29	0.022 .022 .032 .032 .034	-4 to 18				
7(d)				15	0.06 .06 .13 .29	0.025 .028 .034 .034	-4 to 20				
7(e)				30	0 .06 .06 .14 .29	0.020 .020 .029 .028 .028	-4 to 18				
8(a)		30		0	0 .06 .13 .29	0.014	-4 to 20	Off		Effect of jet exhaust deflector off	
8(b)				-10	0 .06 .13 .29		-4 to 22				
8(c)				15	0 .06 .13 .29		-4 to 20				
8(d)				30	0 .06 .13 .29		-4 to 22				
8(e)				40	0 .06 .13 .29		-4 to 20				

TABLE I.- LONGITUDINAL CHARACTERISTICS OF THE MODEL - Continued

Figure	Main flap arrangement	δf_m , deg	Aux. flap chord	δf_{aux} , deg	C_T	C_μ	α_u , deg	δ_d , deg	δ_{sp} , deg	Remarks
9(a)	A	50	Extended	0	0 .06 .06 .13 .29	0.022 .020 .030 .030 .033	-4 to 18 ↓ -4 to 20	Off	Off	Effect of jet exhaust deflector off
9(b)				-25	0 .06 .06 .13 .29	0.023 .023 .033	-4 to 18 ↓ -4 to 20			
9(c)				30	0 .06 .06 .13 .29	0.023 .023 .033 .033 .032	-4 to 18 ↓ -4 to 20			
10(a)	30	Normal		0	0 0 .06 .14 .21 .30	0 .0064	-4 to 20 -4 to 22 -4 to 22 -4 to 28 -4 to 20 -4 to 20	15		Normal auxiliary chord effect
10(b)				30	0 0 .06 .13 .20 .30	0 .017	-4 to 28 -4 to 24 -4 to 20 -4 to 28 -4 to 20 -4 to 20			
11(a)				Extended	0 .06 .13 .29	0.018	-4 to 20	5	Spoilers on	
11(b)					0 .06 .13 .29					
11(c)				30	0 .06 .13 .29		-4 to 18 -4 to 18 -4 to 20 -4 to 20			
11(d)					0 .06 .13 .29	0.019	-4 to 18 -4 to 18 -4 to 20 -4 to 20			

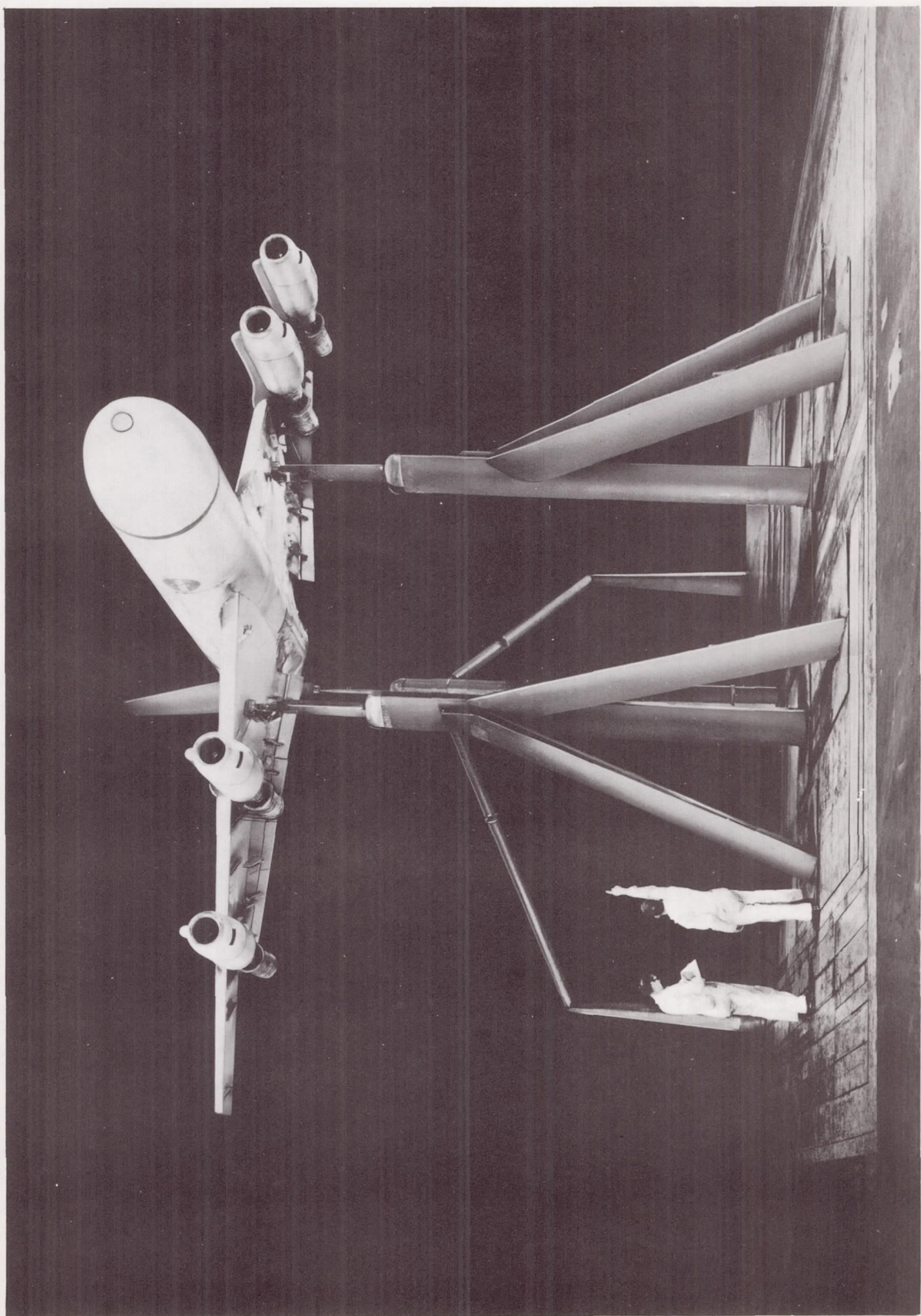
TABLE I.- LONGITUDINAL CHARACTERISTICS OF THE MODEL - Concluded

Figure	Main flap arrangement	δ_{f_m} , deg	Aux. flap chord	$\delta_{f_{aux}}$, deg	C_T	C_μ	α_u , deg	δ_d , deg	δ_{sp} , deg	Remarks
12(a)	A	30	Extended	-25 (Inbd) 15 (OB)	0 .06 .13 .30	0.016 	-4 to 18 -4 to 18 -4 to 20 -4 to 20	15	Off	Symmetrical differential auxiliary flap effect
12(b)				30 (Inbd) 15 (OB)	0 .06 .13 .30	0.017 	-4 to 16 			
12(c)				40 (Inbd) 15 (OB)	0 .06 .13 .29	0.018 	-4 to 18 -4 to 16 -4 to 18 -4 to 20			
Lift coefficient variation with momentum coefficient										
13(a)	A	30	Normal	0	0 .31	0 to 0.009 	0 15 Off	0 15 Off		
13(b)				30	0 .31	0 to 0.017 0 to 0.016				
14		40	Extended	0 30	0.13 0.13	0 to 0.045 0 to 0.038				
15(a)		50		0	0 .29	0 to 0.023 0 to 0.038				
15(b)				30	0 .29	0 to 0.022 0 to 0.041				

A-38257.1

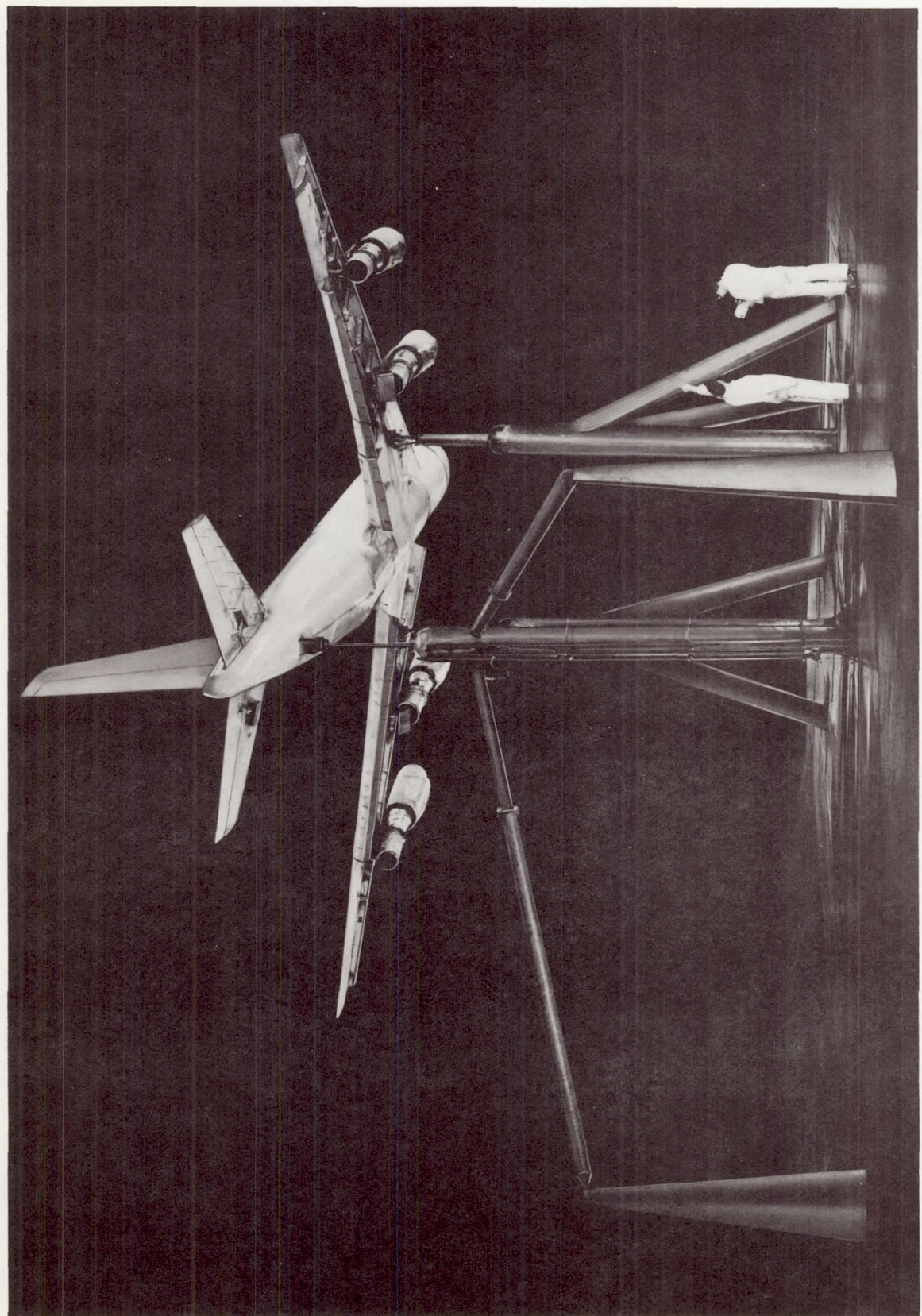
(a) Three-quarter front view.

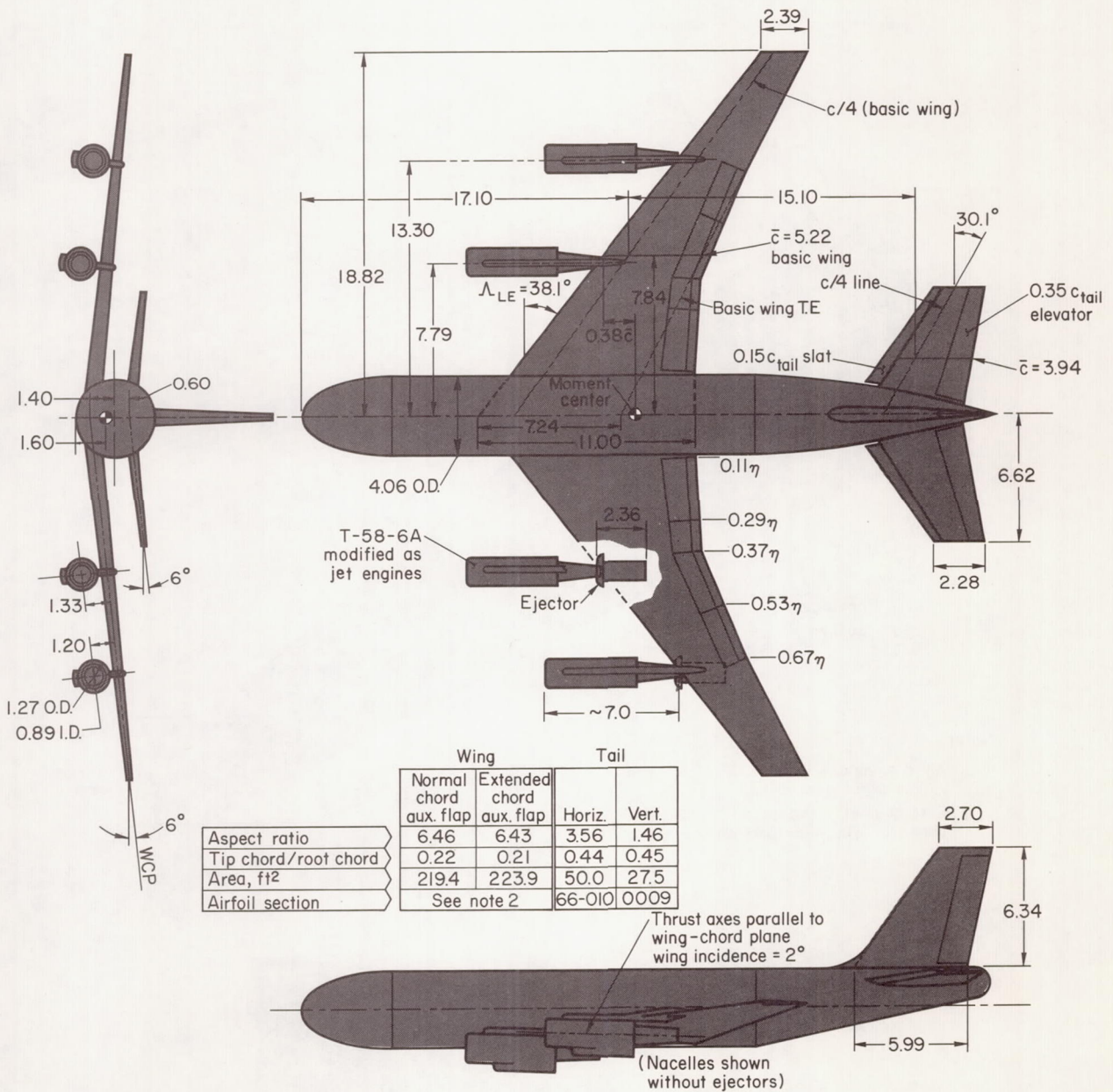
Figure 1.- Photograph of the model as mounted in the Ames 40- by 80-Foot Wind Tunnel.



A-38258, 1

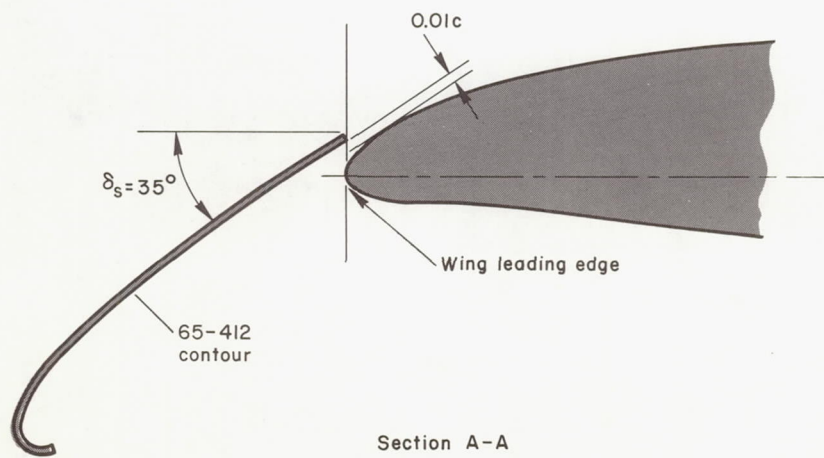
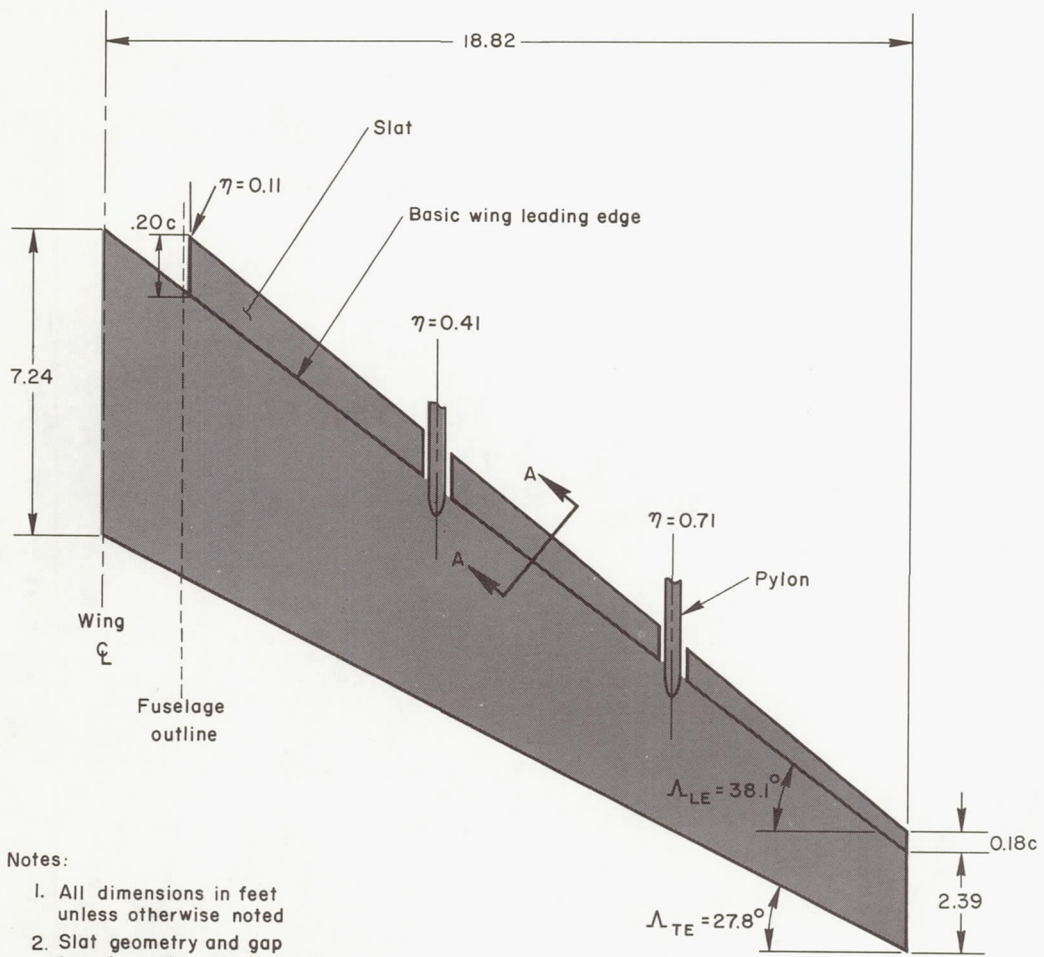
Figure 1.- Concluded.





(a) General arrangement of model.

Figure 2.- Geometric details of the model.



Section A-A

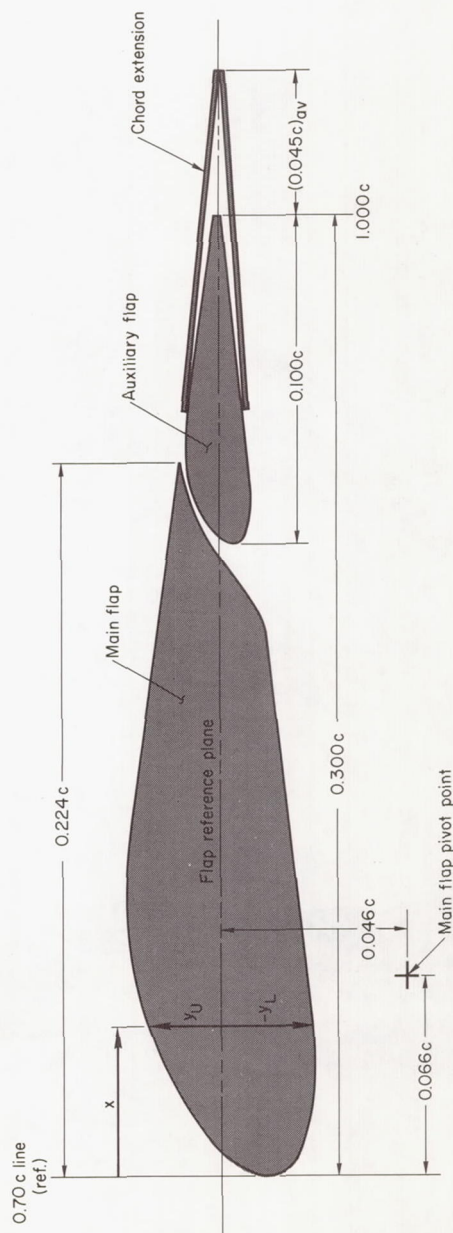
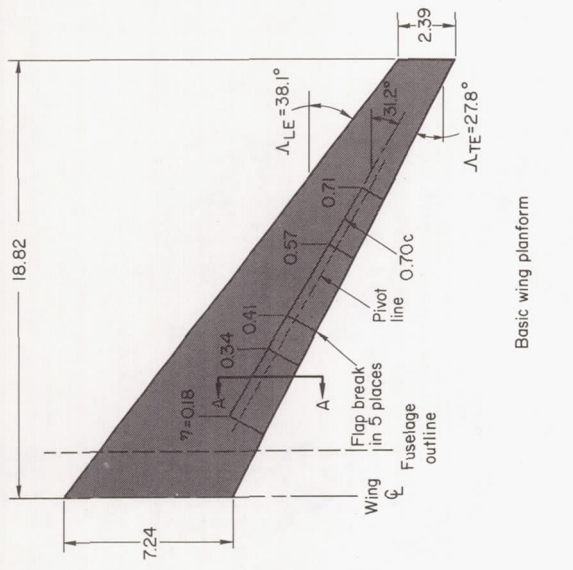
(b) Leading-edge slat.

Figure 2.- Continued.

Main flap ordinates				Auxiliary flap ordinates			
$x, \%, c$	$y_U, \%, c$	$y_L, \%, c$	$x, \%, c$	$y_U, \%, c$	$y_L, \%, c$	$x, \%, c$	
0	-1.274	-1.274	20.000	-0.348	-0.348		
0.448	-3.14	-2.018	20.274	.049	-.679		
.814	.041	-2.166	20.502	.251	-.743		
1.543	603	-2.420	20.731	.396	-.792		
2.269	1.023	-2.550	21.416	.686	-.823		
3.003	1.377	-2.548	21.872	.799	-.807		
4.448	1.902	-	22.328	.871	-		
5.888	2.252	-2.342	22.783	.903	-		
7.333	2.519	-2.207	23.238	.902	-.700		
8.755	2.564	-	23.692	.853	-		
10.181	2.511	-	26.308	.500	-.410		
11.612	2.392	-1.764	30.000	.058	-.062		
16.902	-	-1.250					
17.547	1.685	-					
17.823	-	-997					
18.743	-	-.502					
19.660	-	.073					
19.962	1.375	-					
20.585	-	.501					
21.498	-	.856					
22.410	1.097	.968					

Notes:

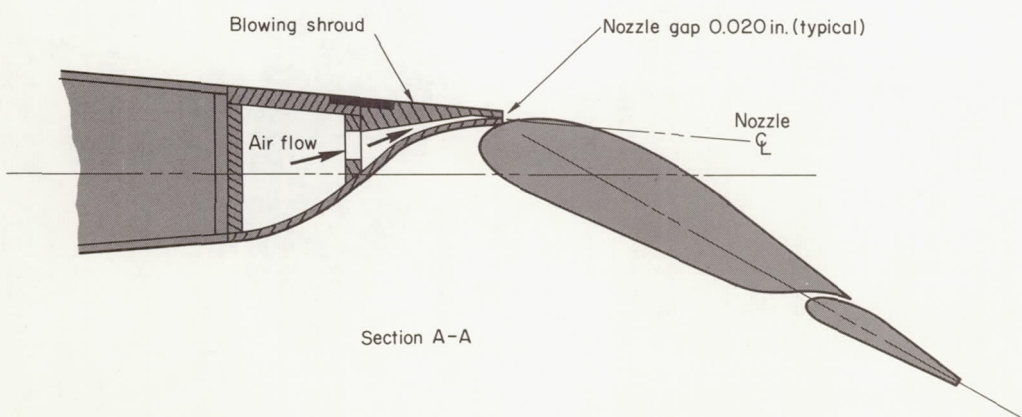
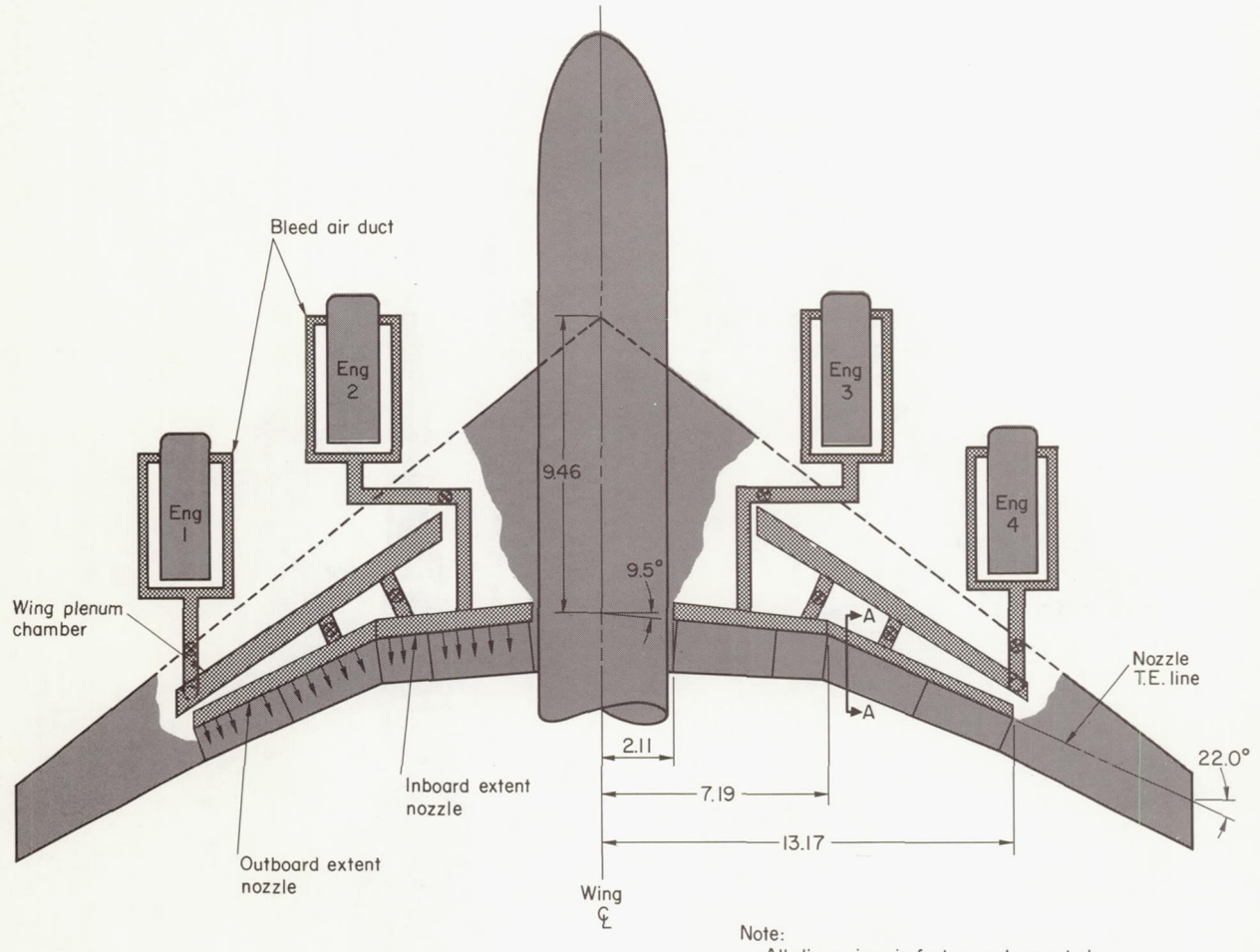
1. All dimensions in feet except as noted
2. Flap geometry and dimensions obtained from basic wing planform



Section A-A (typical)

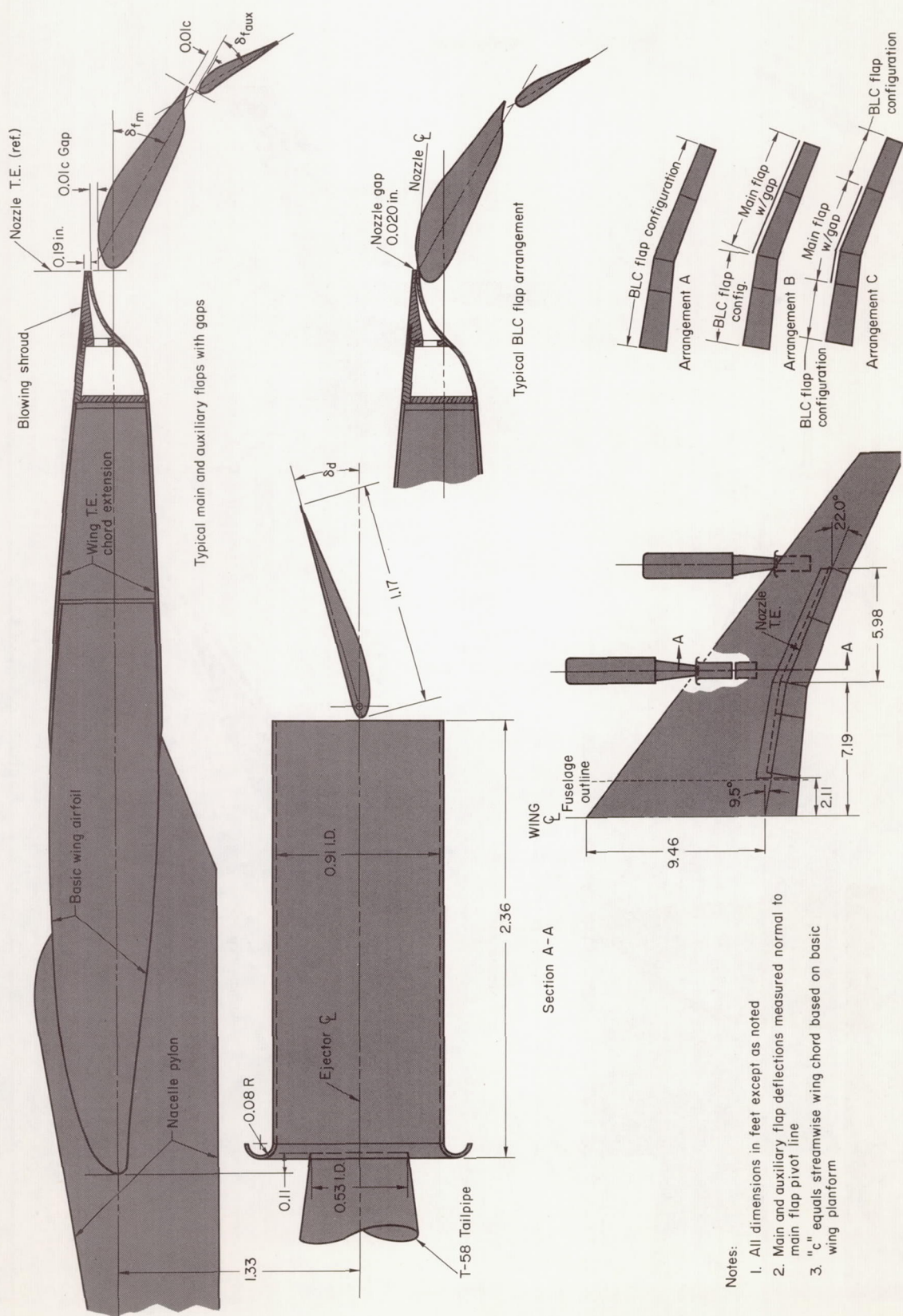
(c) Trailing-edge flap.

Figure 2.- Continued.



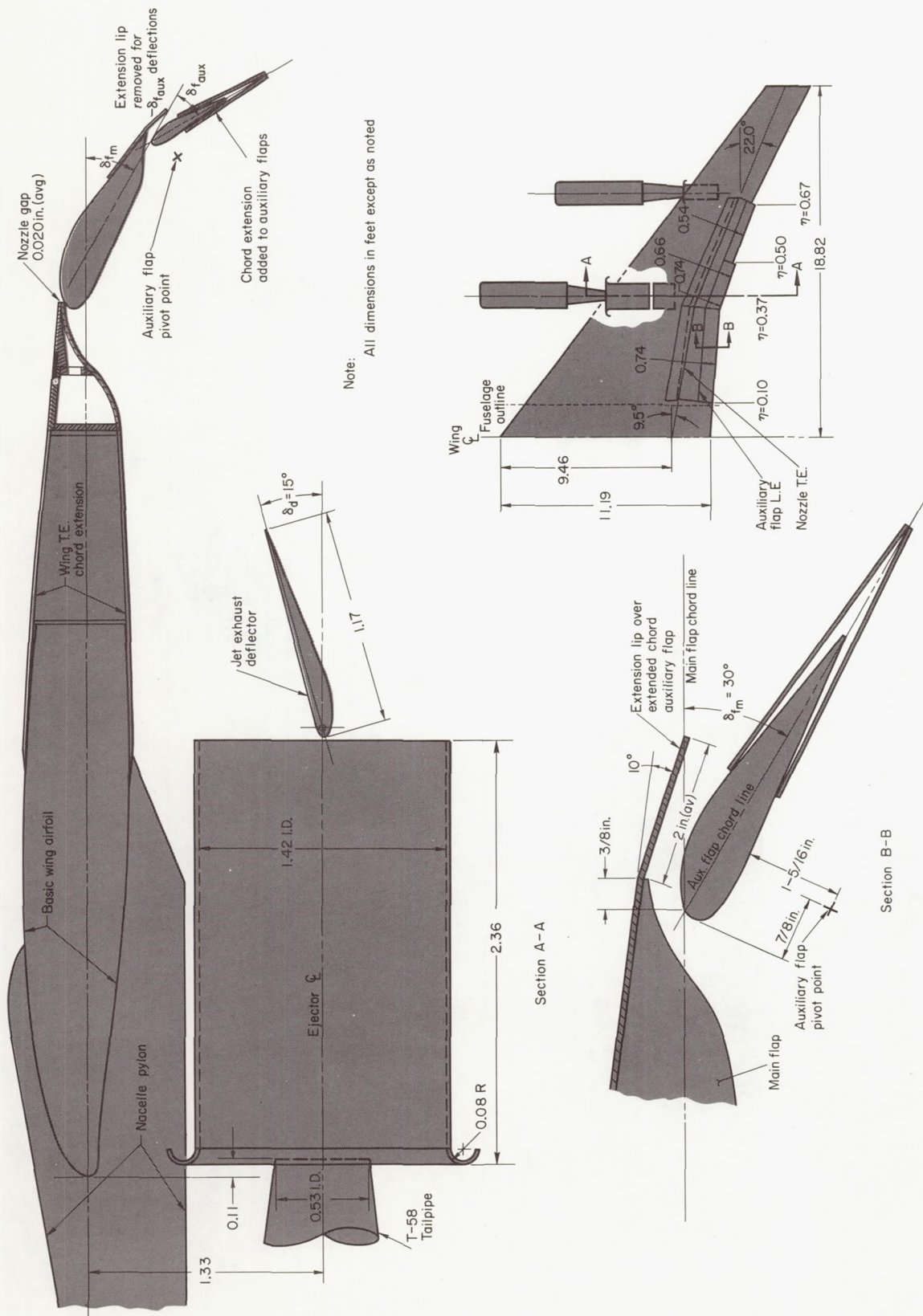
(d) Boundary-layer-control system ducting and blowing nozzle arrangement.

Figure 2.- Continued.

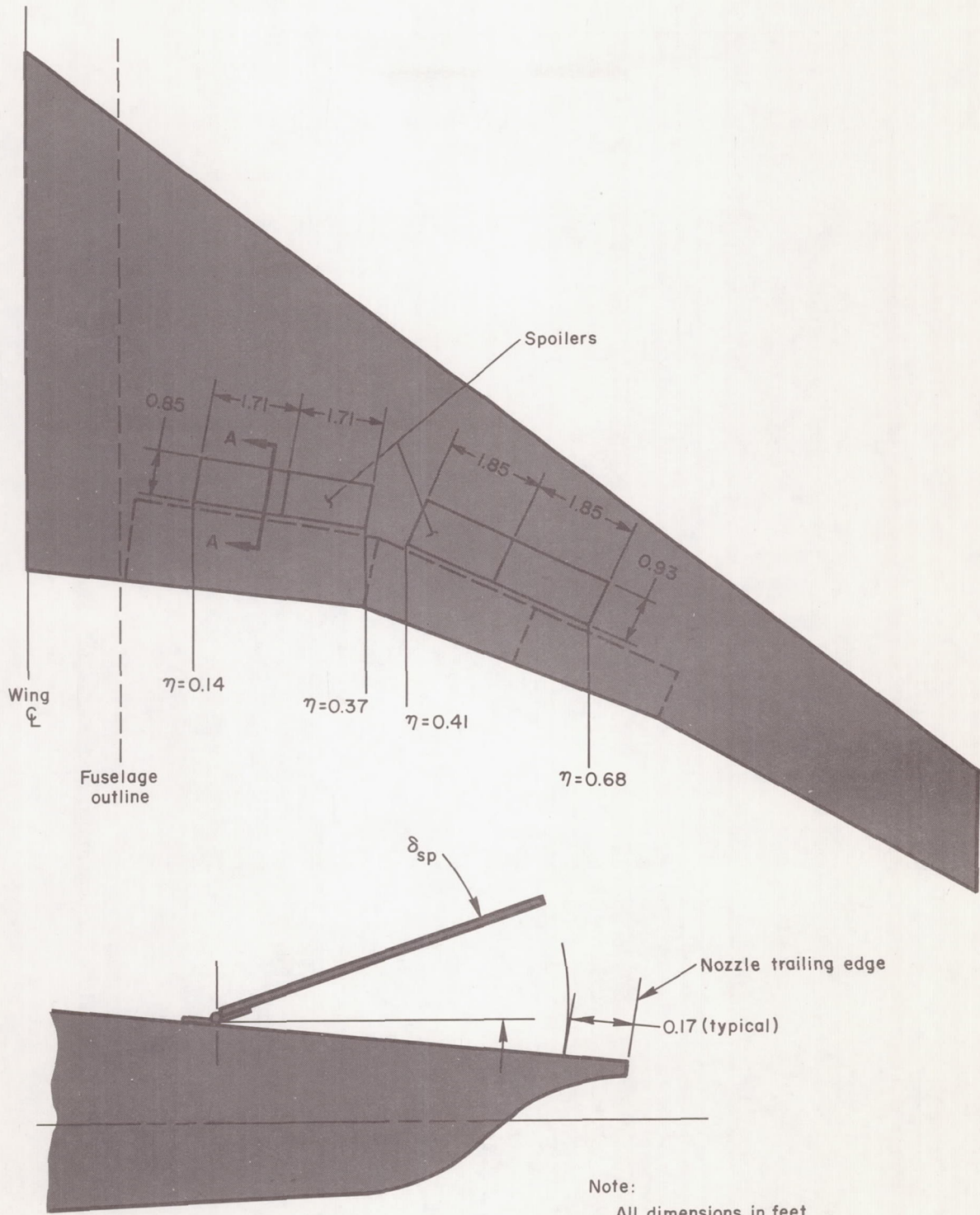


(e) Flap arrangement.

Figure 2.- Continued.



(f) Extended chord auxiliary flap arrangement.
Figure 2.- Continued.



Section A-A

(g) Wing spoiler arrangement.

Figure 2.- Concluded.

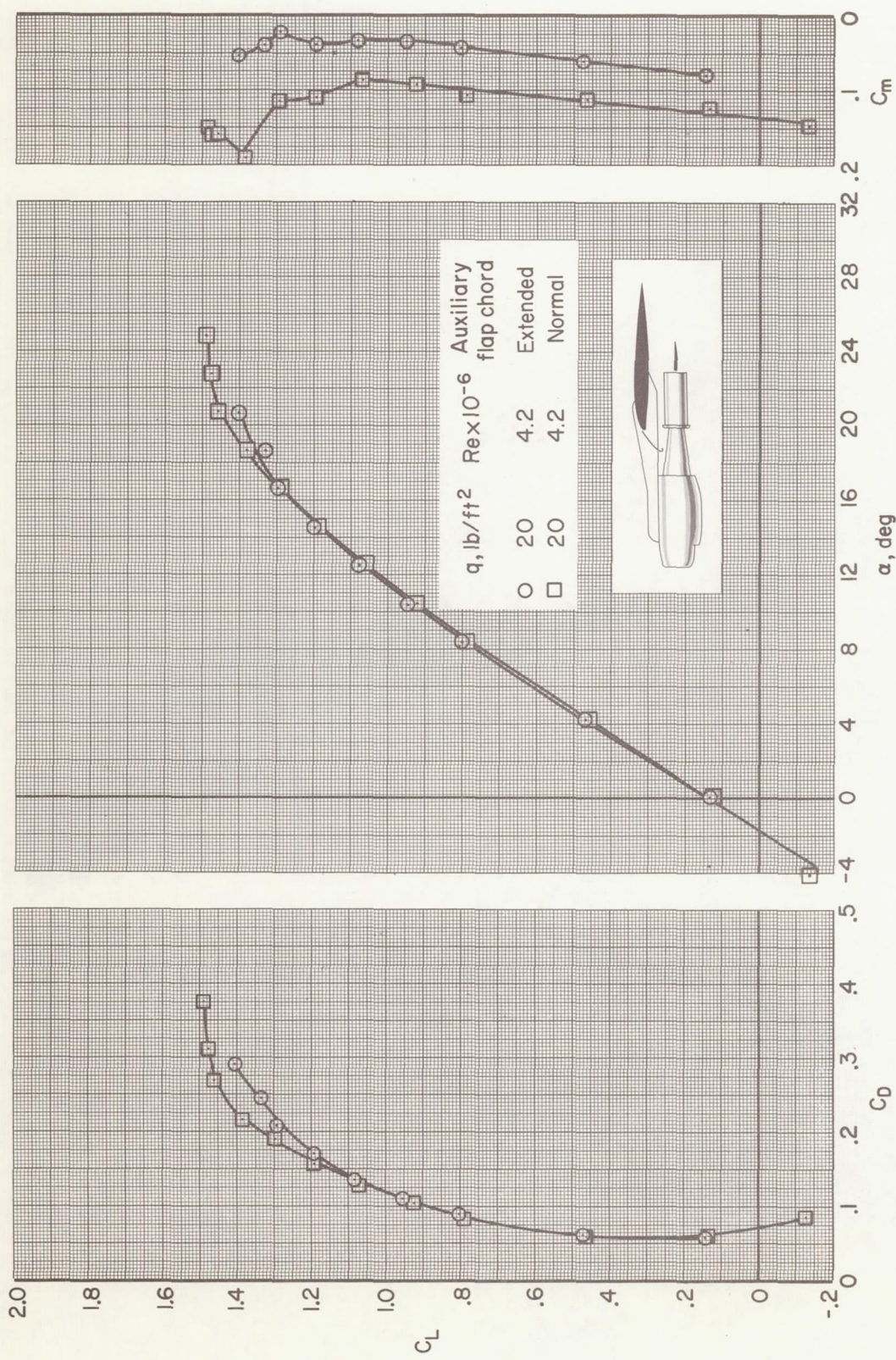


Figure 3.- Longitudinal characteristics of the model with plain wing; $\delta_d = 0^\circ$, $\delta_s = 35^\circ$, $i_t = -5^\circ$, $\delta_e = 0^\circ$, power off.

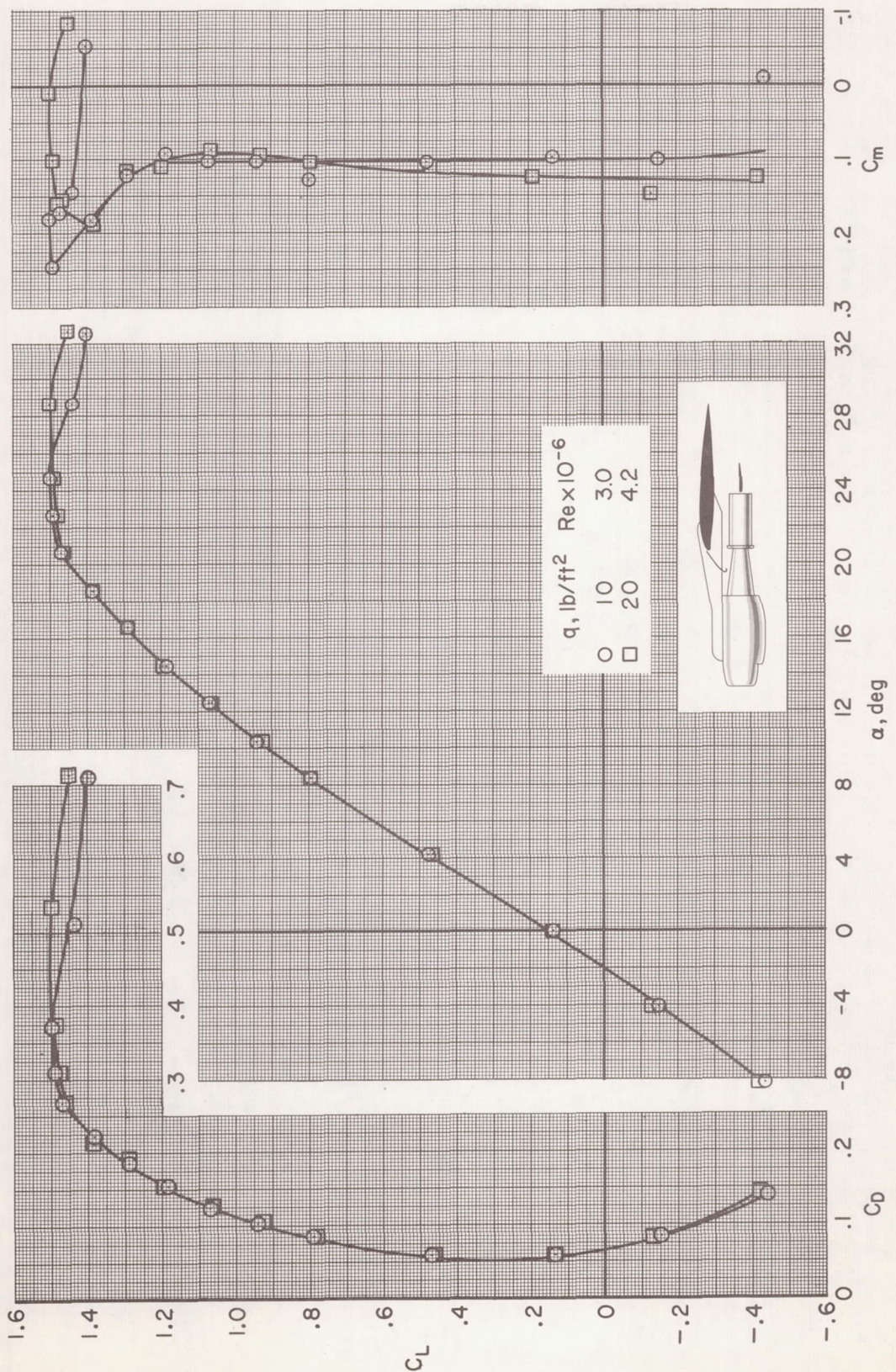


Figure 4.- Effect of Reynolds number on the longitudinal characteristics of the model with plain wing; normal chord auxiliary flap, $\delta_d = 0^\circ$, $\delta_s = 0^\circ$, $\delta_t = 35^\circ$, $\delta_e = -5^\circ$, power off.

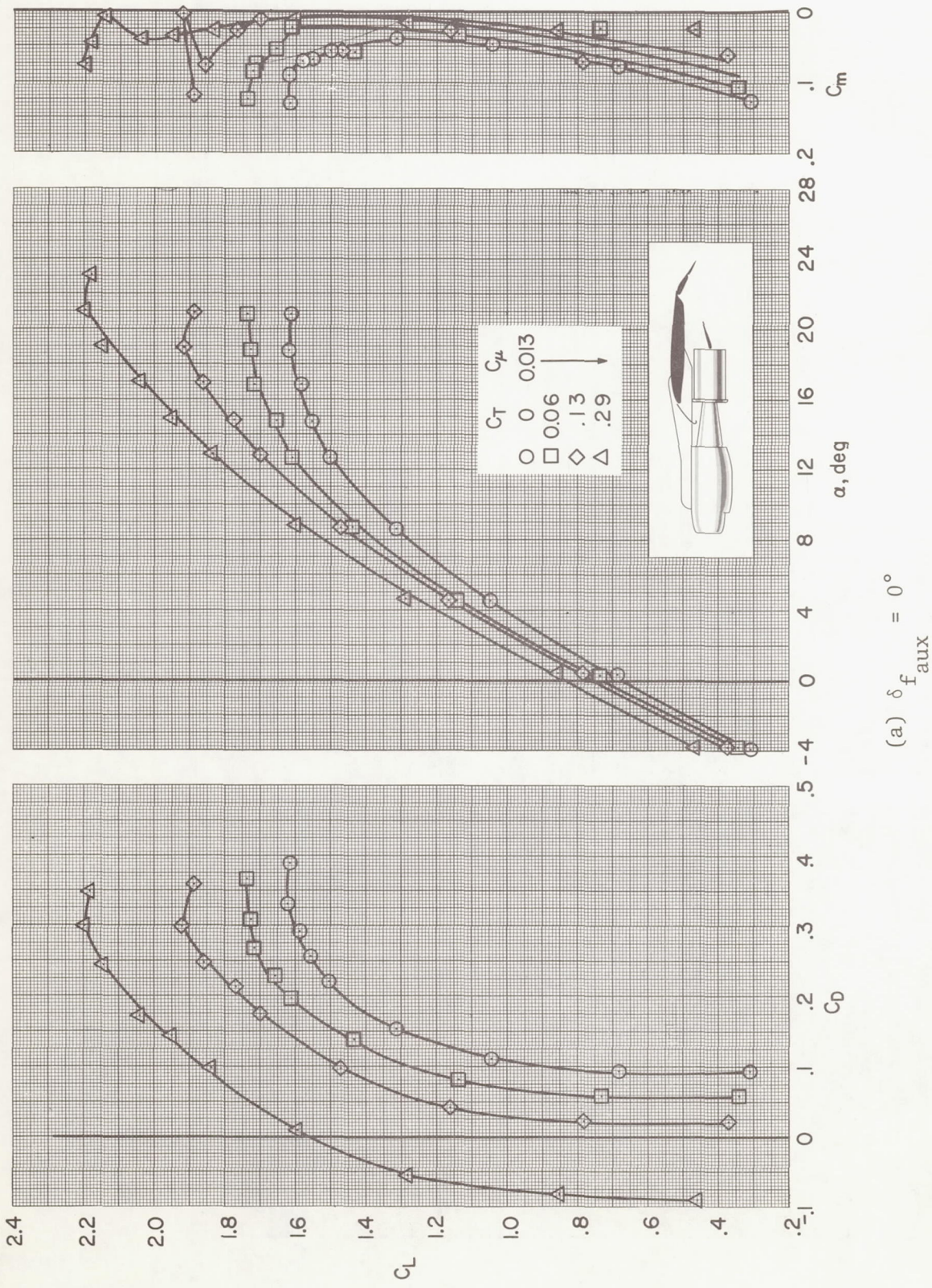
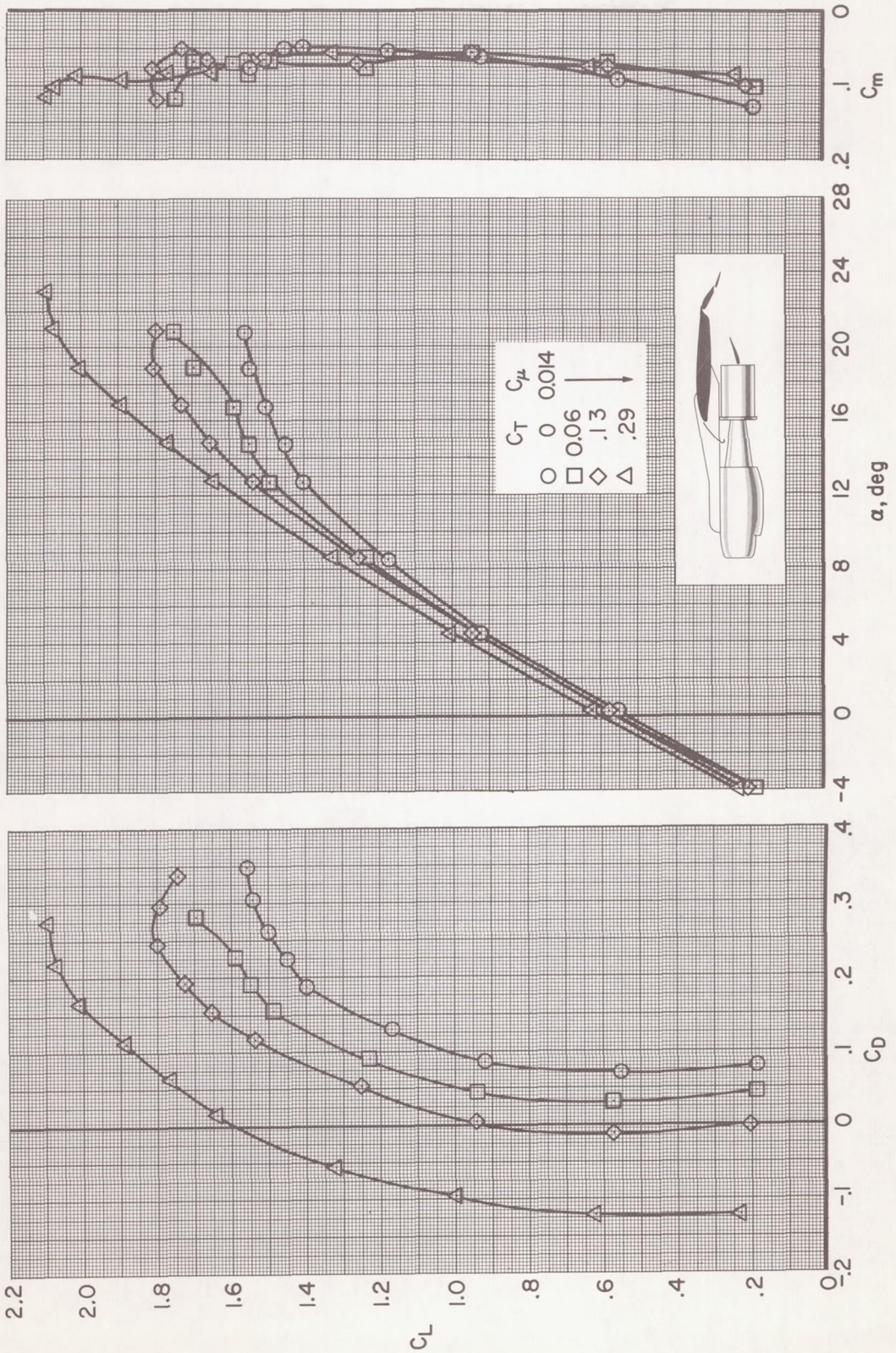
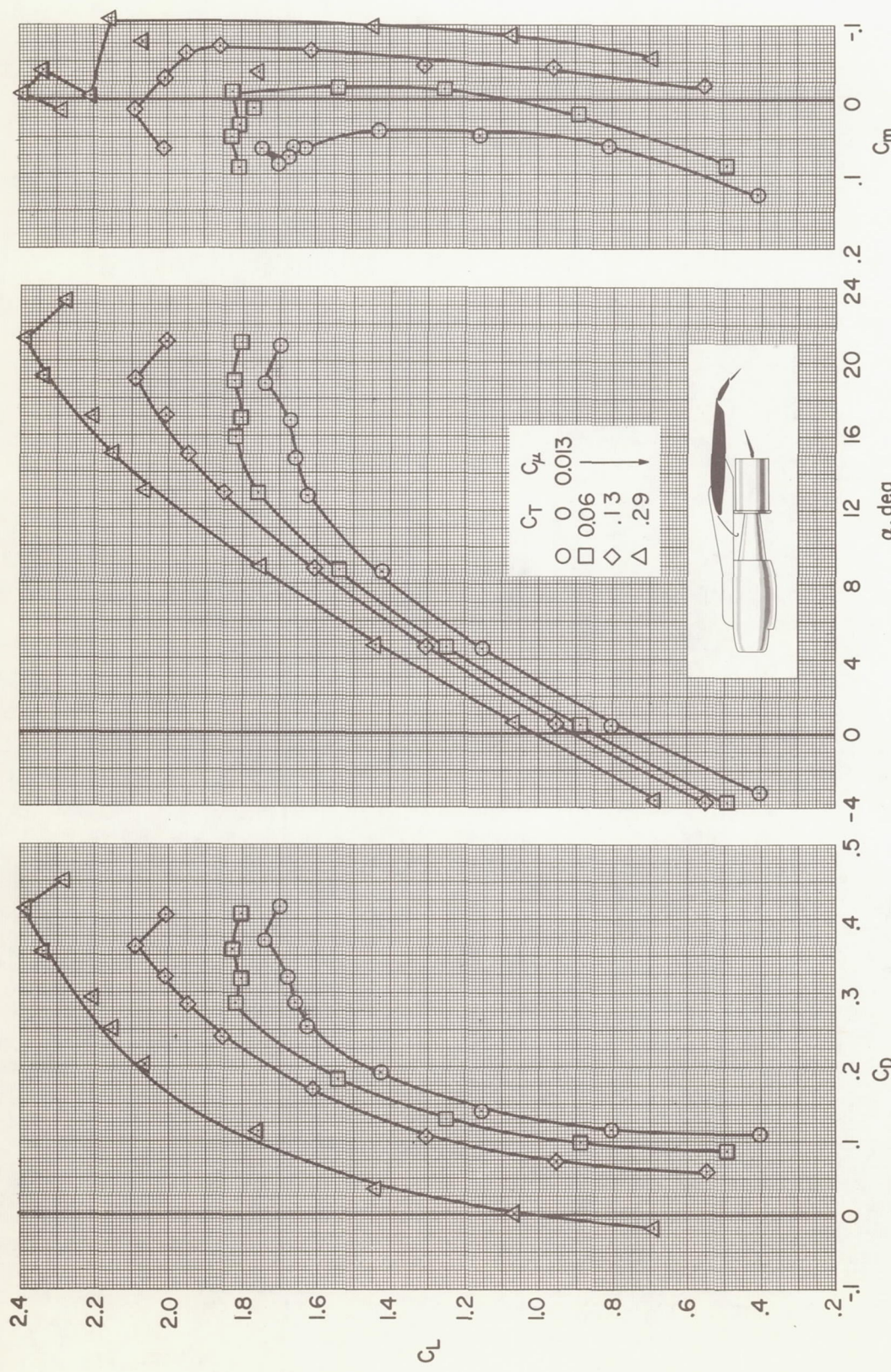


Figure 5.- Longitudinal characteristics of the model with main flap deflected 30° ; BLC flap at 0° .
 arrangement A with extended chord auxiliary flap, $\delta_d = 15^\circ$, $s_s = 35^\circ$, $\delta_i = -5^\circ$, $\delta_e = 0^\circ$.



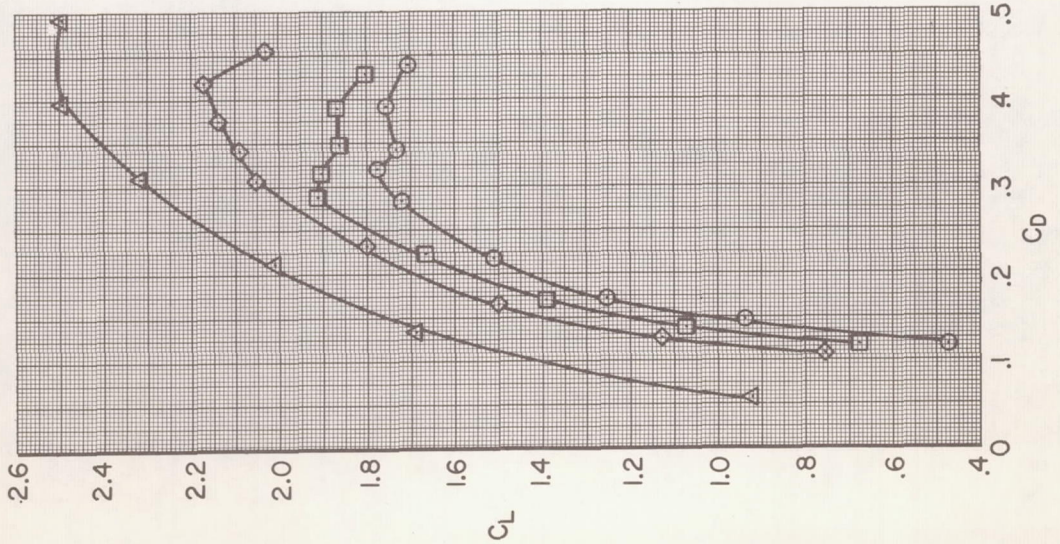
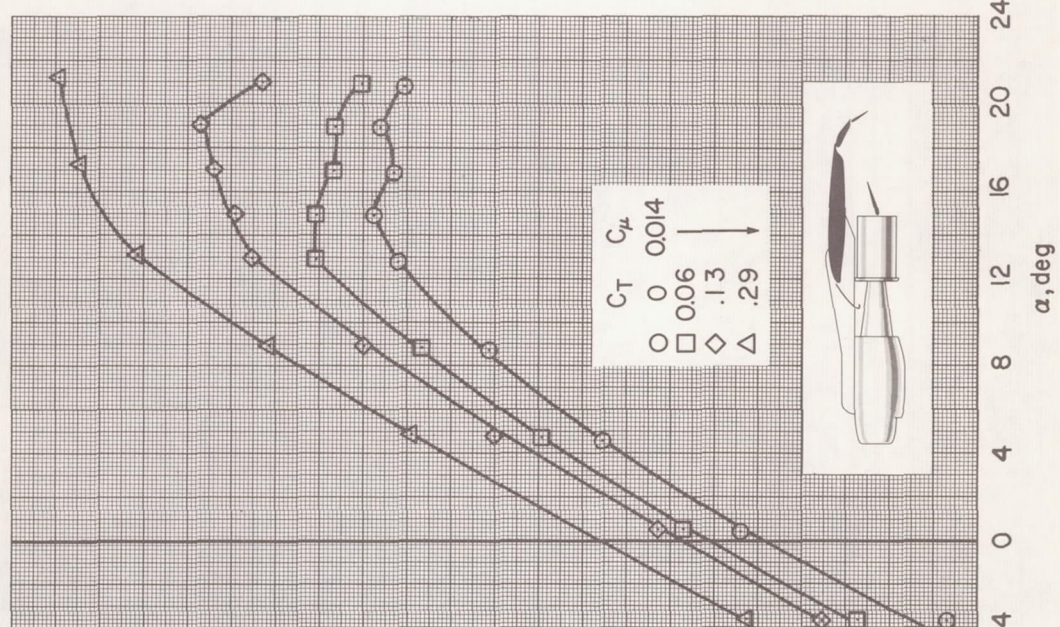
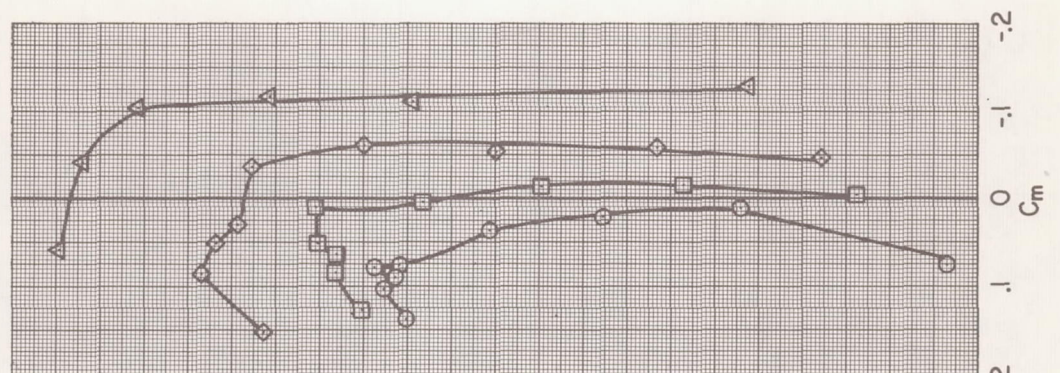
(b) $\delta f_{aux} = -10^\circ$

Figure 5.- Continued.



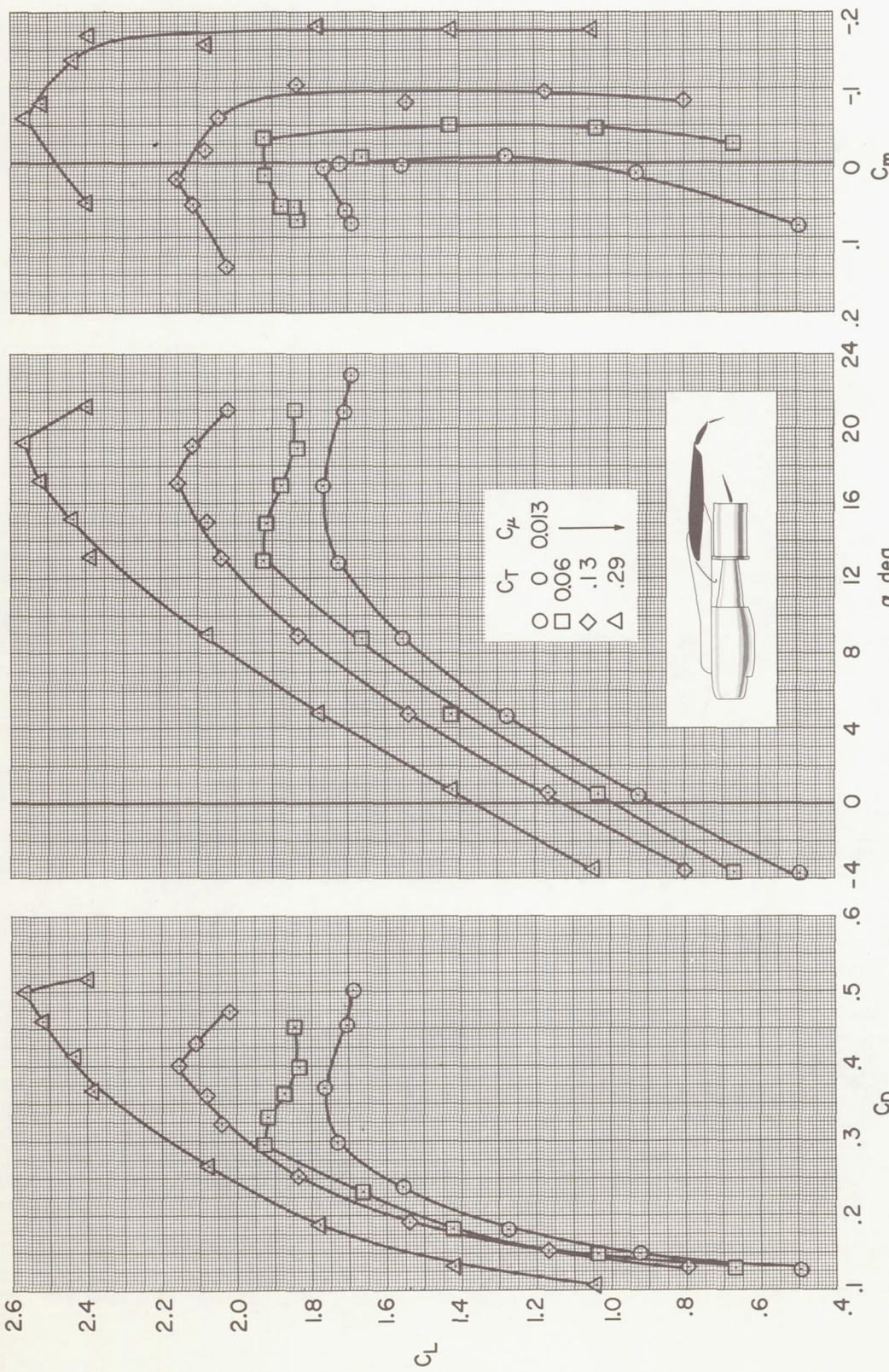
(c) $\delta_f_{aux} = 15^\circ$

Figure 5.- Continued.



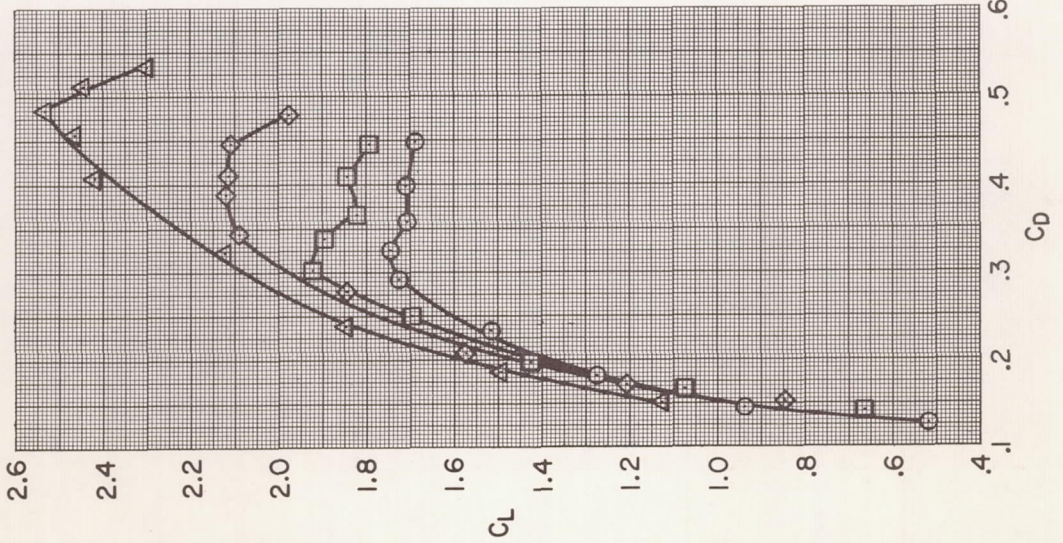
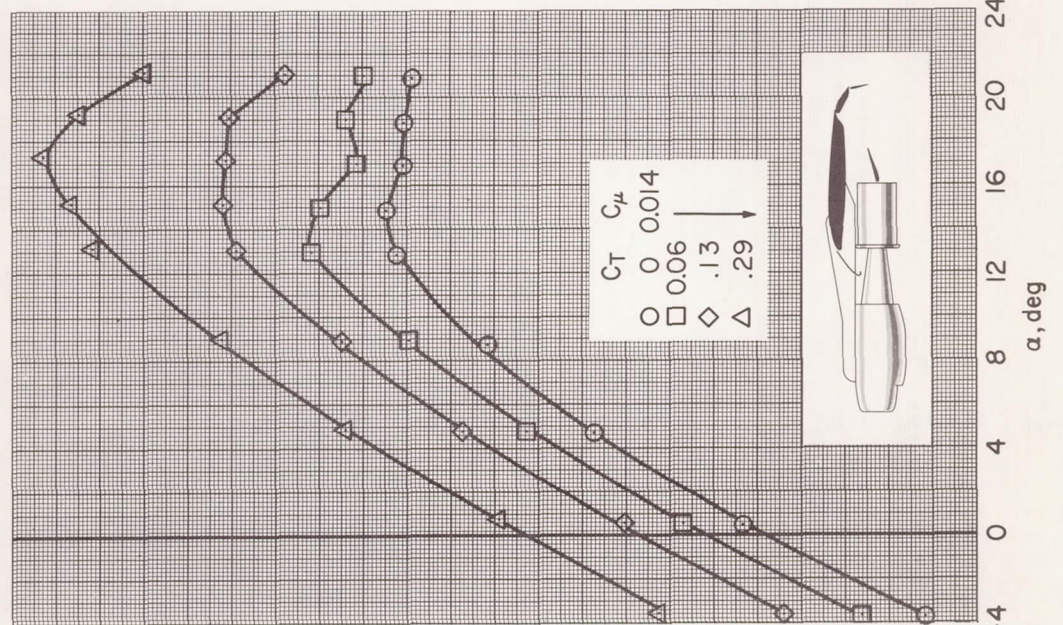
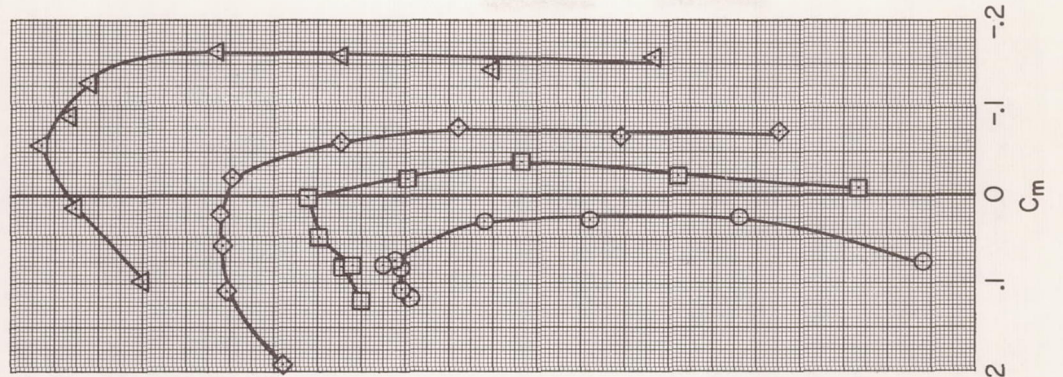
(d) $\delta_{f_{aux}} = 30^\circ$

Figure 5.- Continued.



(e) $\delta_{f_{aux}} = 40^\circ$

Figure 5.- Continued.



$$(f) \quad \delta f_{aux} = 50^\circ$$

Figure 5.- Concluded.

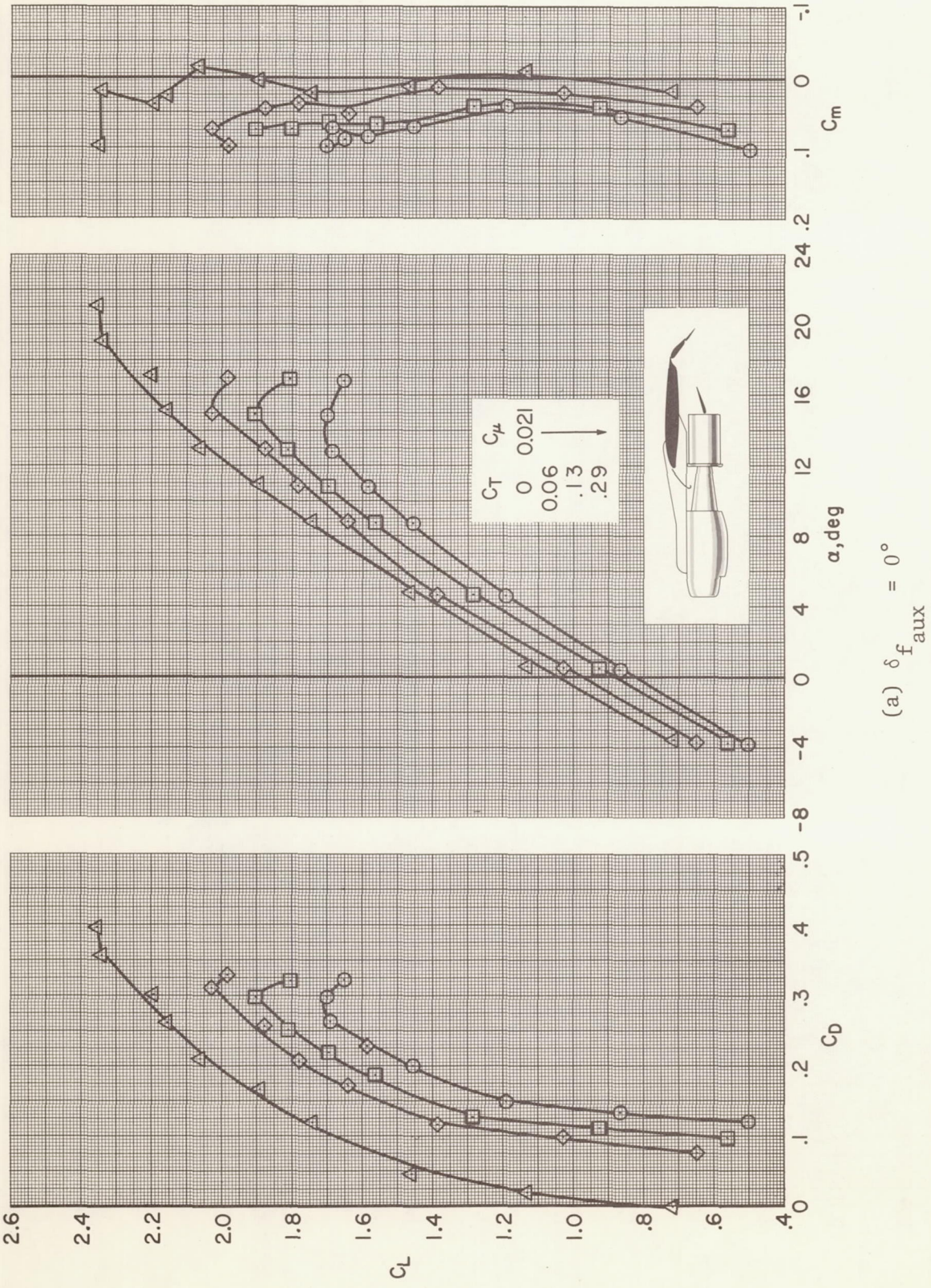
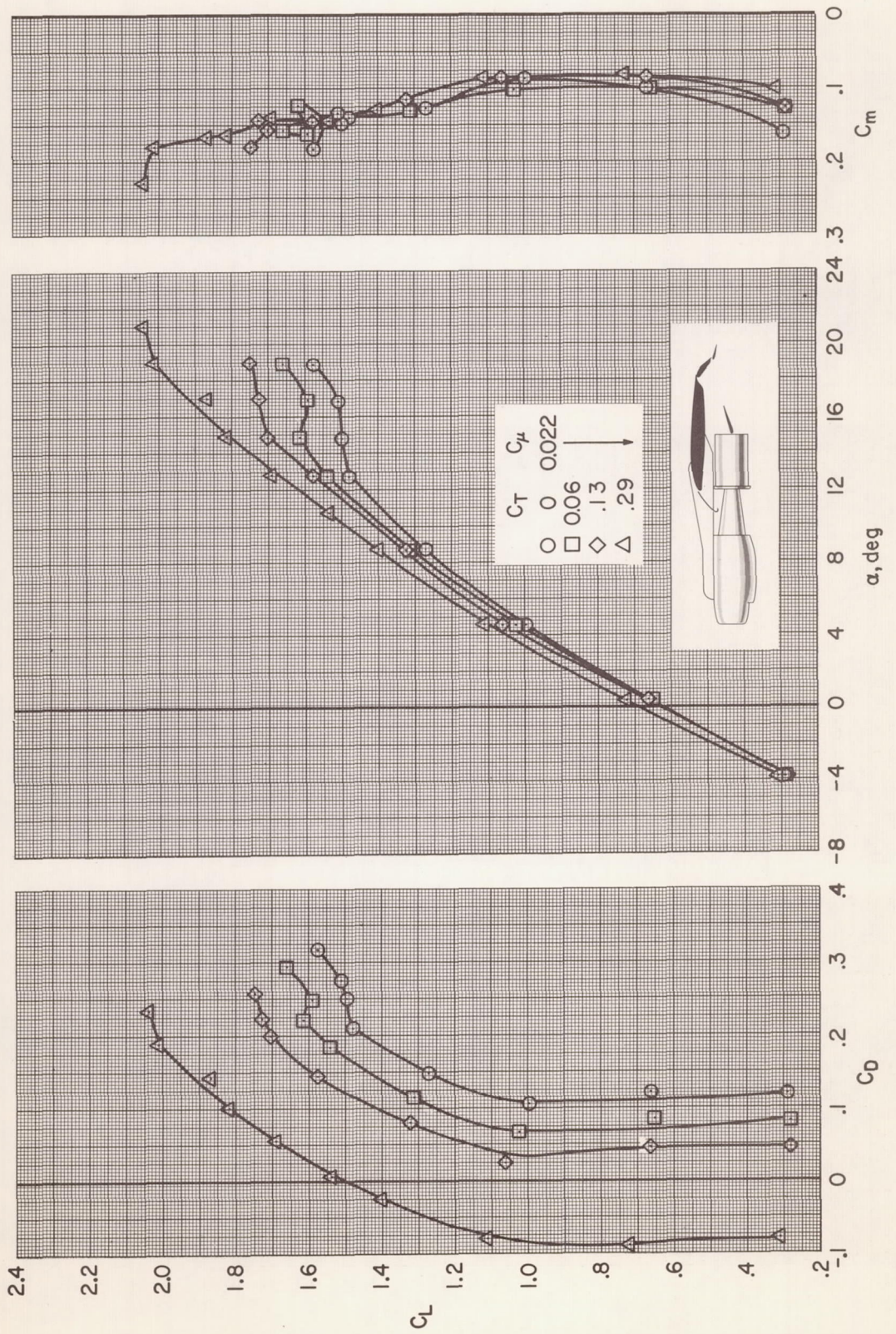
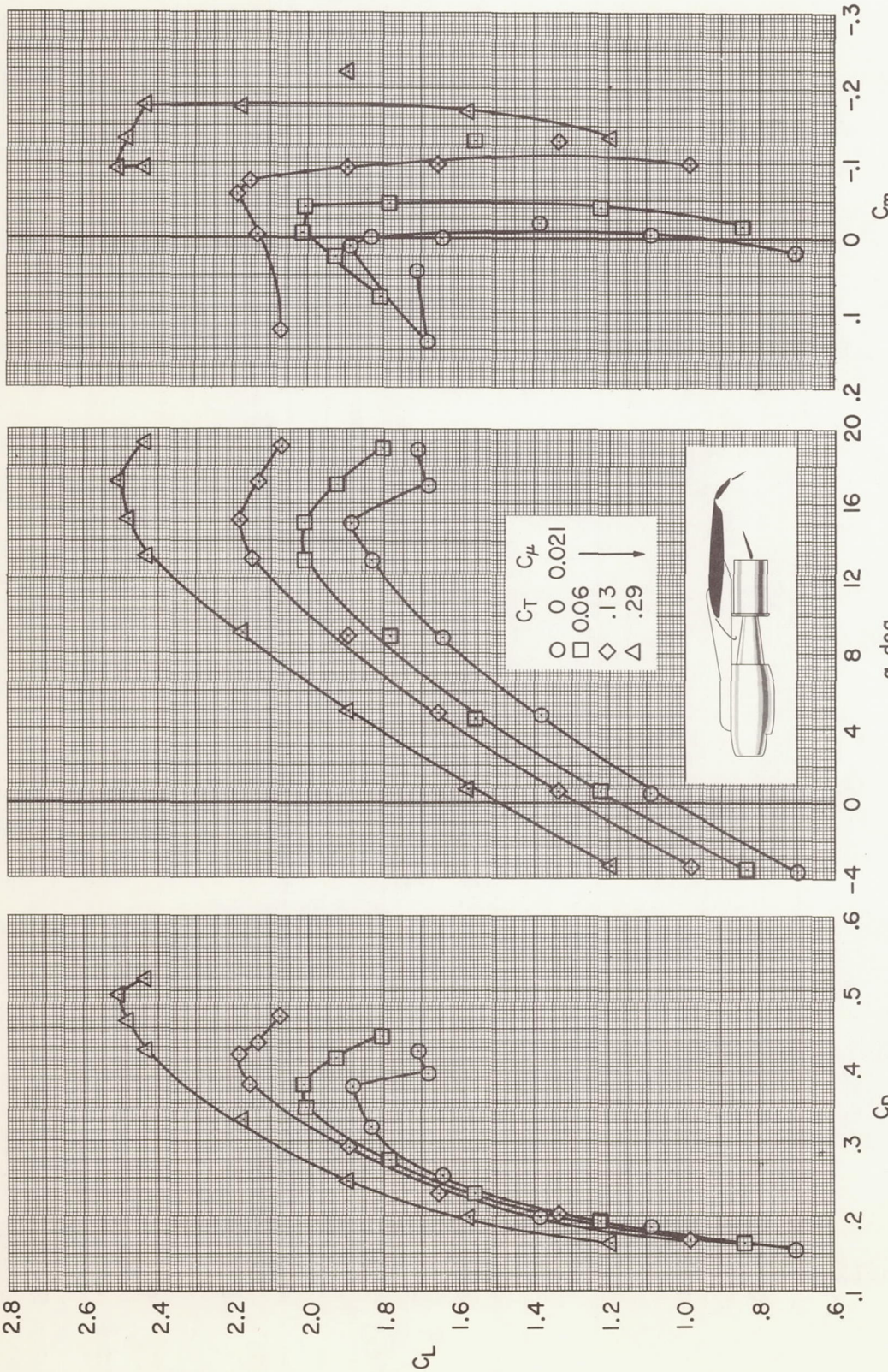


Figure 6.- Longitudinal characteristics of the model with main flap deflected 40°; BLC flap arrangement A with extended chord auxiliary flap, $\delta_d = 15^\circ$, $\delta_s = 35^\circ$, $i_t = -5^\circ$, $\delta_e = 0^\circ$.



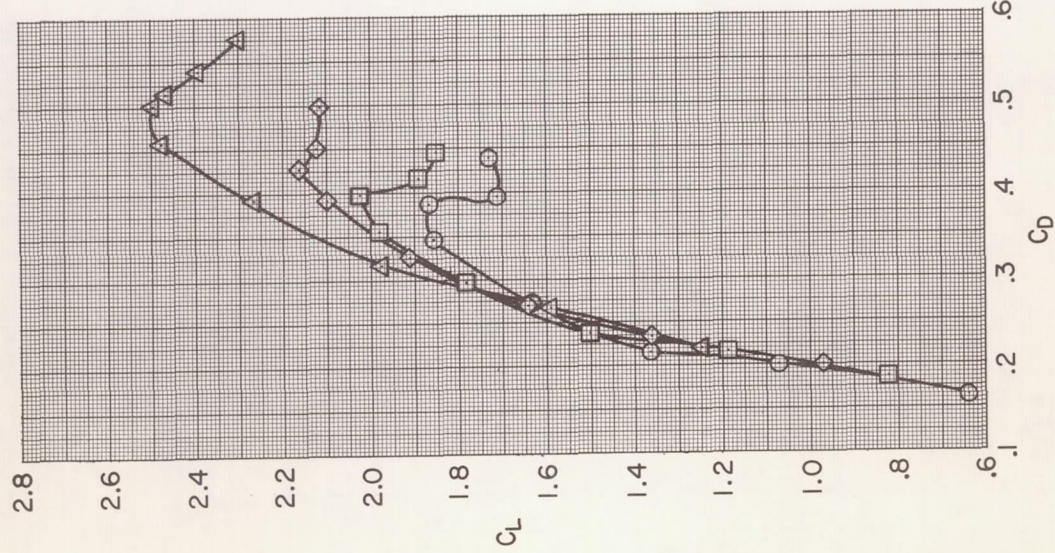
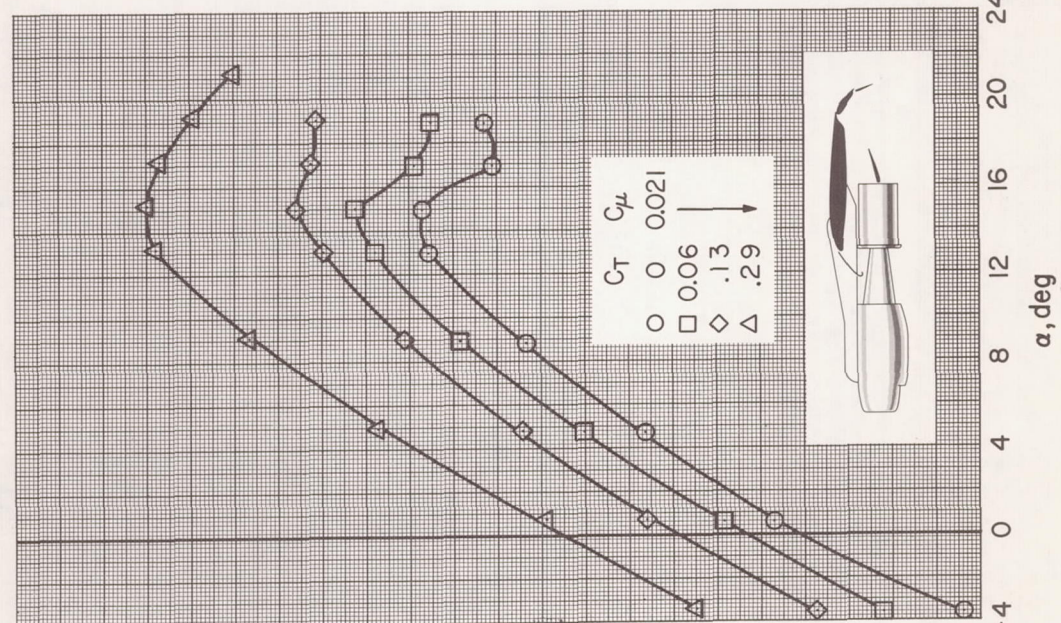
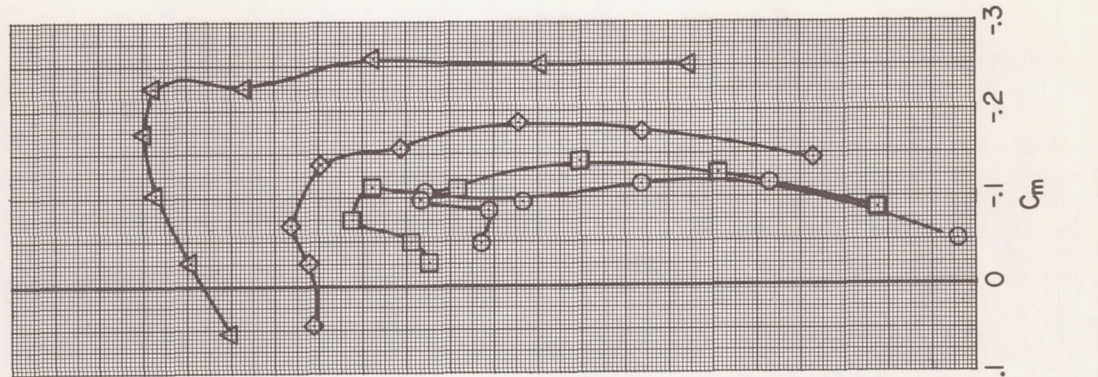
(b) δ_f aux = -25°

Figure 6.- Continued.



(c) $\delta f_{aux} = 30^\circ$

Figure 6.- Continued.



$$(d) \quad \delta_f_{aux} = 40^\circ$$

Figure 6.- Concluded.

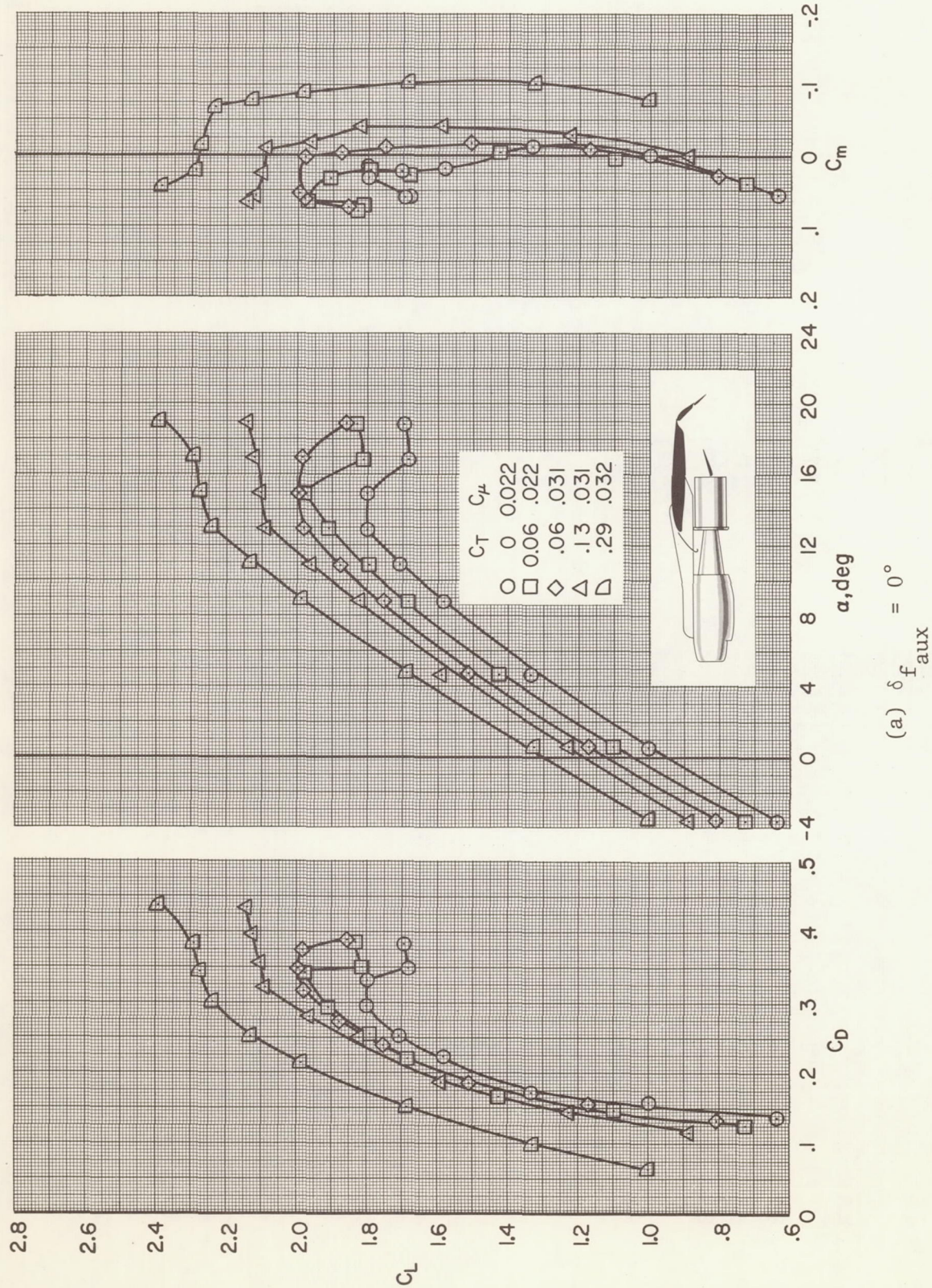
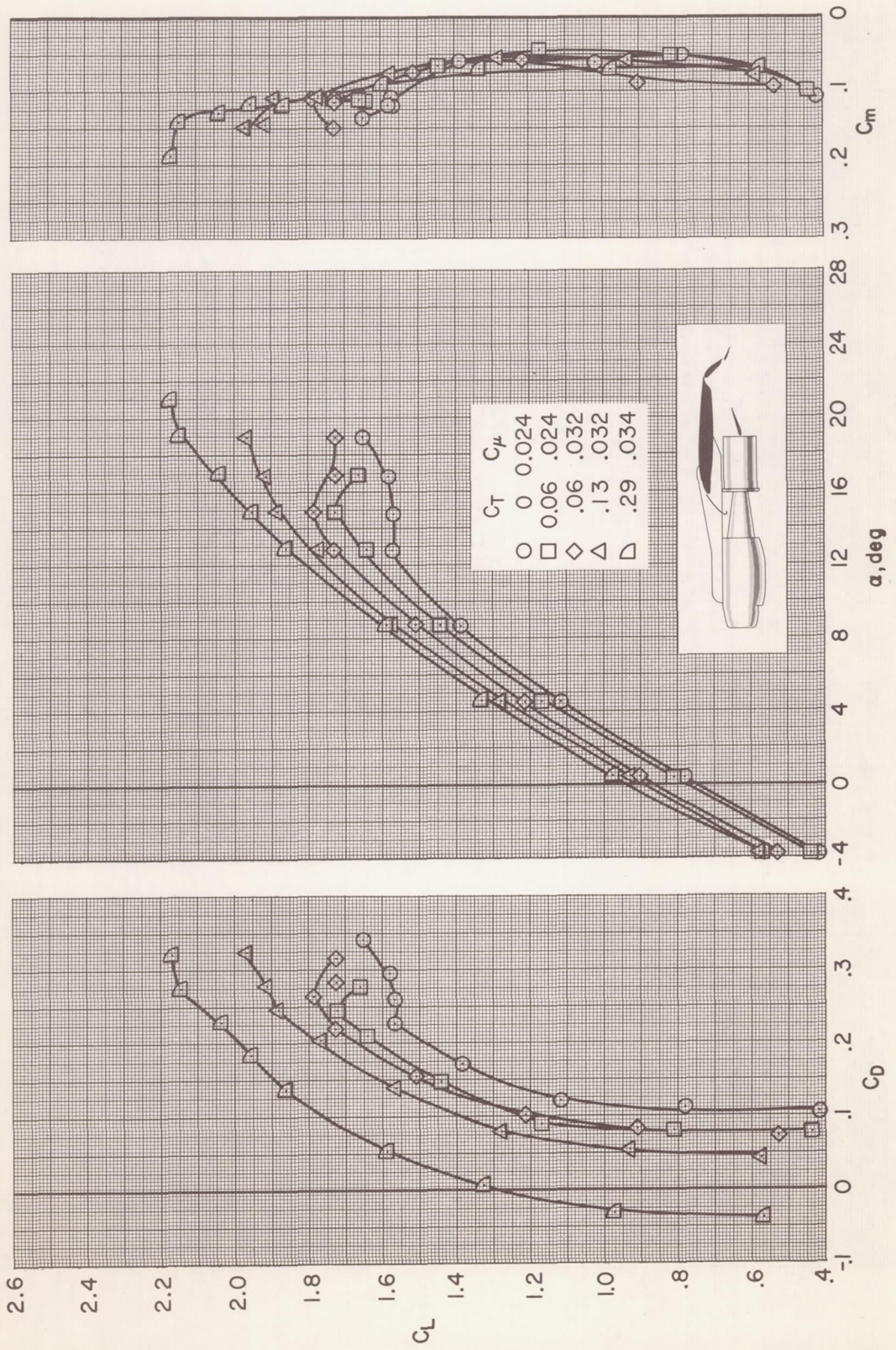
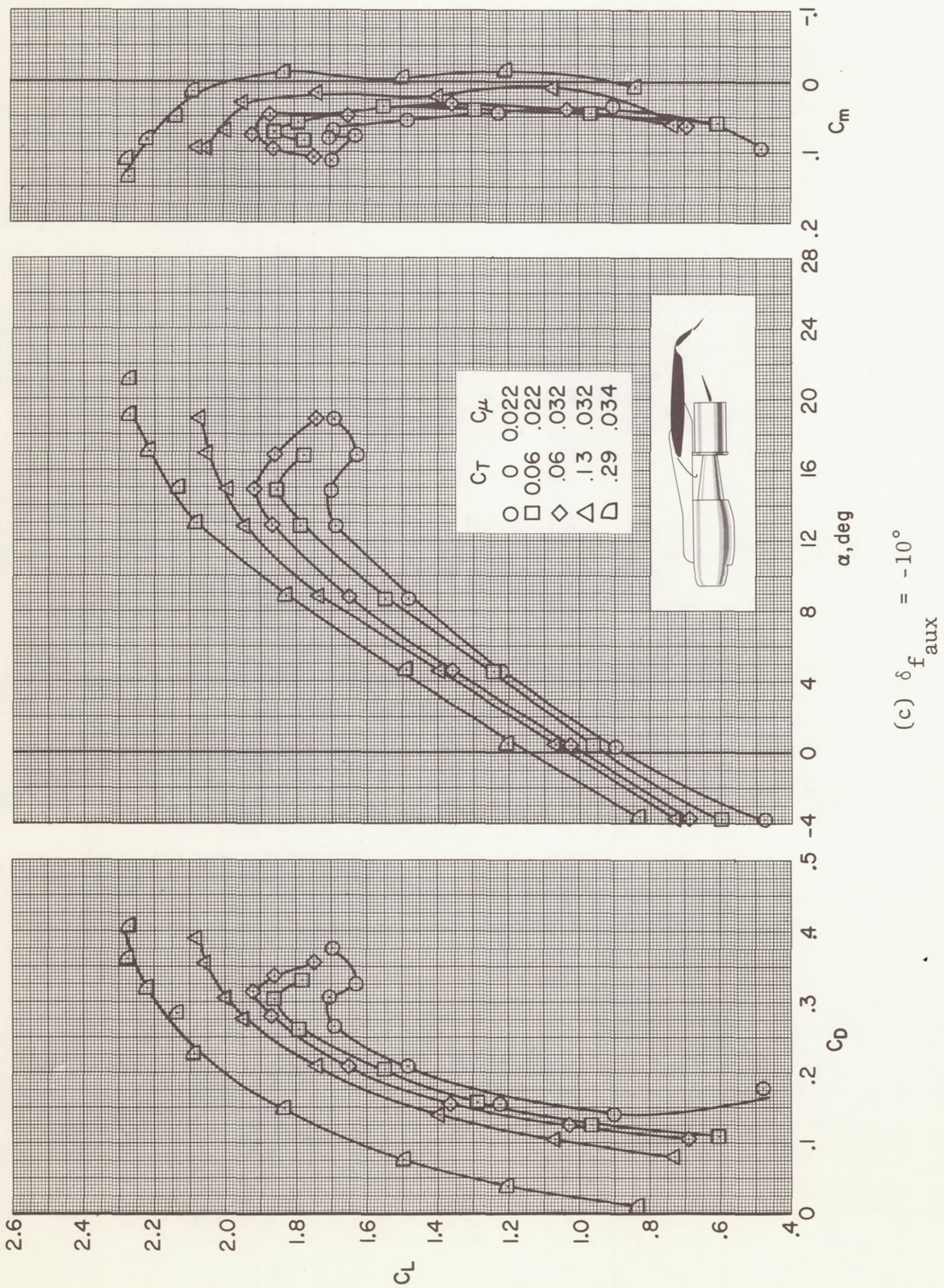


Figure 7.- Longitudinal characteristics of the model with main flap deflected 50°; BLC flap arrangement A with extended chord auxiliary flap, $\delta_d = 15^\circ$, $\delta_s = 35^\circ$, $i_t = -5^\circ$, $\delta_e = 0^\circ$.



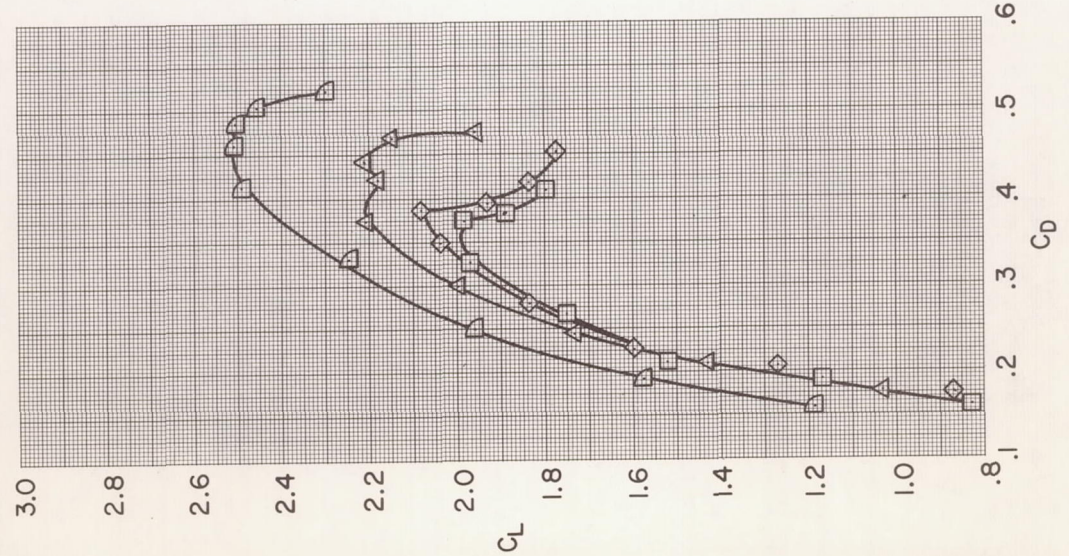
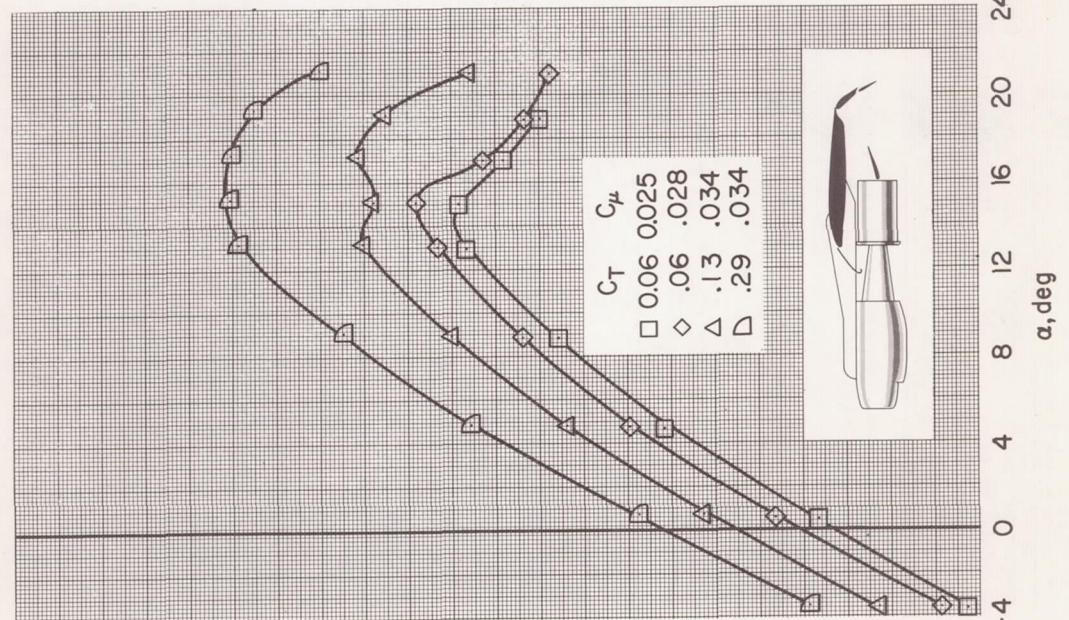
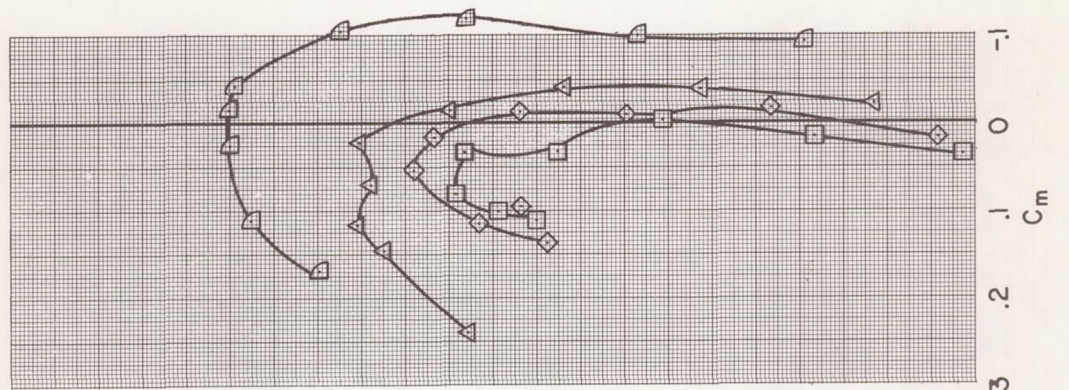
(b) δ_f aux = -25°

Figure 7.- Continued.



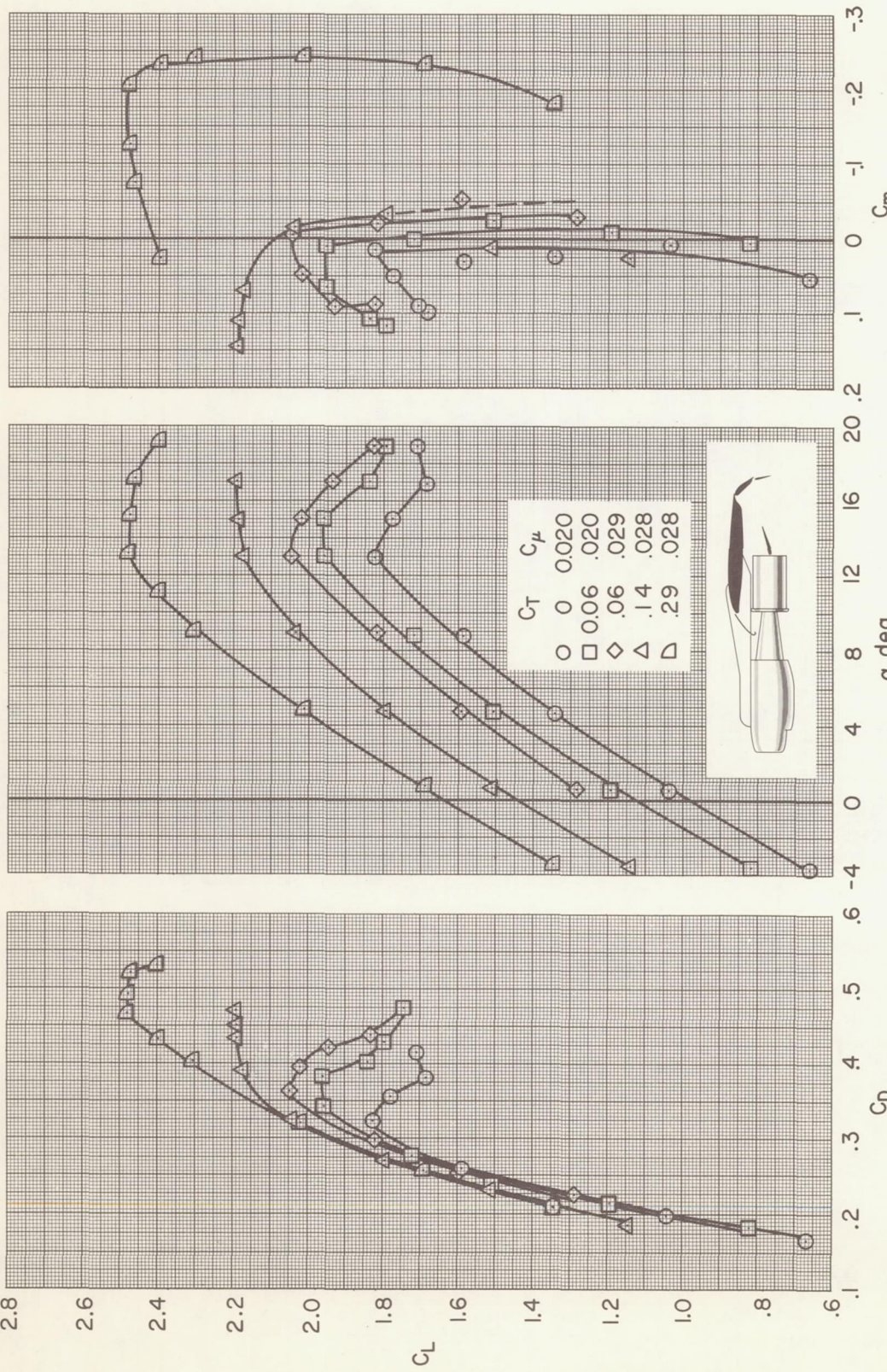
(c) δ_f _{aux} = -10°

Figure 7.- Continued.



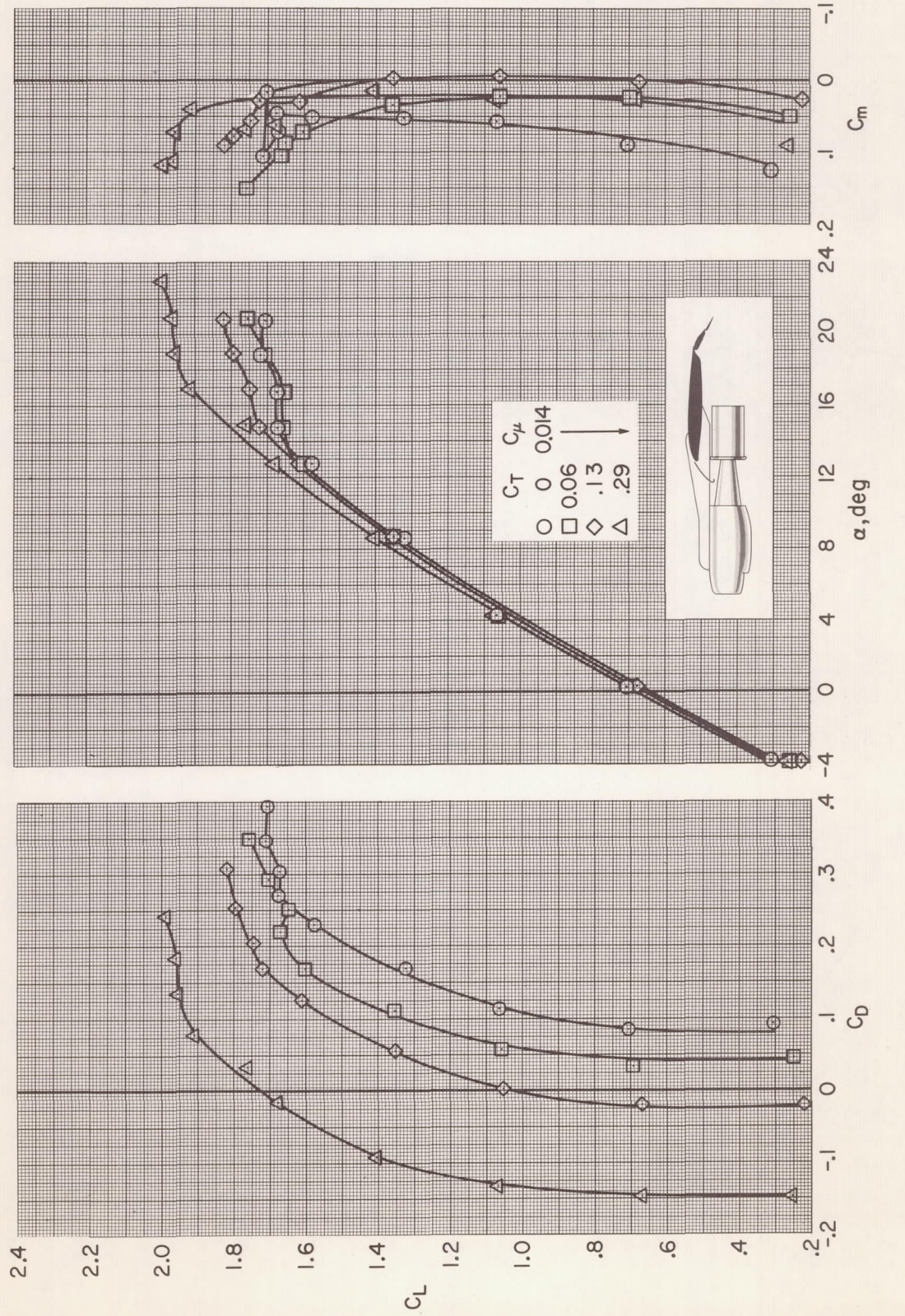
(d) $\delta_f_{aux} = 15^\circ$

Figure 7.- Continued.



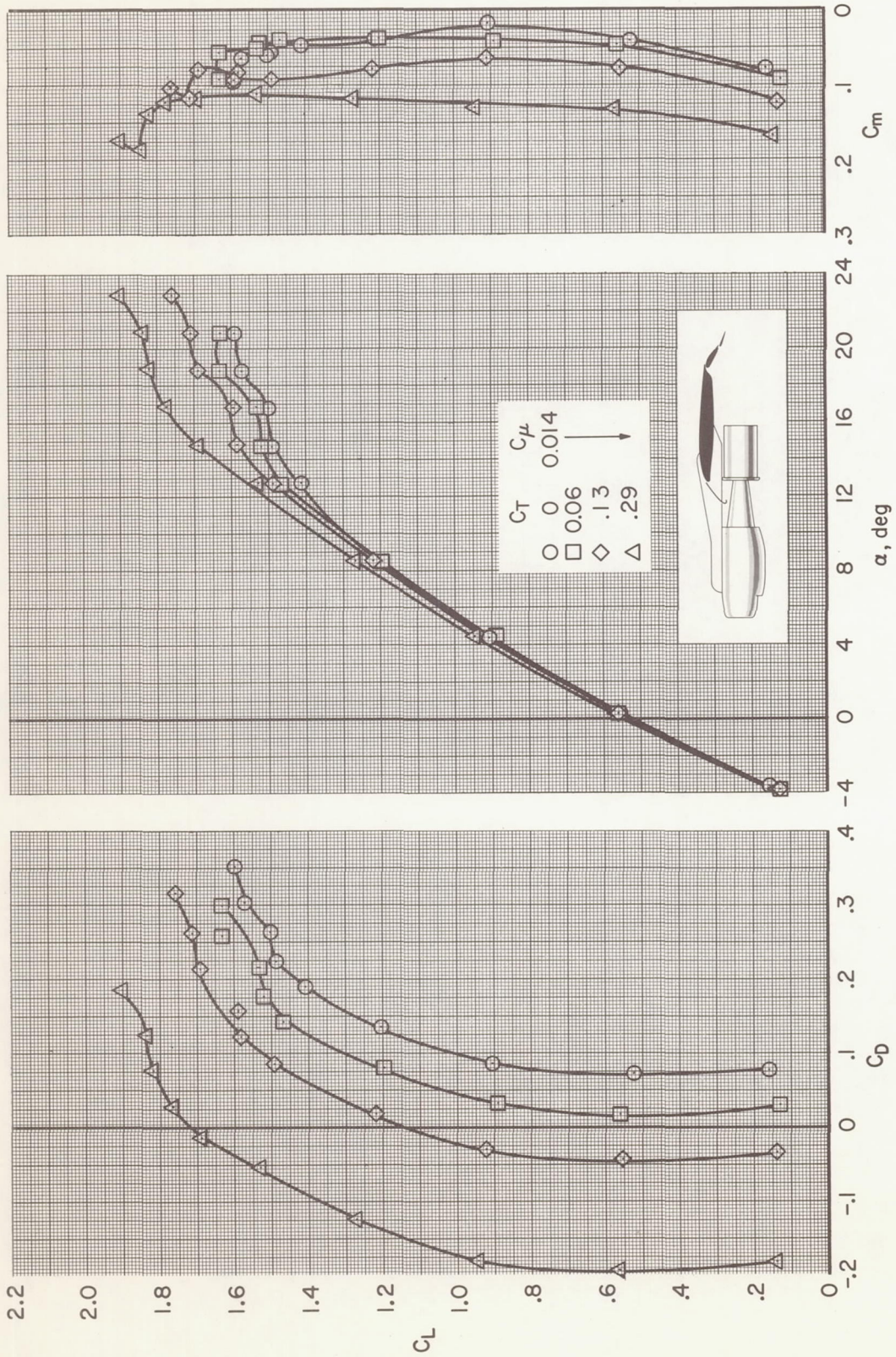
(e) $\delta_f_{aux} = 30^\circ$

Figure 7.- Concluded.



(a) $\delta_{f_{\text{aux}}} = 0^\circ$

Figure 8.- Longitudinal characteristics of the model with jet exhaust deflector off; BLC flap arrangement A with extended chord auxiliary flap, $\delta_f = 30^\circ$, $\delta_s = 35^\circ$, $\delta_t = -5^\circ$, $\delta_e = 0^\circ$.



(b) δ_f _{aux} = -10°

Figure 8.- Continued.

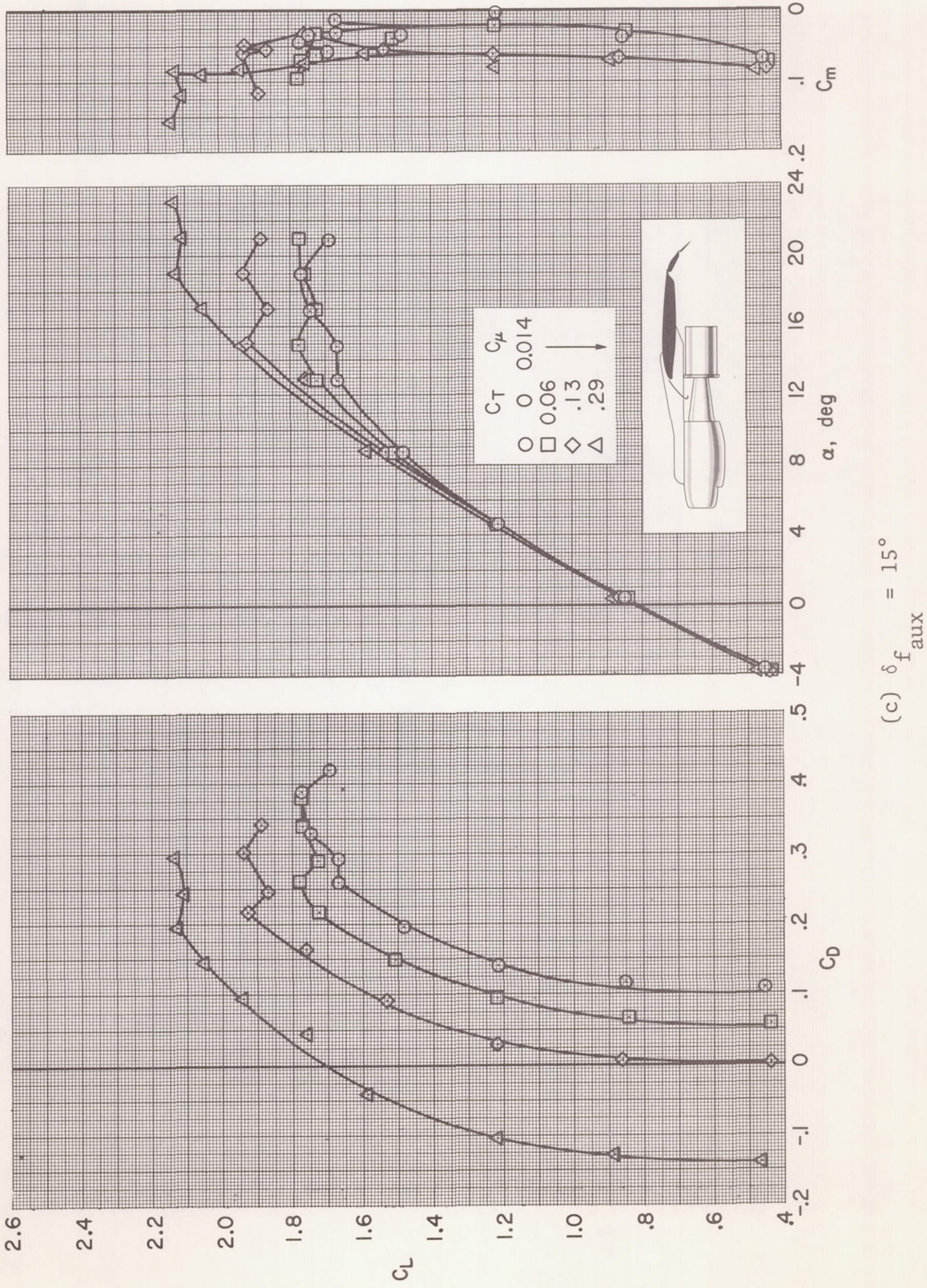


Figure 8.- Continued.
(c) δ_f aux = 15°

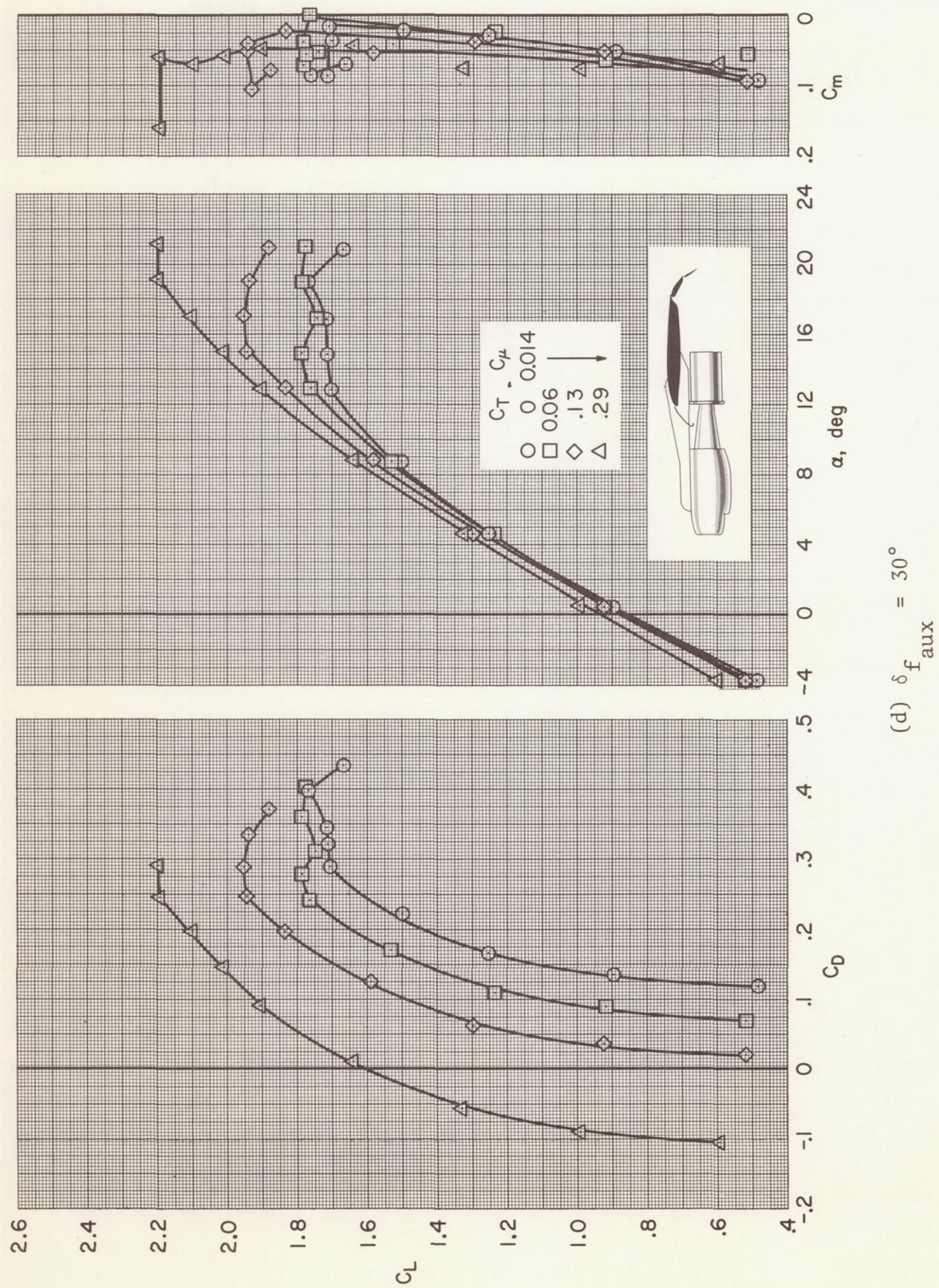
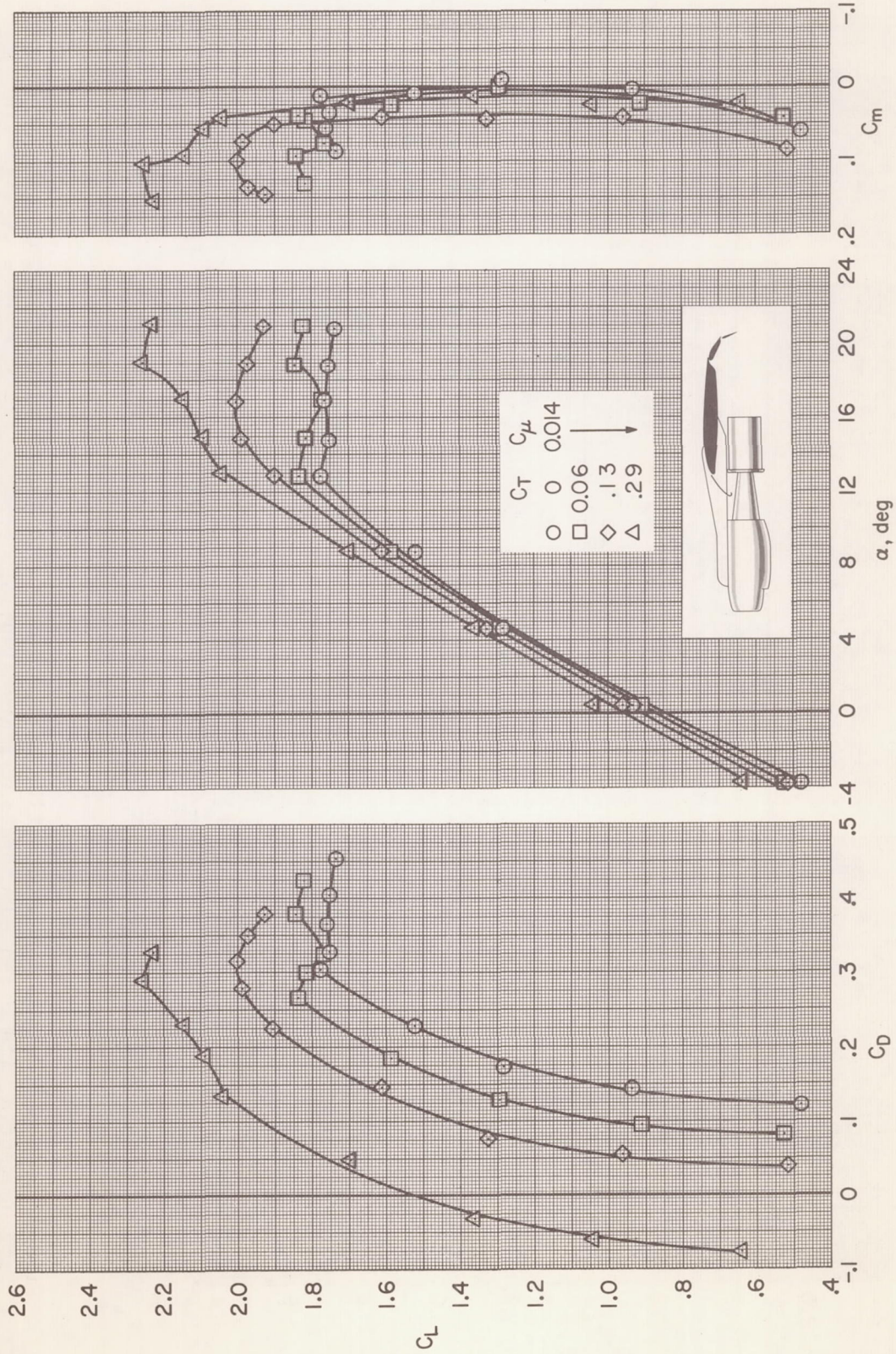


Figure 8.- Continued.



(e) $\delta f_{aux} = 40^\circ$

Figure 8.- Concluded.

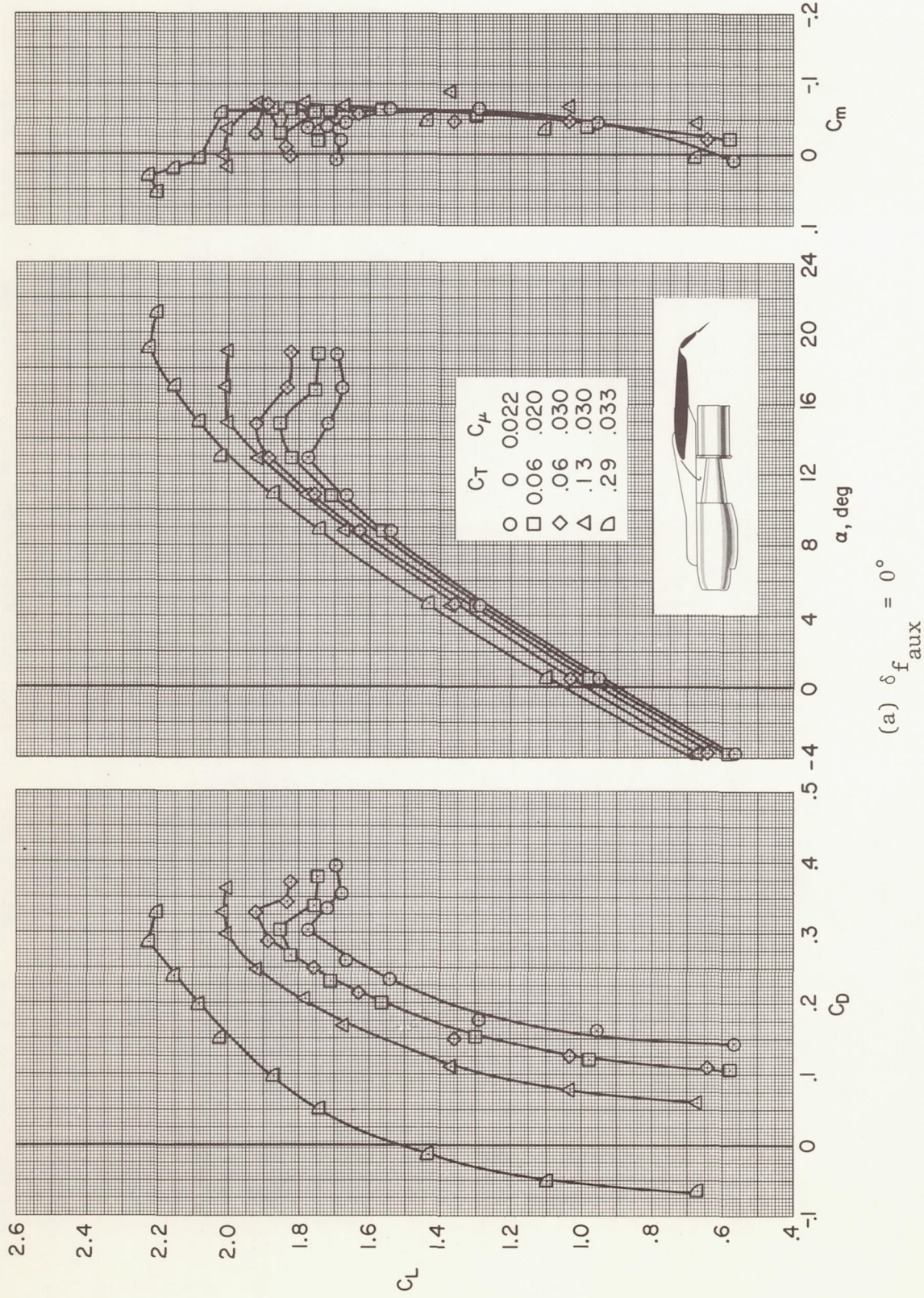
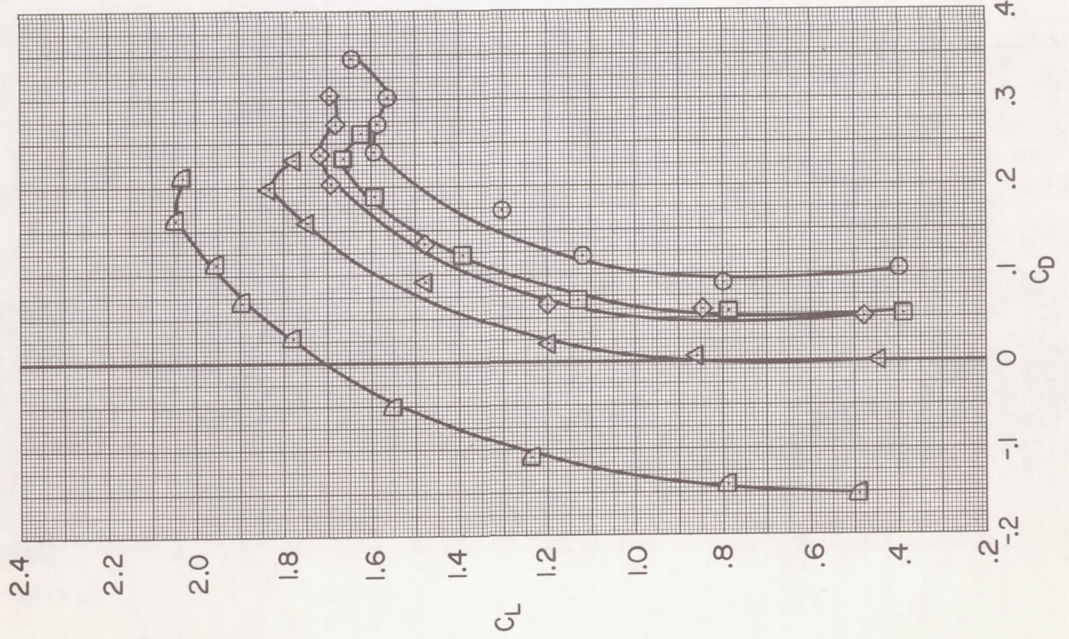
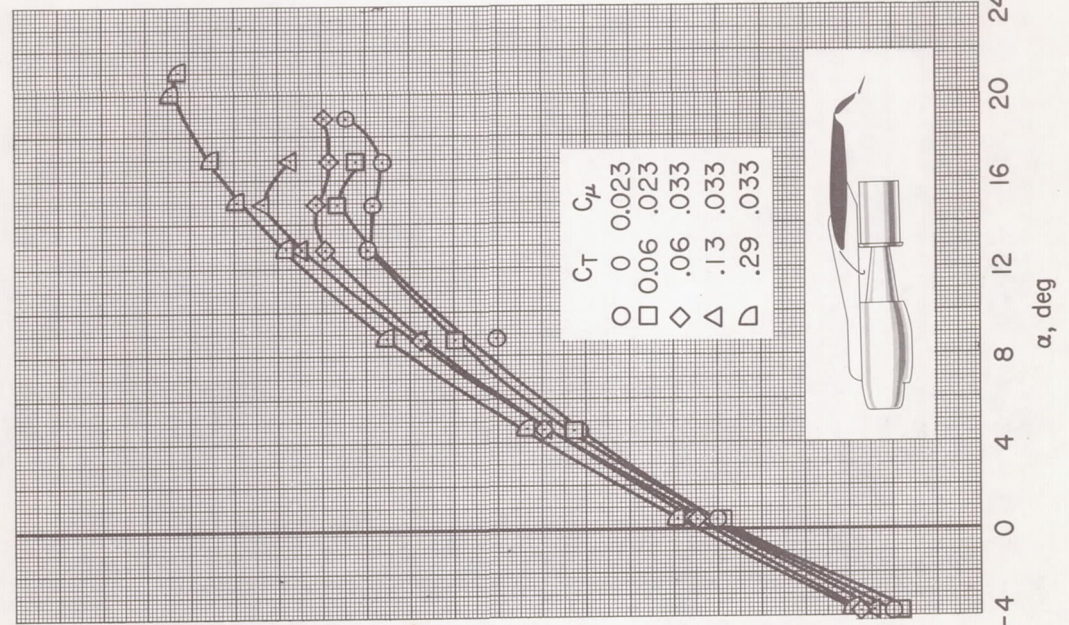
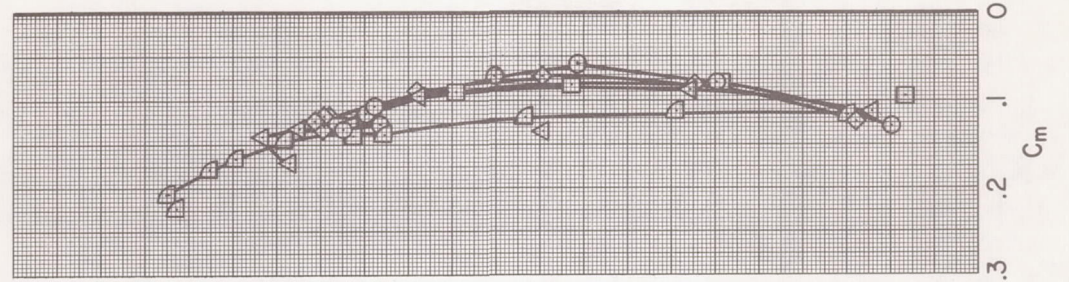


Figure 9.- Longitudinal characteristics of the model with jet exhaust deflector off; BLC flap arrangement A with extended chord auxiliary flap, $\delta_f = 50^\circ$, $\delta_s = 50^\circ$, $\delta_t = 35^\circ$, $i_t = -5^\circ$, $\delta_e = 0^\circ$.



(b) δ_f aux = -25°

Figure 9.- Continued.

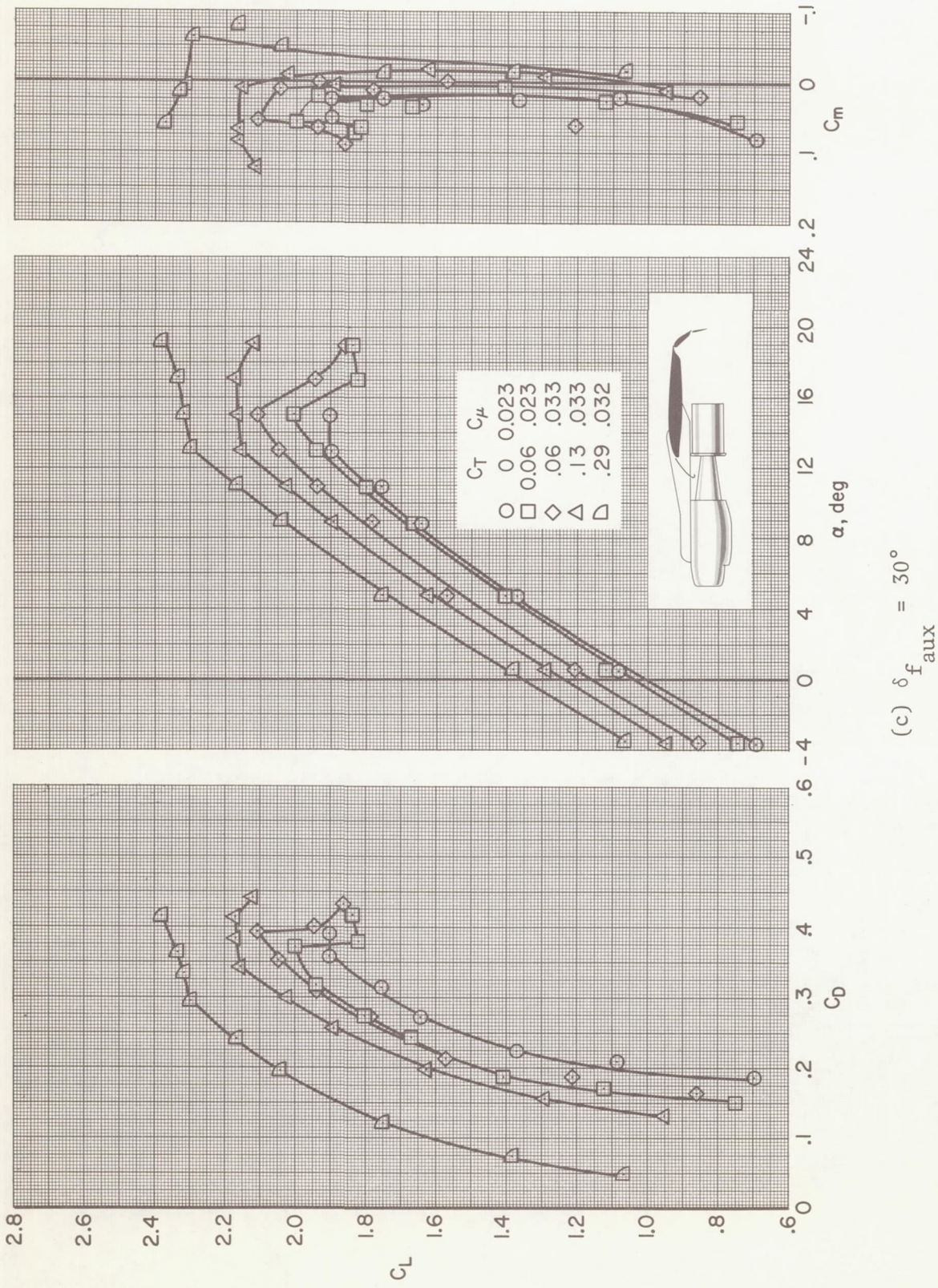


Figure 9.- Concluded.
(c) δ_f aux = 30°

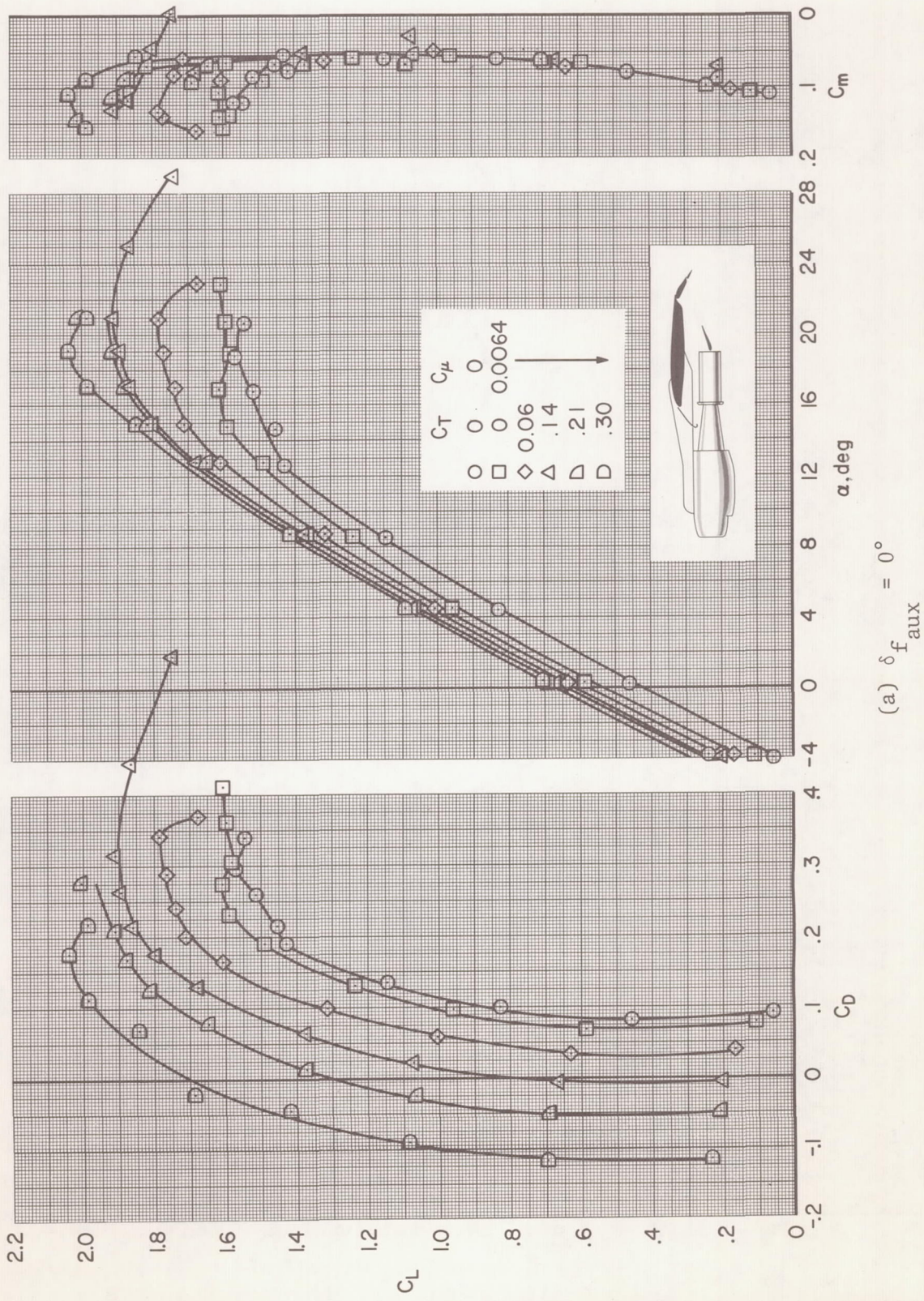
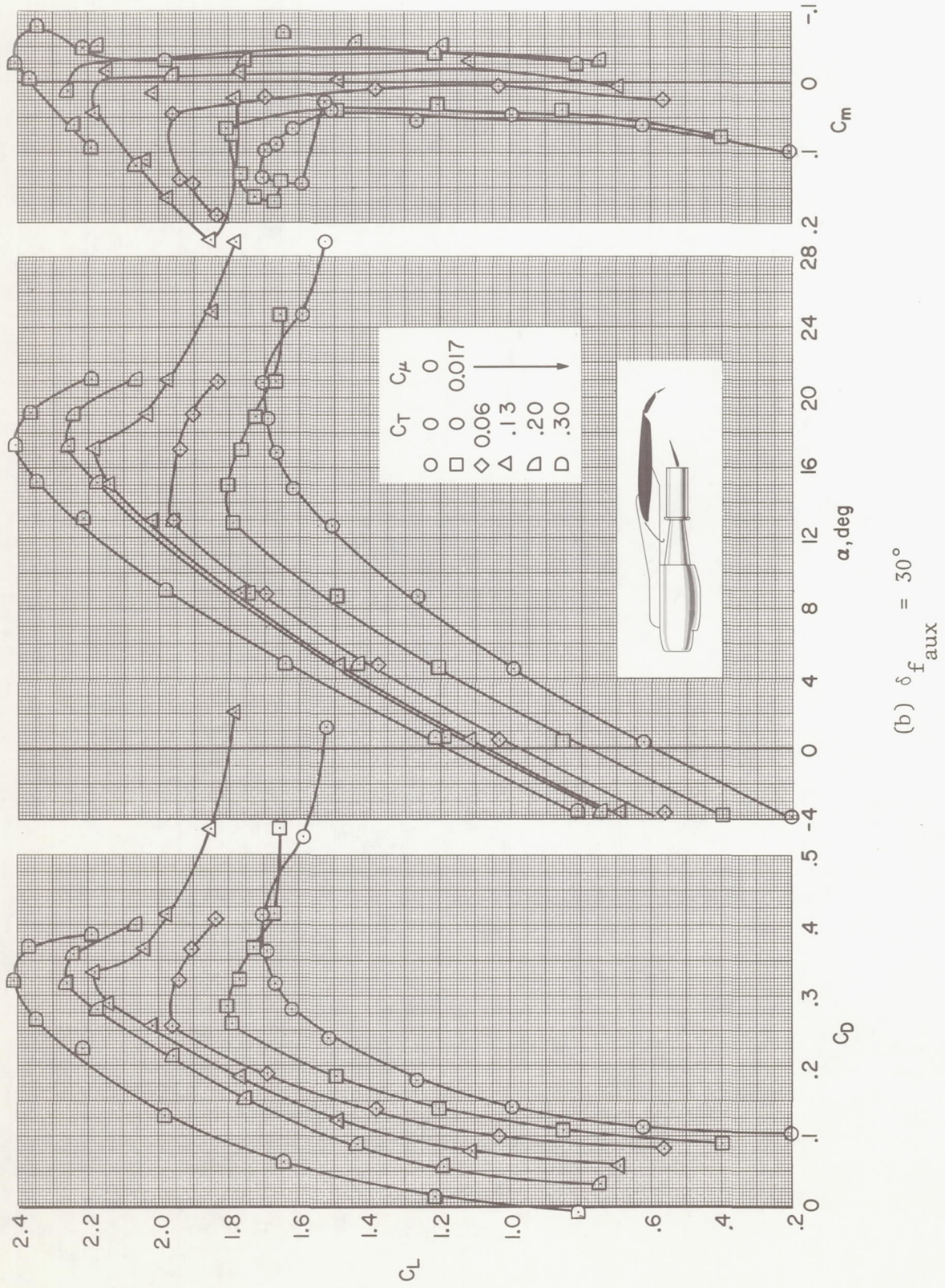
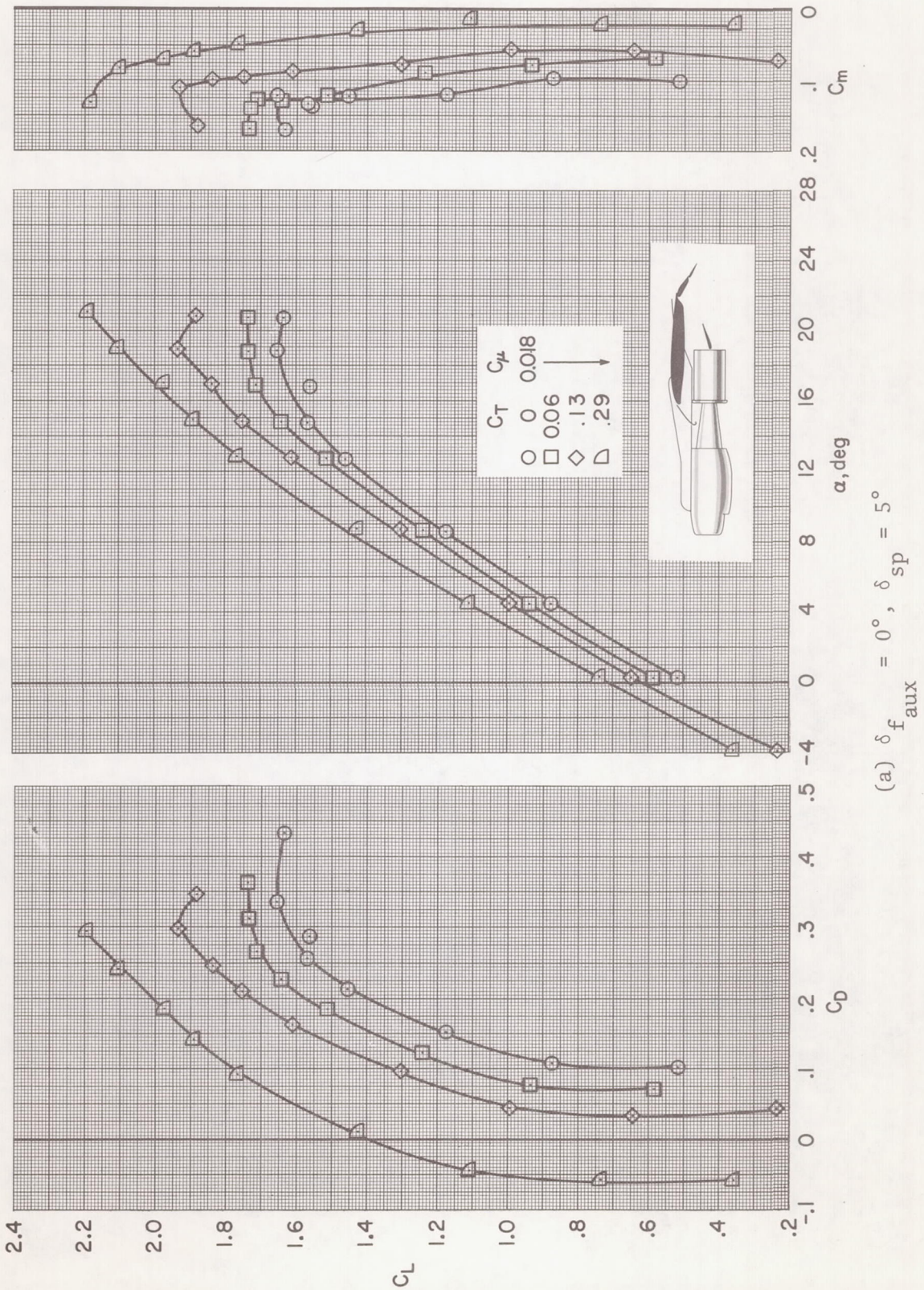


Figure 10.- Longitudinal characteristics of the model with main flap deflected 30°; BLC flap arrangement A with normal chord auxiliary flap, $\delta_d = 15^\circ$, $\delta_s = 15^\circ$, $\delta_t = -5^\circ$, $\delta_e = 0^\circ$.



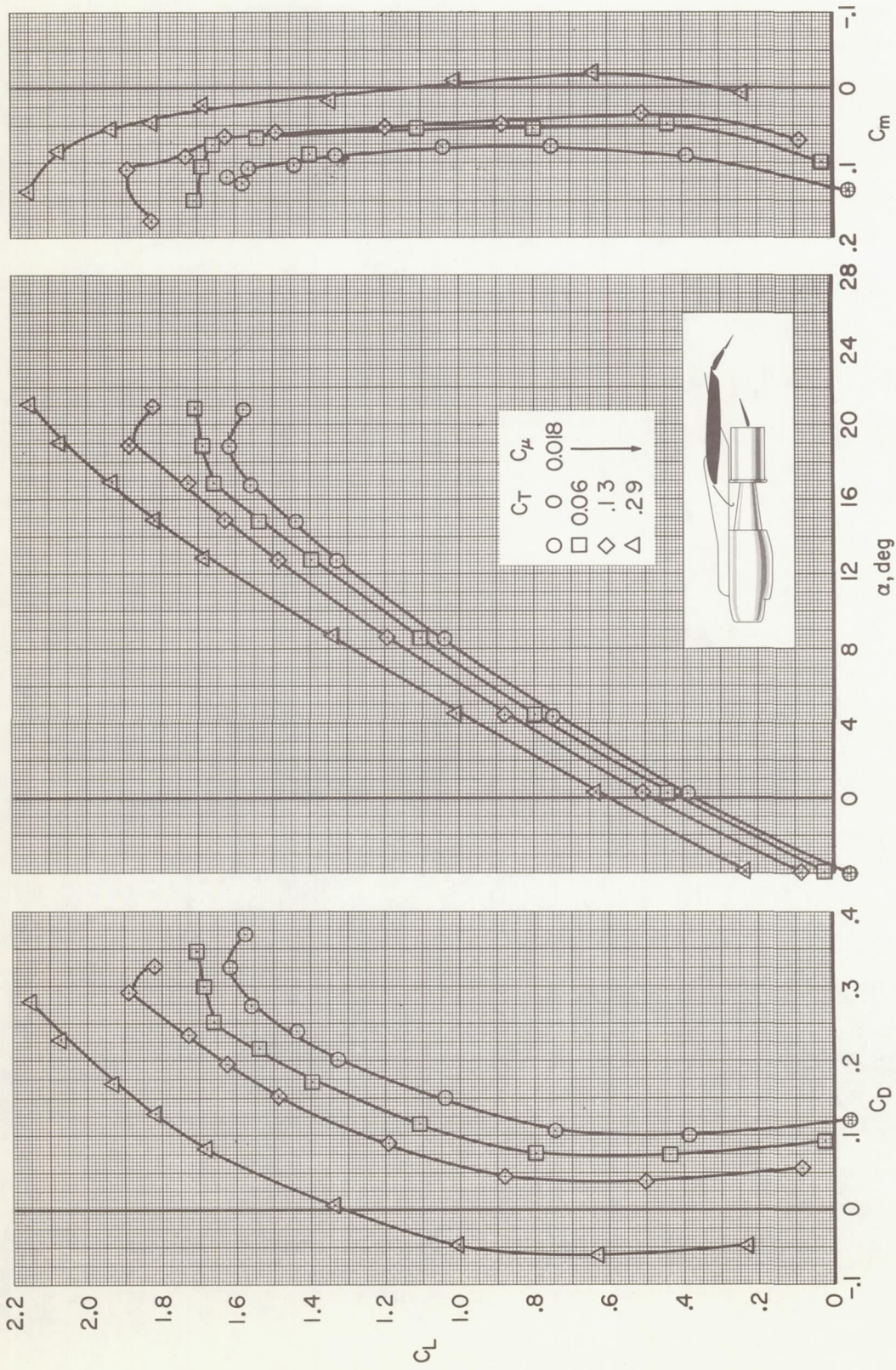
(b) $\delta_{f_{aux}} = 30^\circ$

Figure 10.- Concluded.



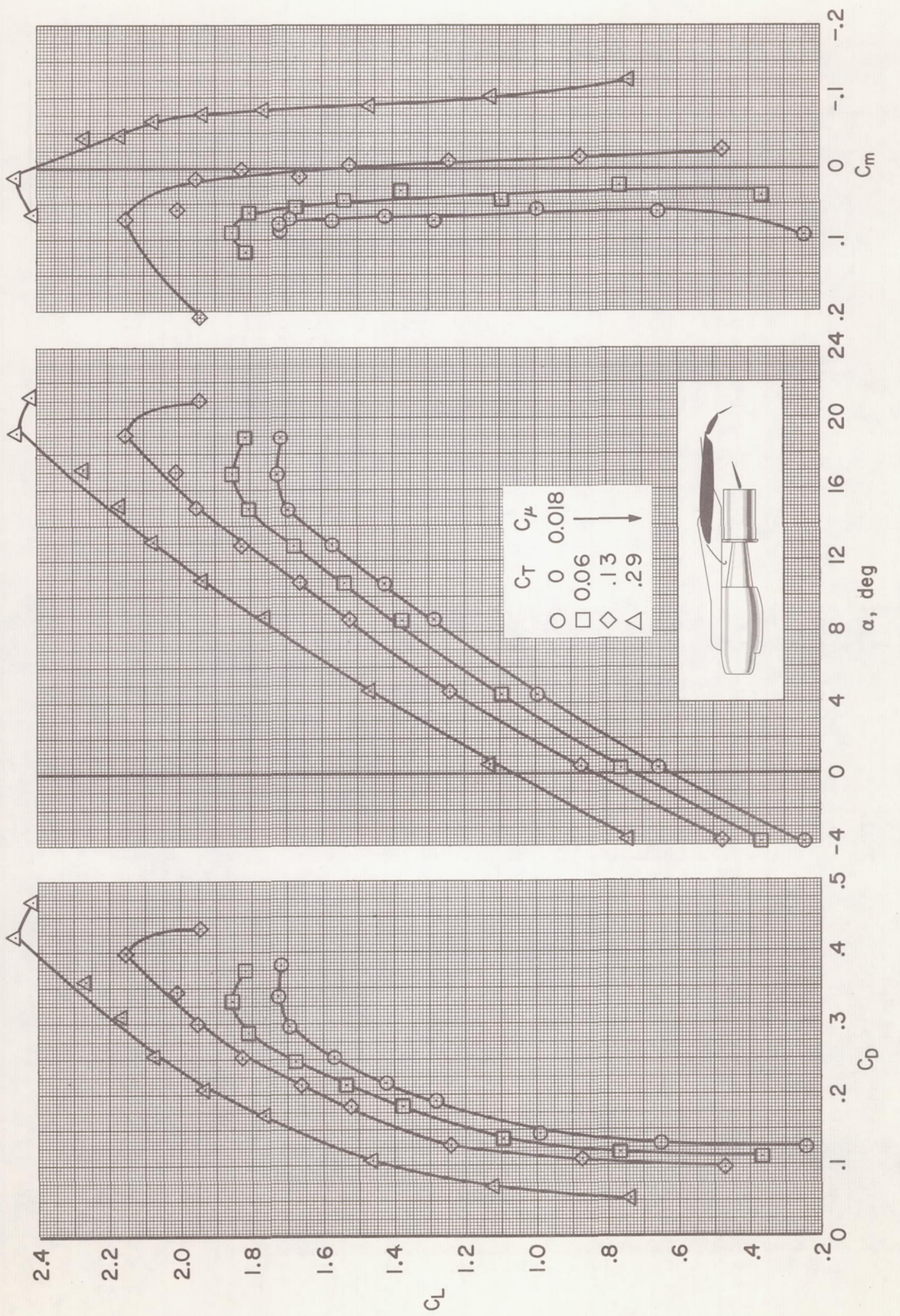
(a) $\delta_{f_{aux}} = 0^\circ, \delta_{sp} = 5^\circ$

Figure 11.- Effect of symmetrically deflected spoilers on the longitudinal characteristics of the model; BLC flap arrangement A with extended chord auxiliary flap, $\delta_f = 30^\circ, \delta_d = 15^\circ, i_t = -5^\circ, \delta_e = 0^\circ$.



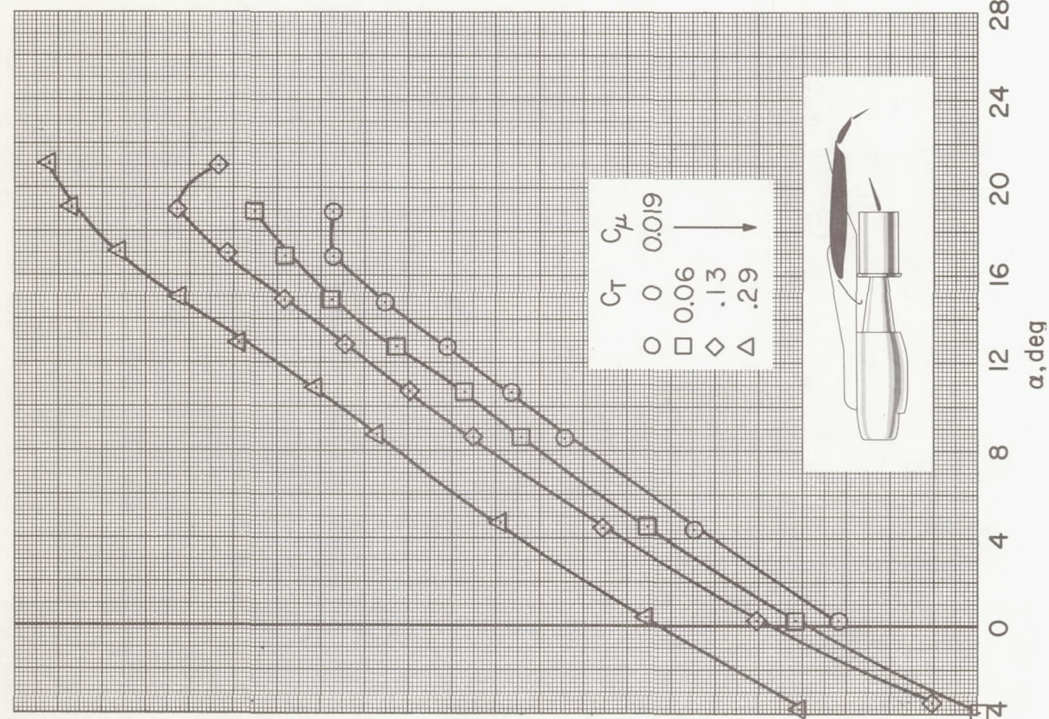
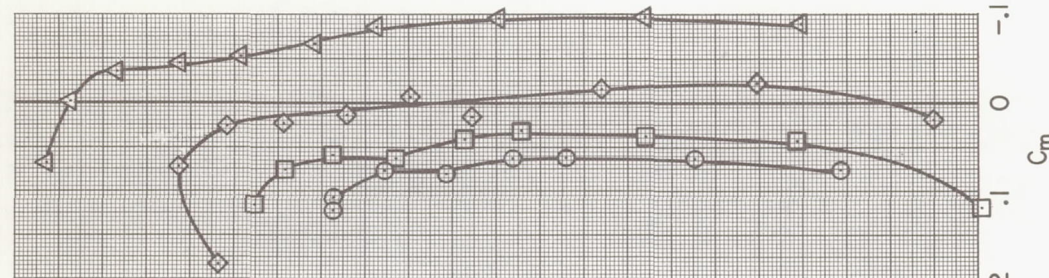
(b) $\delta_{f_{aux}} = 0^\circ$, $\delta_{sp} = 10^\circ$

Figure 11.- Continued.



(c) $\delta_f_{aux} = 30^\circ$, $\delta_{sp} = 5^\circ$

Figure 11.- Continued.



(d) $\delta_{f_{aux}} = 30^\circ$, $\delta_{sp} = 10^\circ$

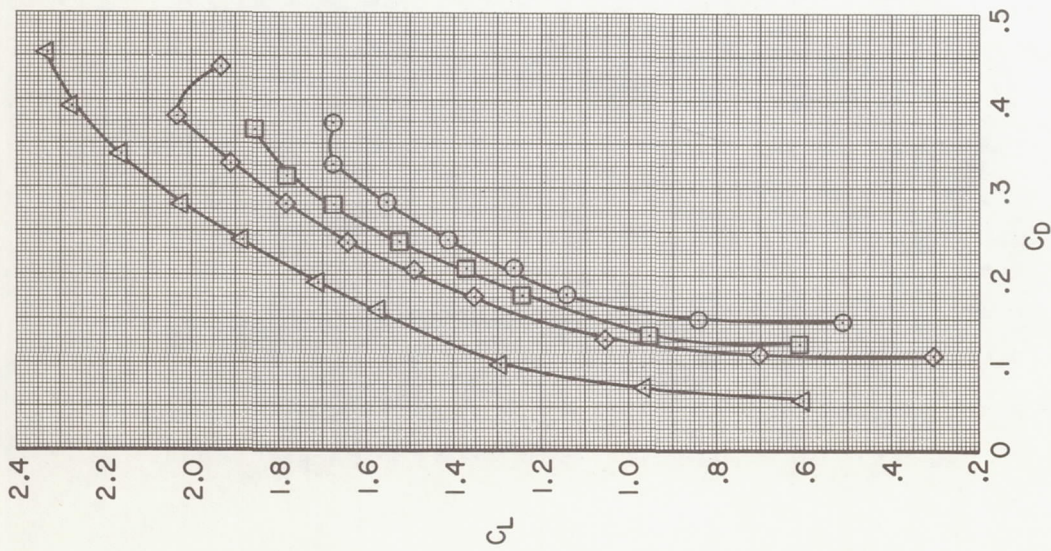
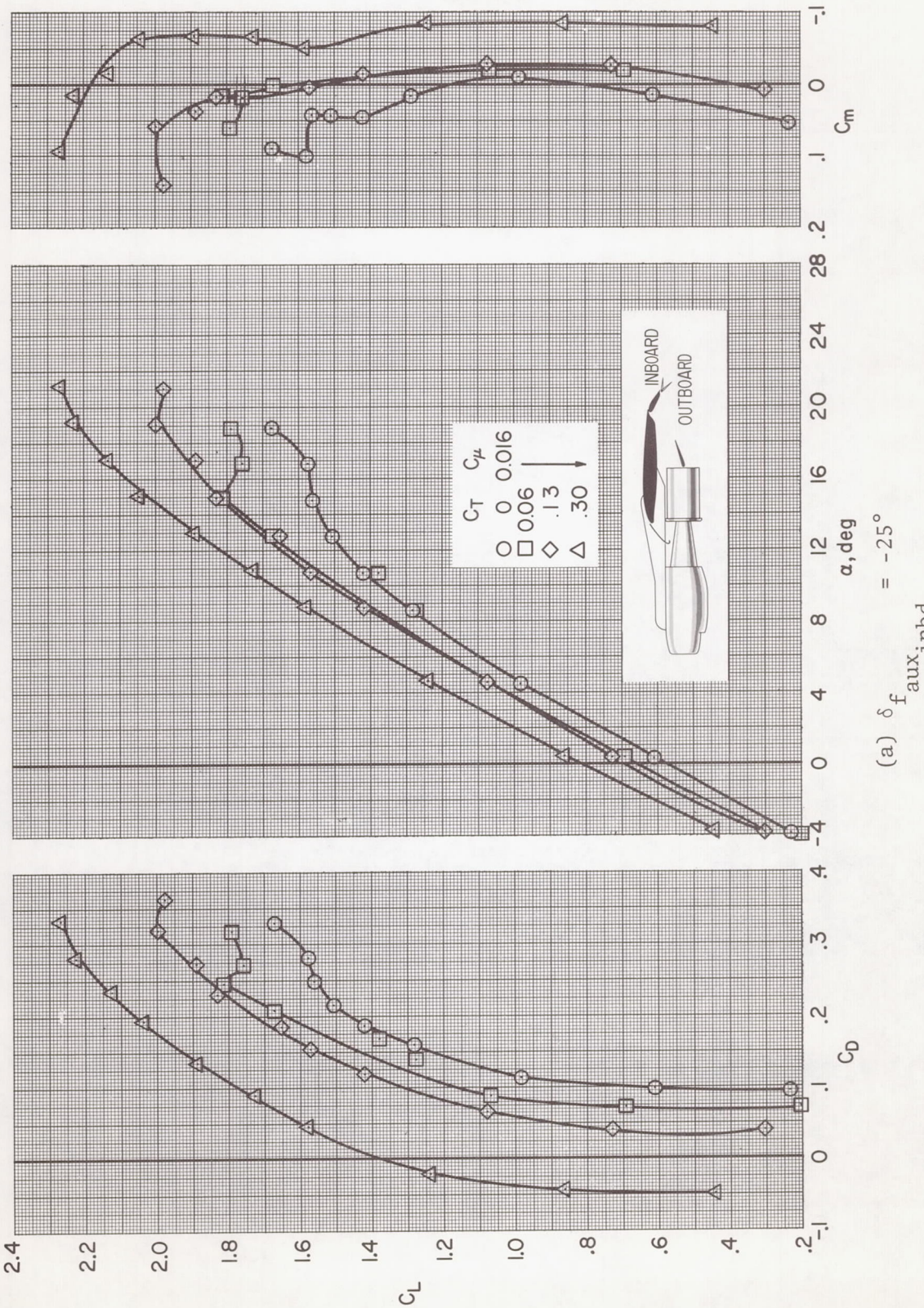
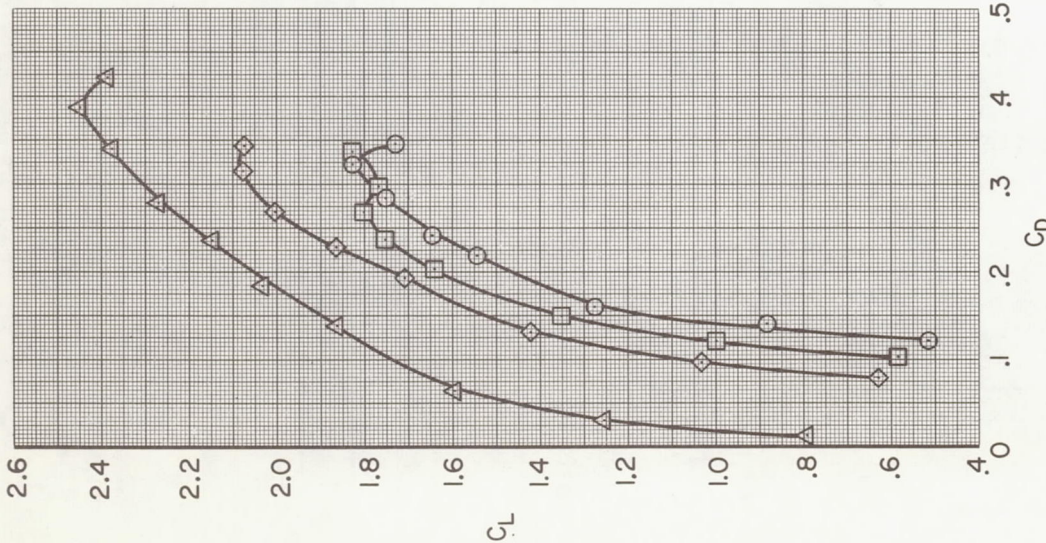
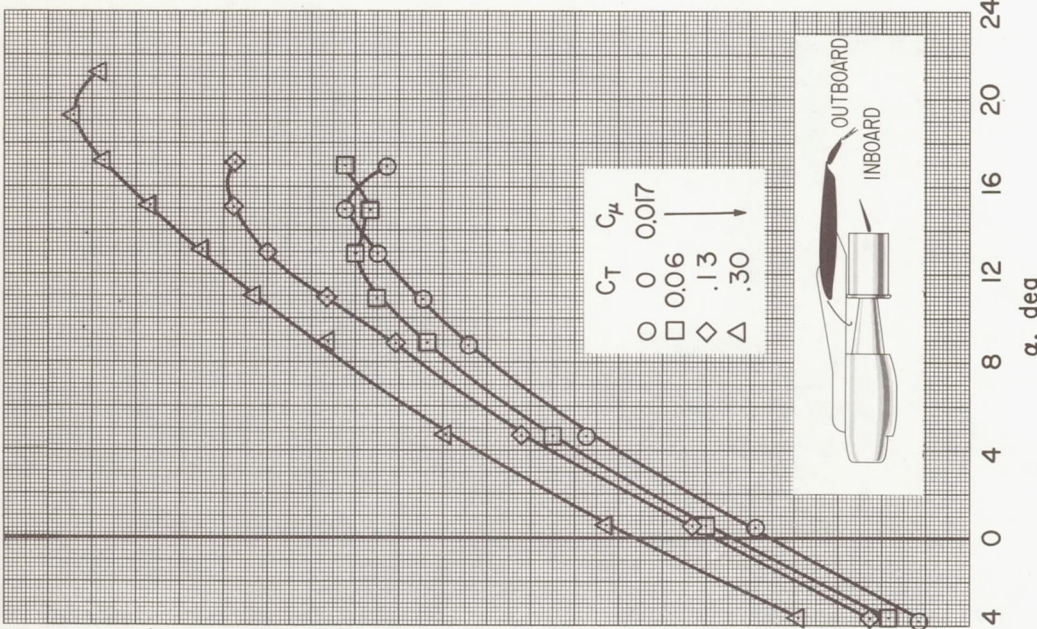
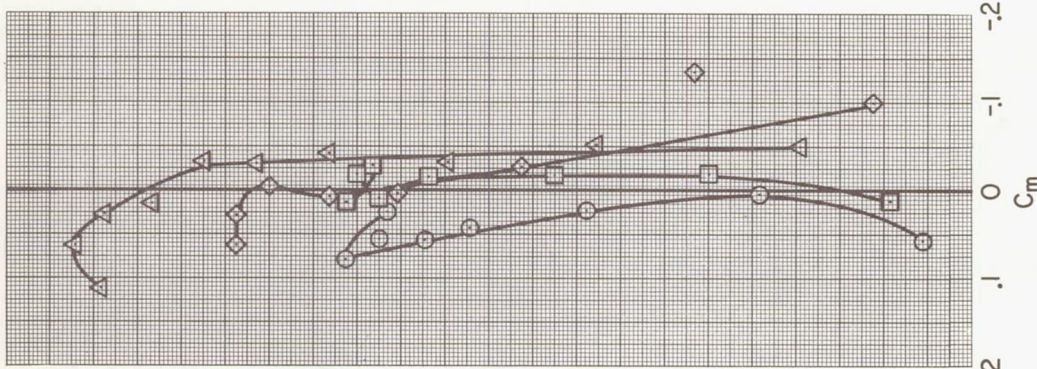


Figure 11.- Concluded.



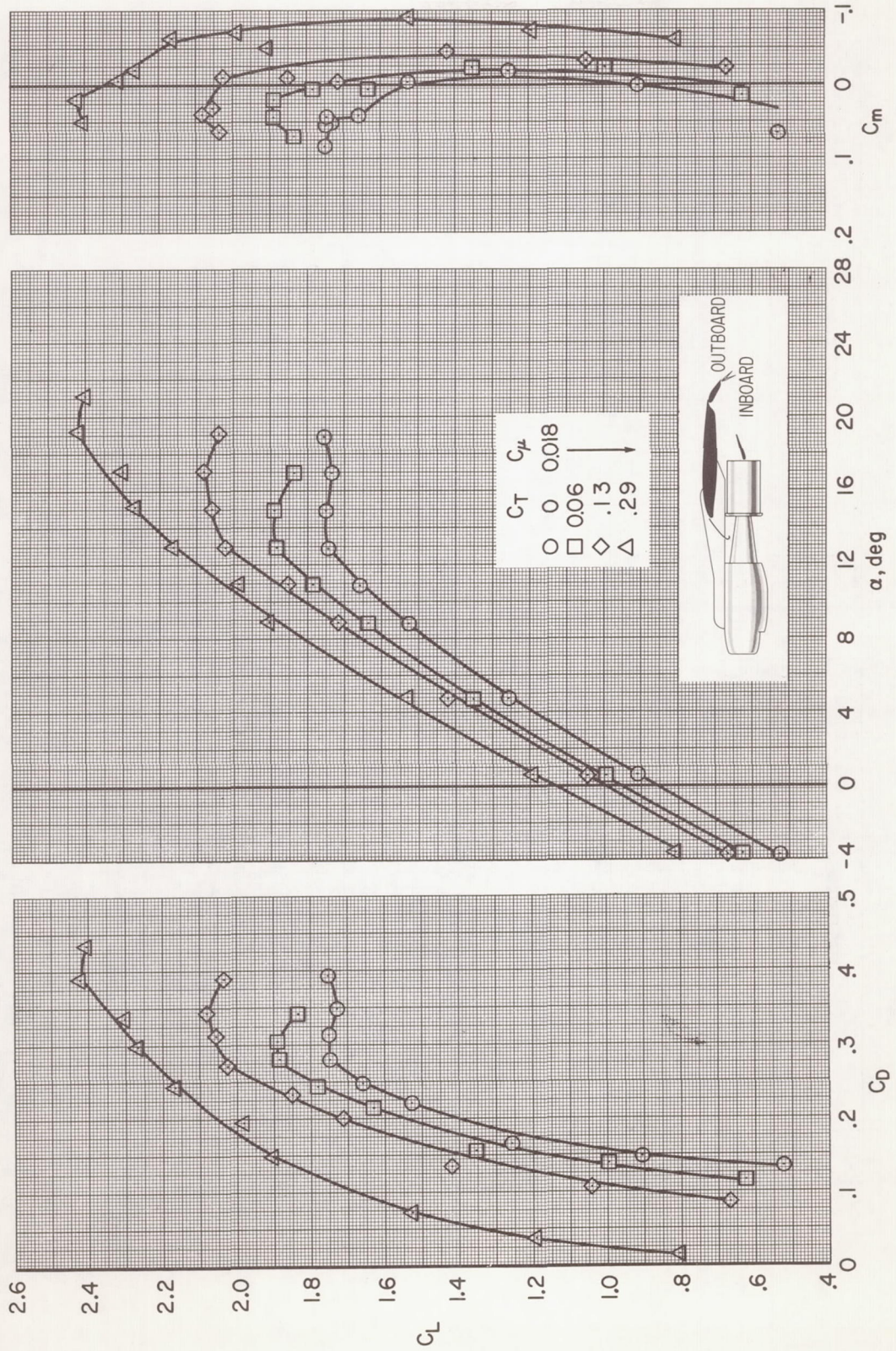
(a) δ_f aux_{inbd} = -25°

Figure 12.- Effect of symmetrical differential auxiliary flap deflection on the longitudinal characteristics of the model; BLC flap arrangement A with extended chord auxiliary flap, $\delta_f = 30^\circ$, $\delta_d = 15^\circ$, $\delta_s = 15^\circ$, $\delta_t = -5^\circ$, $\delta_e = 0^\circ$.



$$(b) \quad \delta_f^{\text{aux,inbd}} = 30^\circ$$

Figure 12.- Continued.



$$(c) \quad \delta_f^{\text{aux,inbd}} = 40^\circ$$

Figure 12.- Concluded.

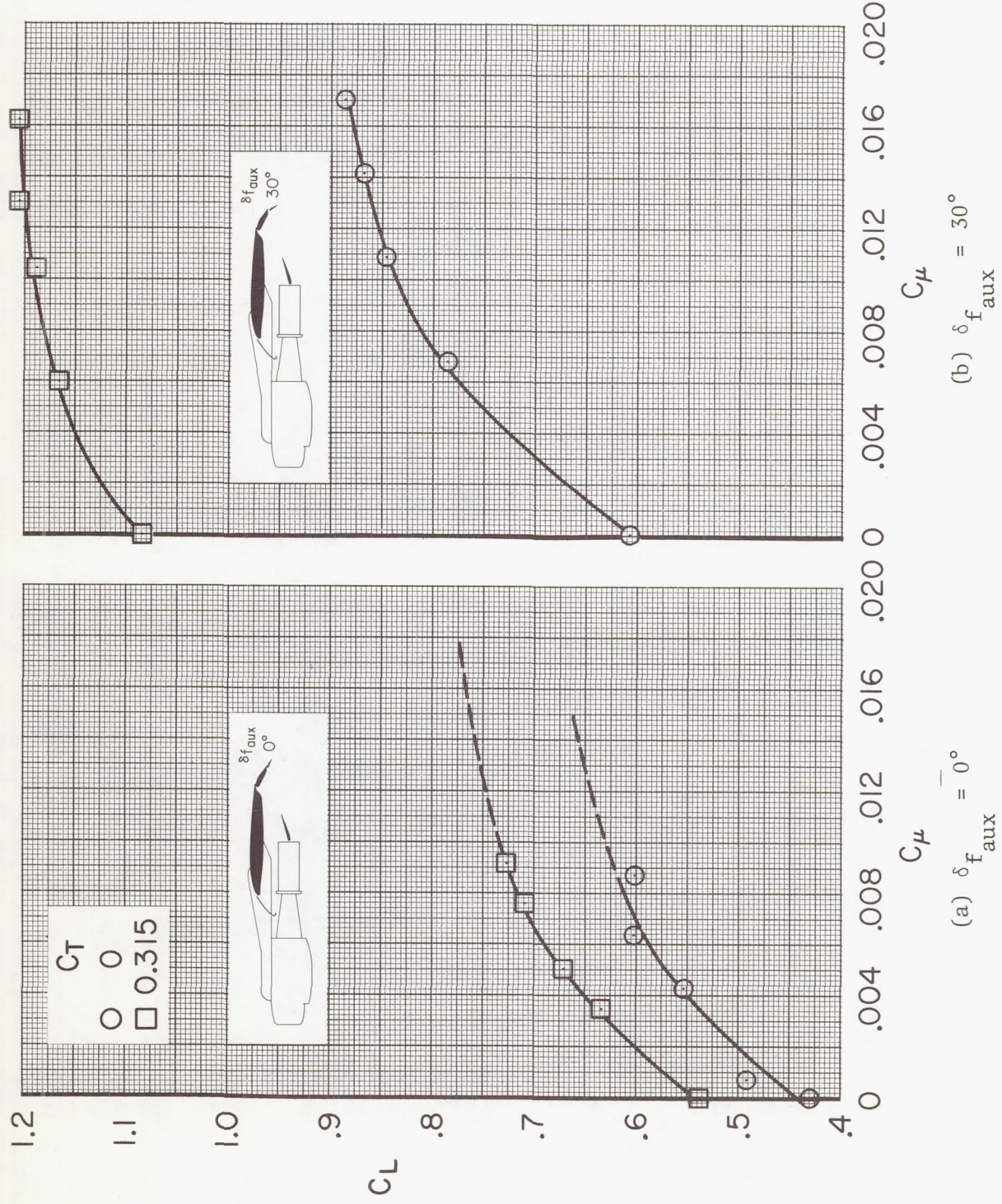


Figure 13.- Variation of lift coefficient with momentum coefficient A with normal chord auxiliary flap, $\delta_d = 15^\circ$, $\delta_s = 35^\circ$, $\alpha_u = 0^\circ$.

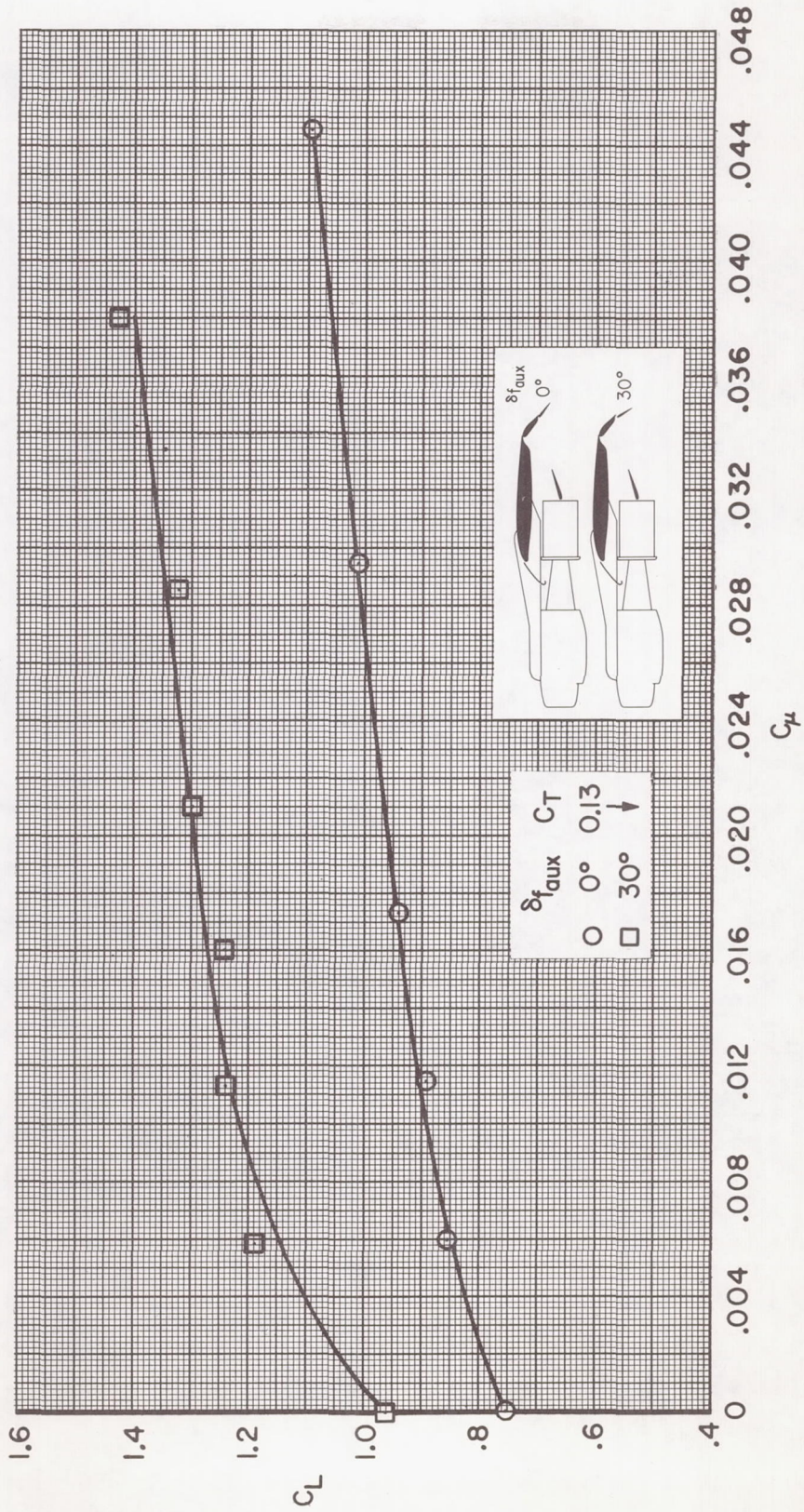
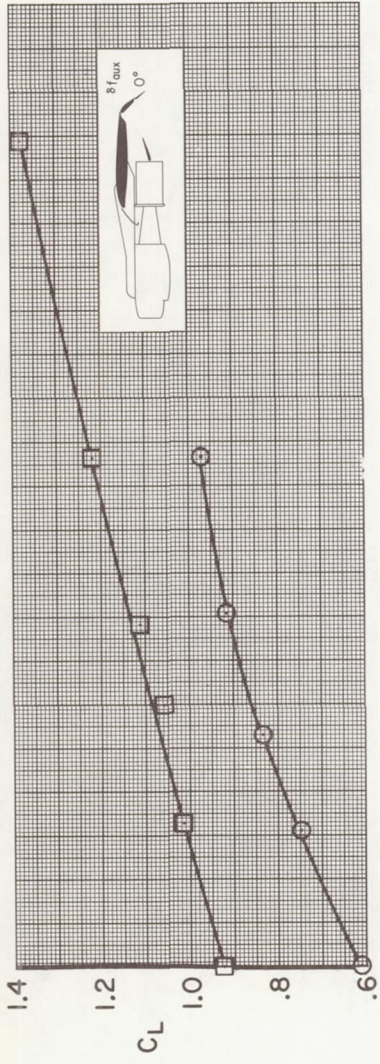
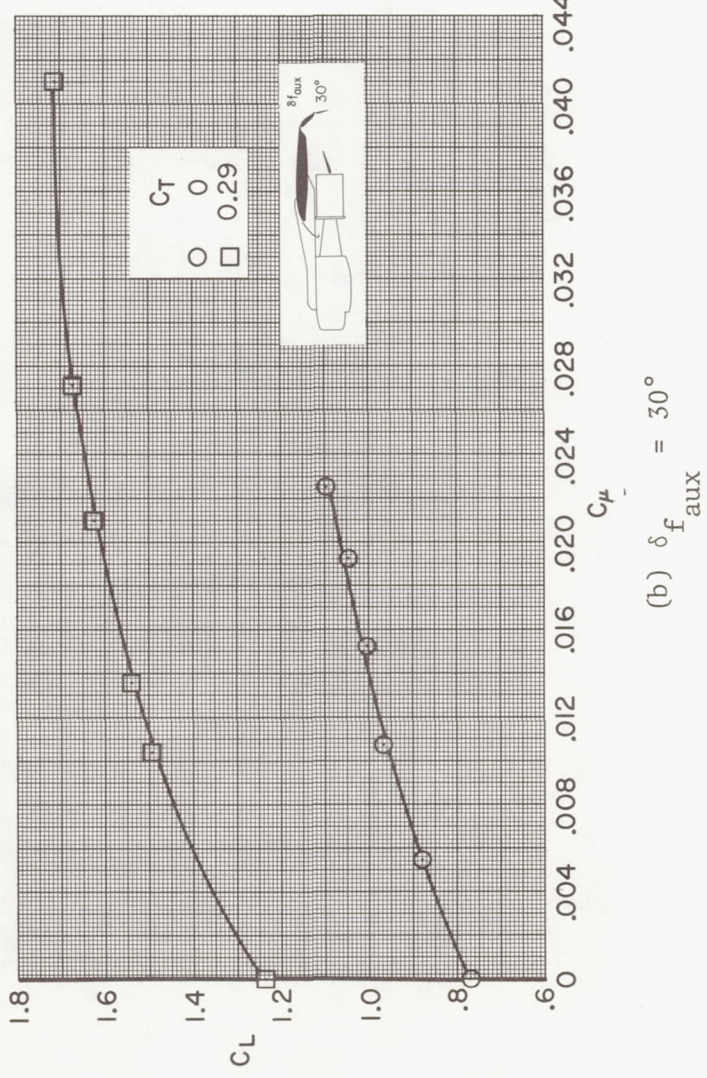


Figure 14.- Variation of lift coefficient with momentum coefficient; BLC flap arrangement A with extended chord auxiliary flap, $\delta_f = 40^\circ$, $\delta_d = 15^\circ$, $\delta_s = 35^\circ$, $\alpha_u = 0^\circ$.

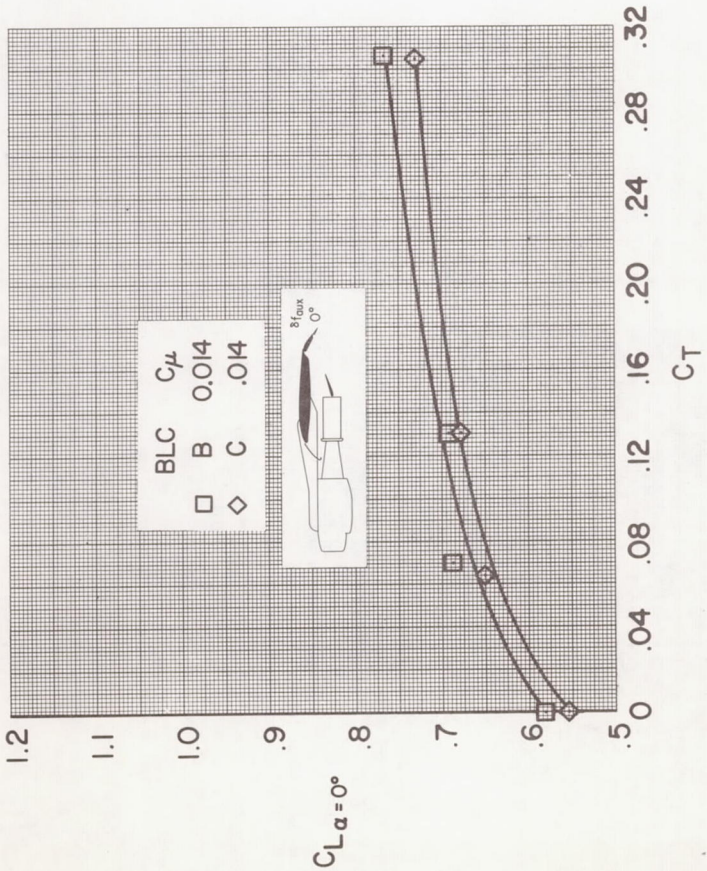


(a) $\delta_{f_{aux}} = 0^\circ$

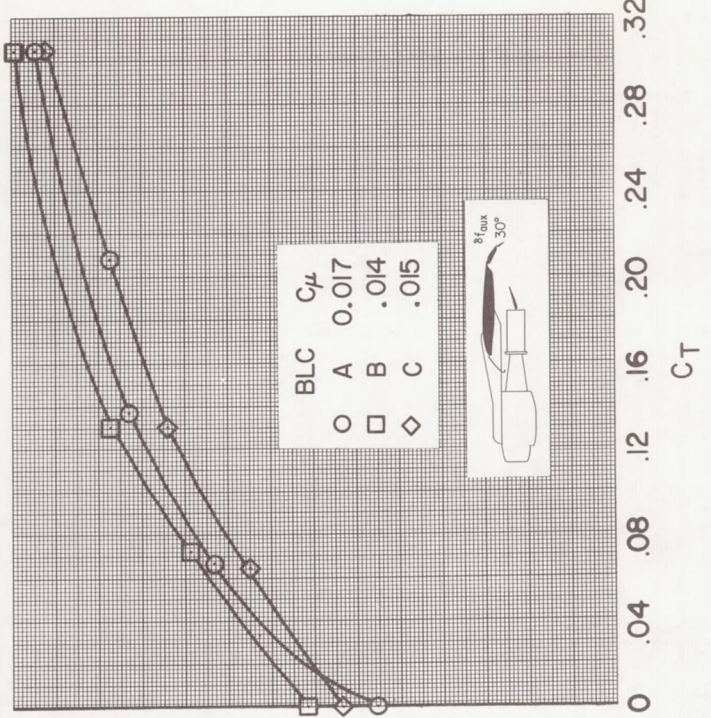


(b) $\delta_{f_{aux}} = 30^\circ$

Figure 15.- Variation of lift coefficient with momentum coefficient; BLC flap arrangement A with extended chord auxiliary flap, $\delta_{f_m} = 50^\circ$, $\delta_d = 15^\circ$, $\delta_s = 35^\circ$, $\alpha_u = 0^\circ$.



(a) $\delta_f_{aux} = 0^\circ$



(b) $\delta_f_{aux} = 30^\circ$

Figure 16.- Effect of BLC flap arrangements on lift coefficient; normal chord auxiliary flap,
 $\delta_f_m = 30^\circ$.

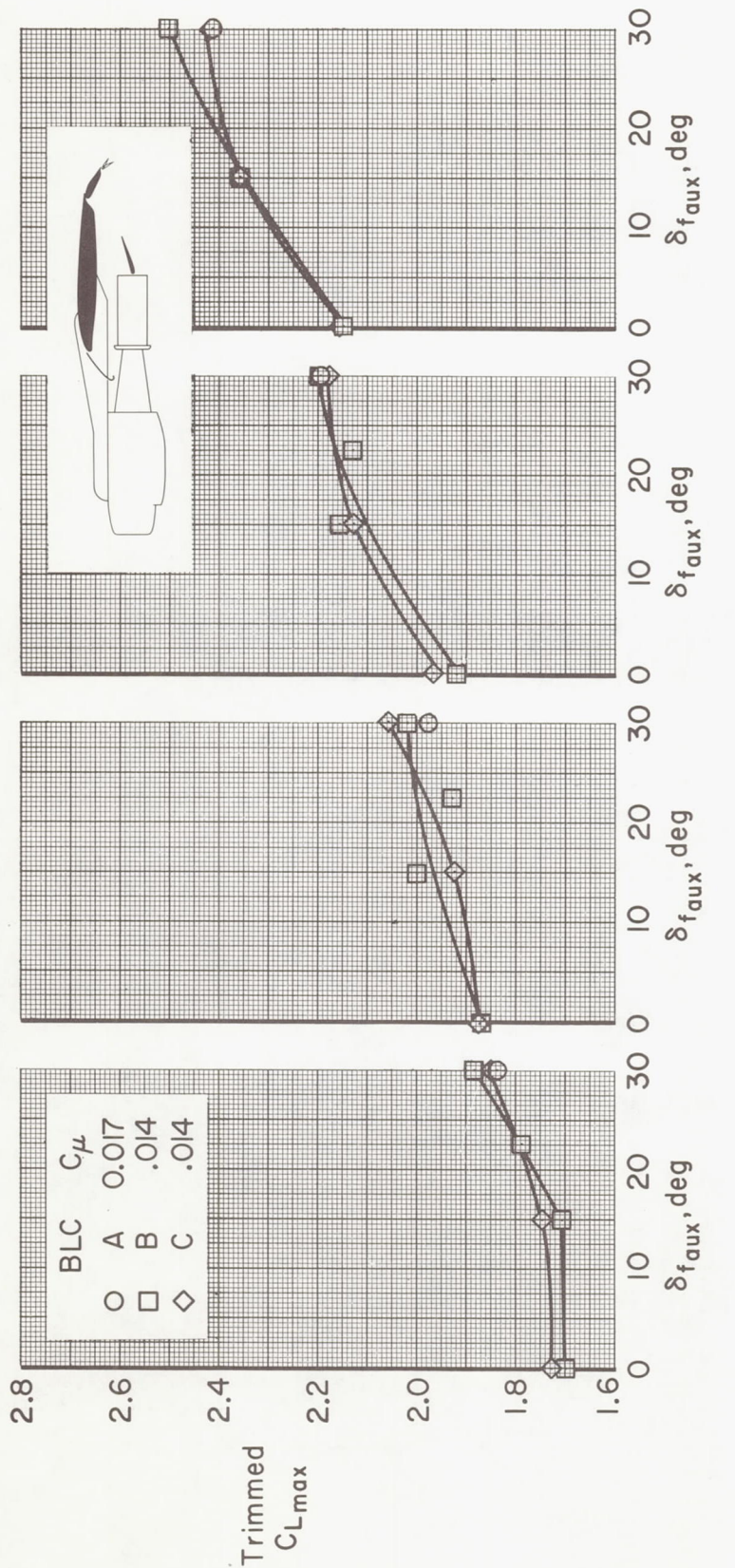


Figure 17.- Effect of BLC flap arrangements on trimmed $C_{L_{max}}$ with normal chord auxiliary flap, $\delta_{f_m} = 30^\circ$, $\delta_d = 15^\circ$, $\delta_s = 35^\circ$.

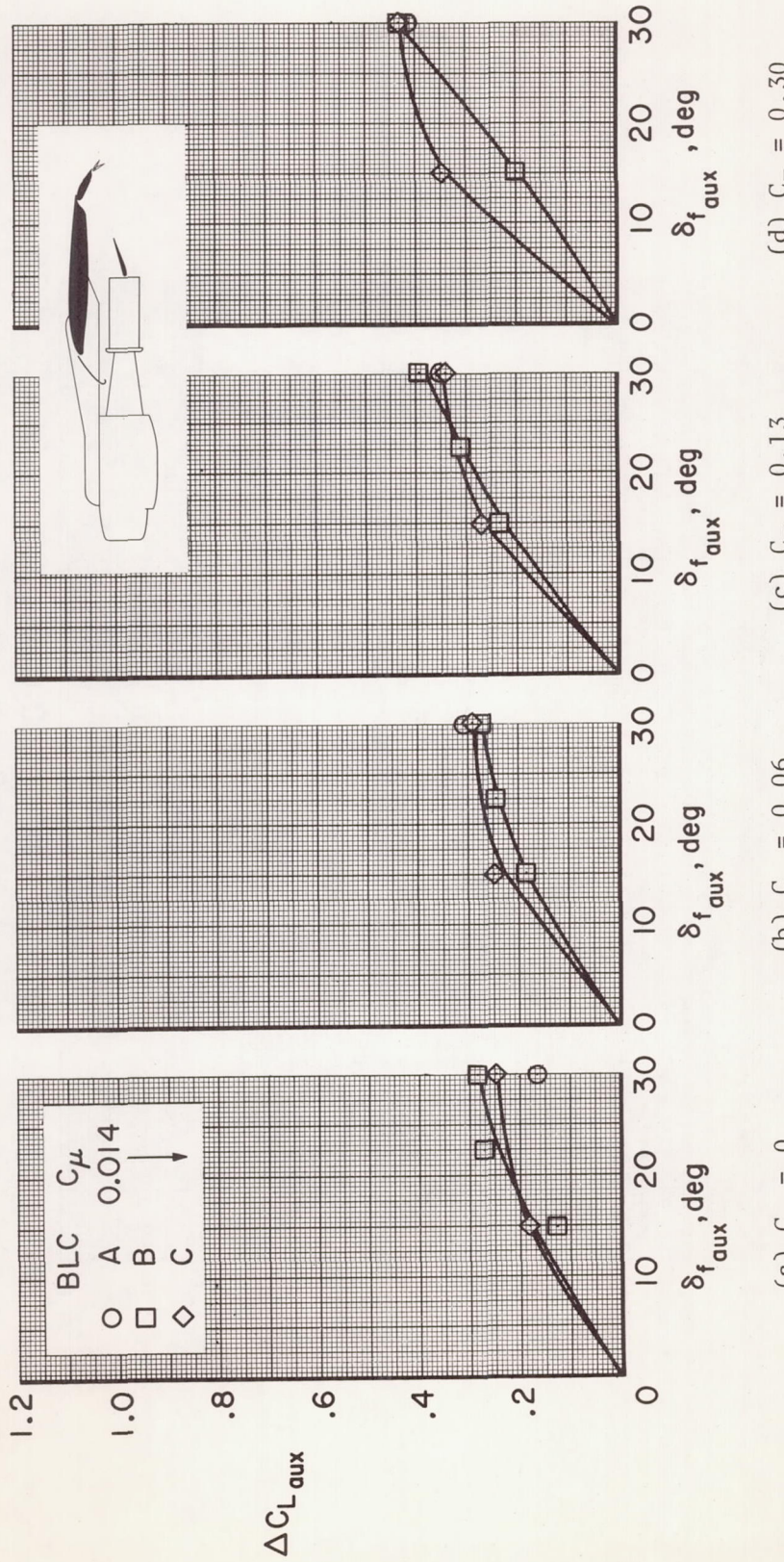


Figure 18.- Effect of BLC flap arrangements on the incremental lift due to normal chord auxiliary flap deflection, $\delta_d = 30^\circ$, $\delta_s = 15^\circ$, $\alpha_u = 0^\circ$.

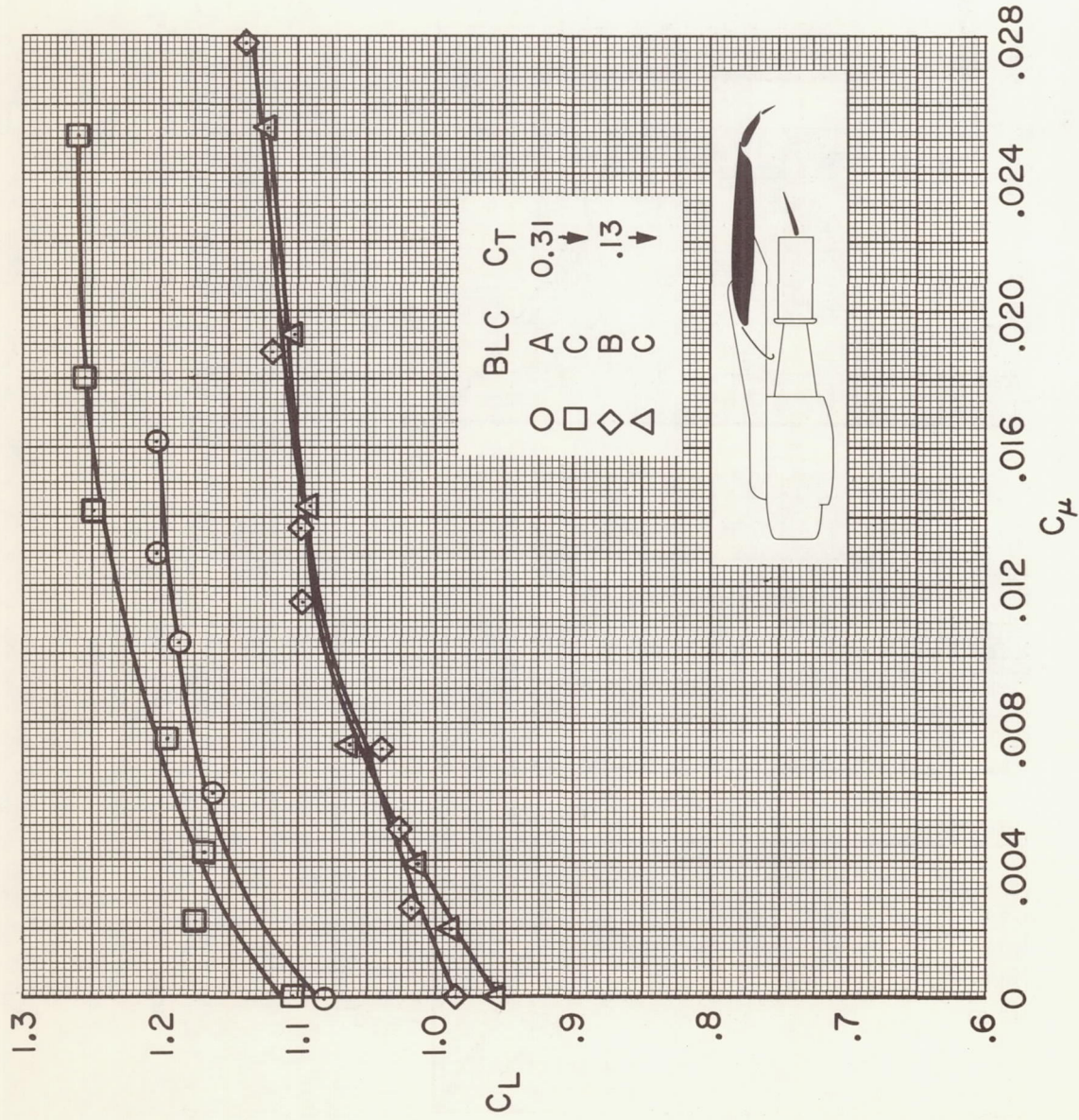


Figure 19.- Effect of BLC flap arrangements on the variation of lift coefficient with momentum coefficient; normal chord auxiliary flap, $\delta_{f_m} = 30^\circ$, $\delta_{f_{aux}} = 30^\circ$, $\delta_d = 15^\circ$, $\delta_s = 35^\circ$

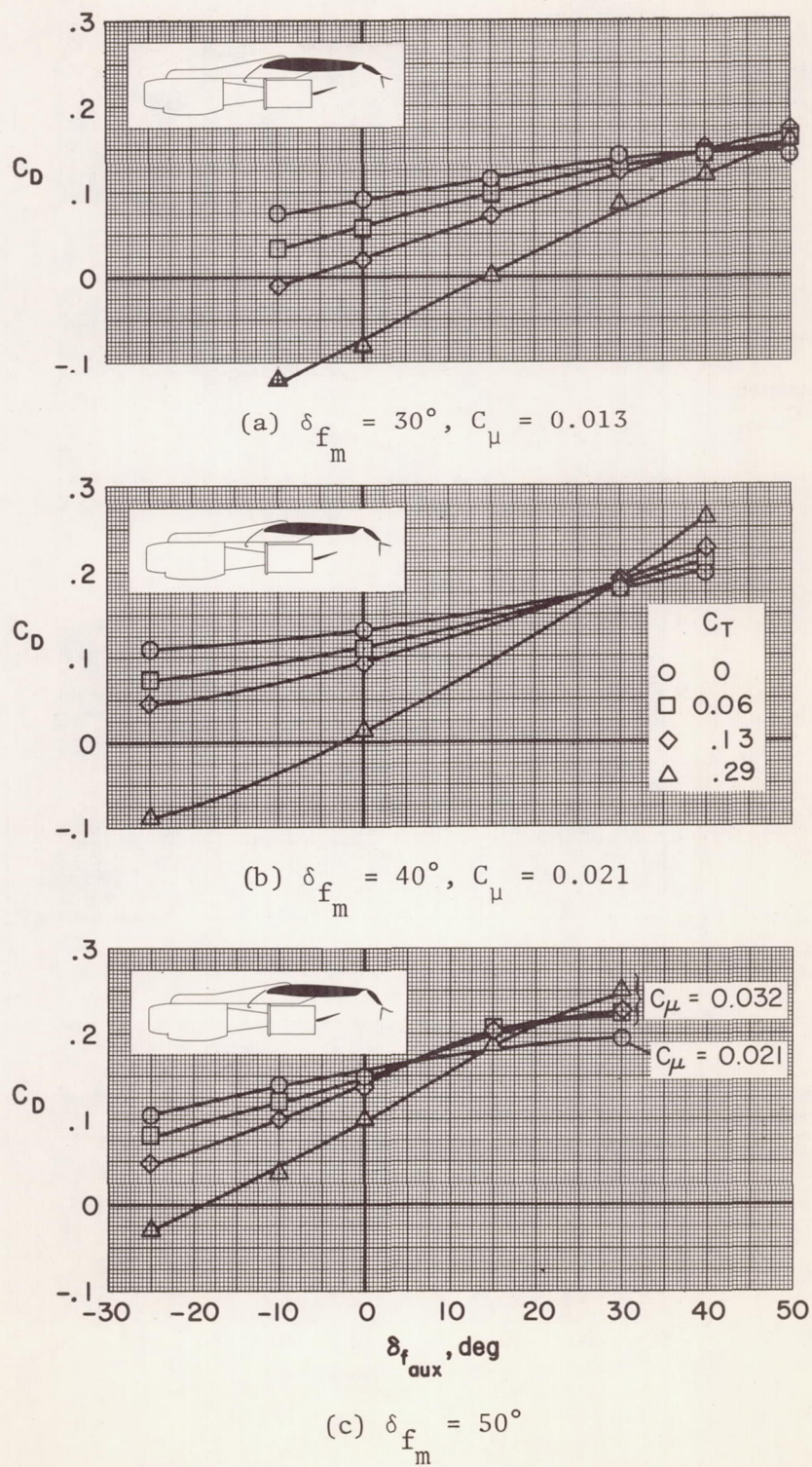


Figure 20.- Effect of auxiliary flap deflection on drag coefficient; BLC flap arrangement A with extended chord auxiliary flap, $\delta_d = 15^\circ$, $\delta_s = 35^\circ$, $i_t = -5^\circ$, $\delta_e = 0^\circ$, $\alpha = 0^\circ$.

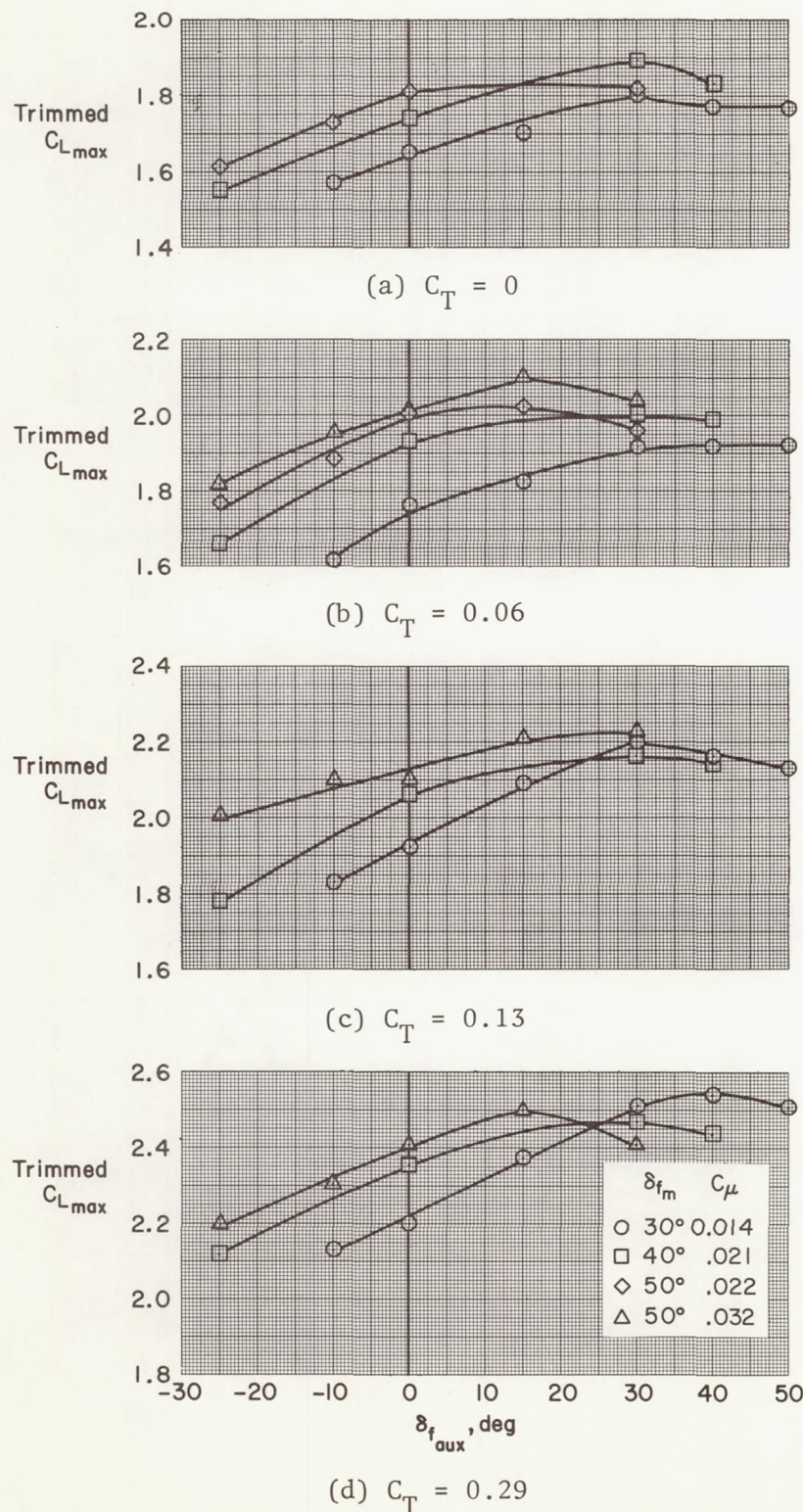


Figure 21.- Effect of auxiliary flap deflection on trimmed $C_{L_{max}}$; BLC flap arrangement A with extended chord auxiliary flap, $\delta_d = 15^\circ$, $\delta_s = 35^\circ$.

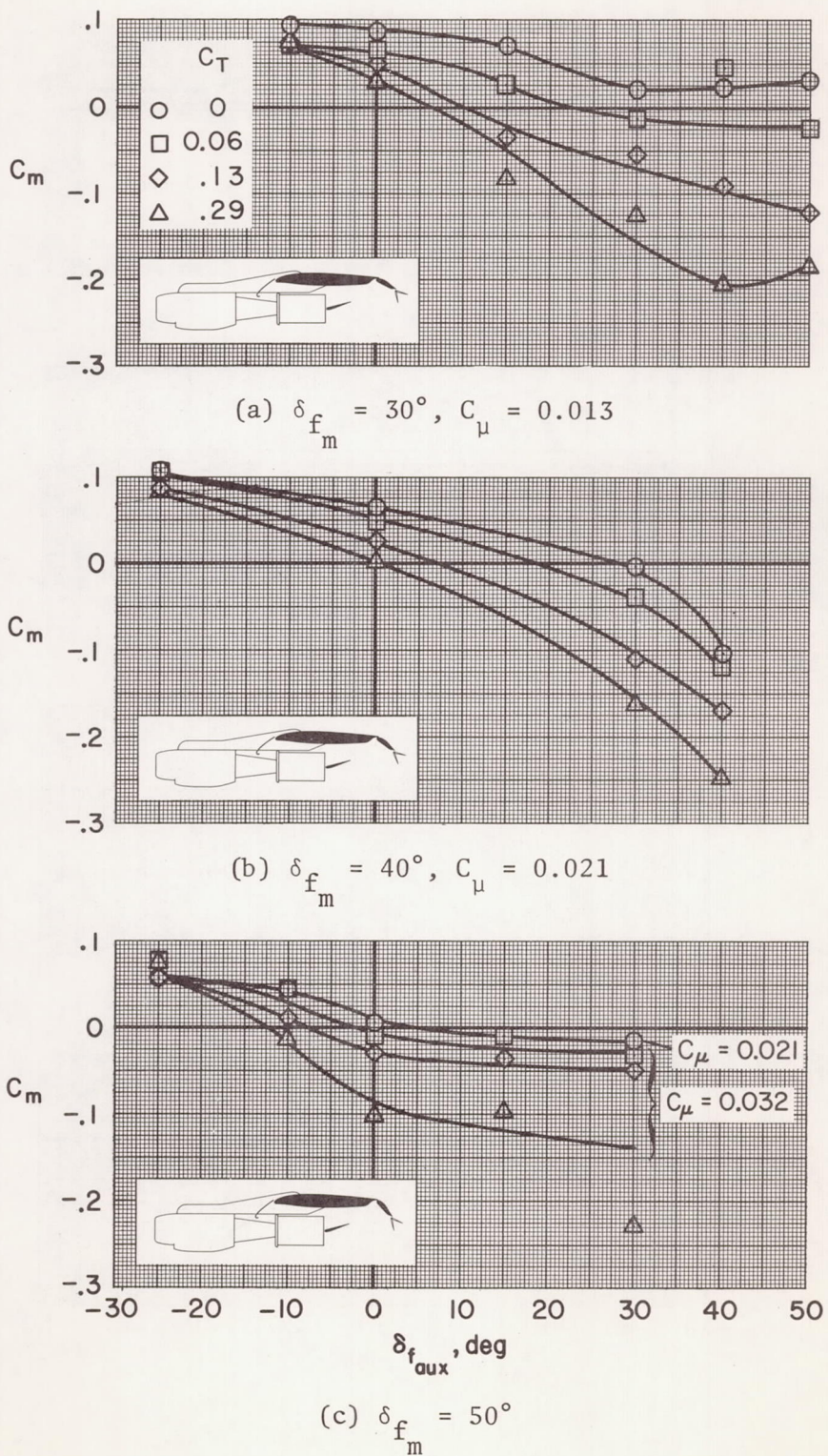
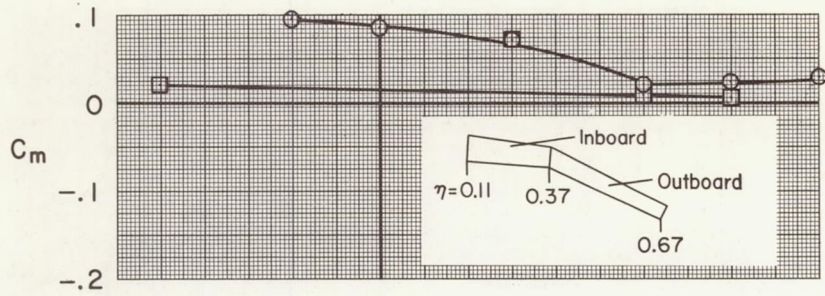
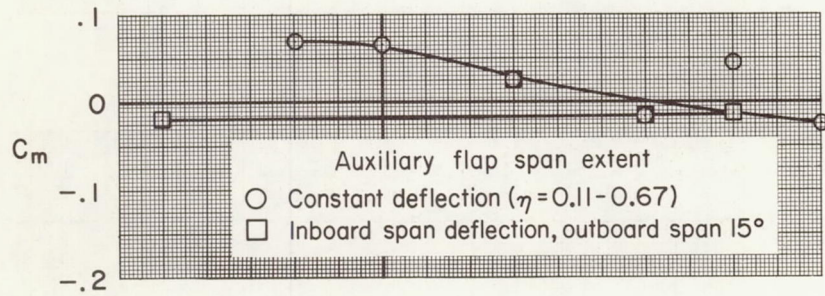


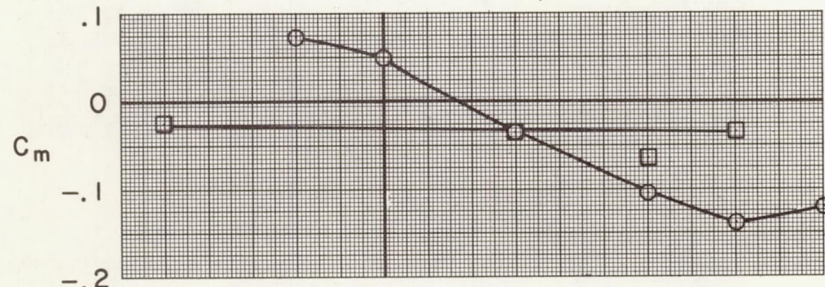
Figure 22.- Effect of auxiliary flap deflection on pitching-moment coefficient; BLC flap arrangement A with extended chord auxiliary flap, $\delta_d = 15^\circ$, $\delta_s = 35^\circ$, $i_t = -5^\circ$, $\delta_e = 0^\circ$, $\alpha = 0^\circ$.



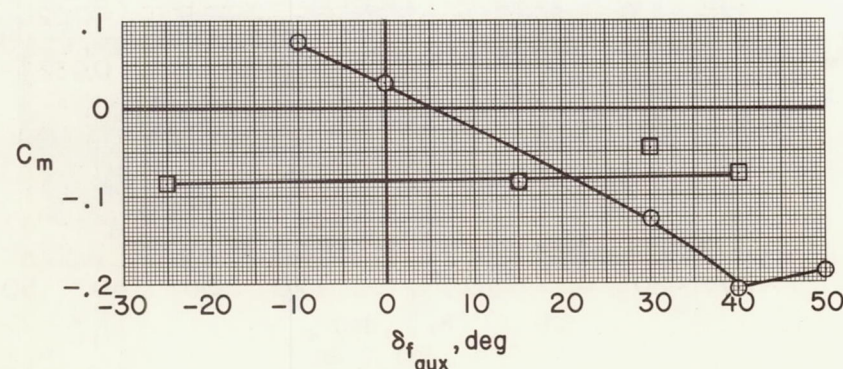
(a) $C_T = 0$



(b) $C_T = 0.06$



(c) $C_T = 0.13$



(d) $C_T = 0.29$

Figure 23.- Effect of varying inboard span auxiliary flap deflection on pitching-moment coefficient; BLC flap arrangement A with extended chord auxiliary flap, $\delta_{f_m} = 30^\circ$, $\delta_d = 15^\circ$, $\delta_s = 35^\circ$, $i_t = -5^\circ$, $\delta_e = 0^\circ$, $\alpha = 0^\circ$.

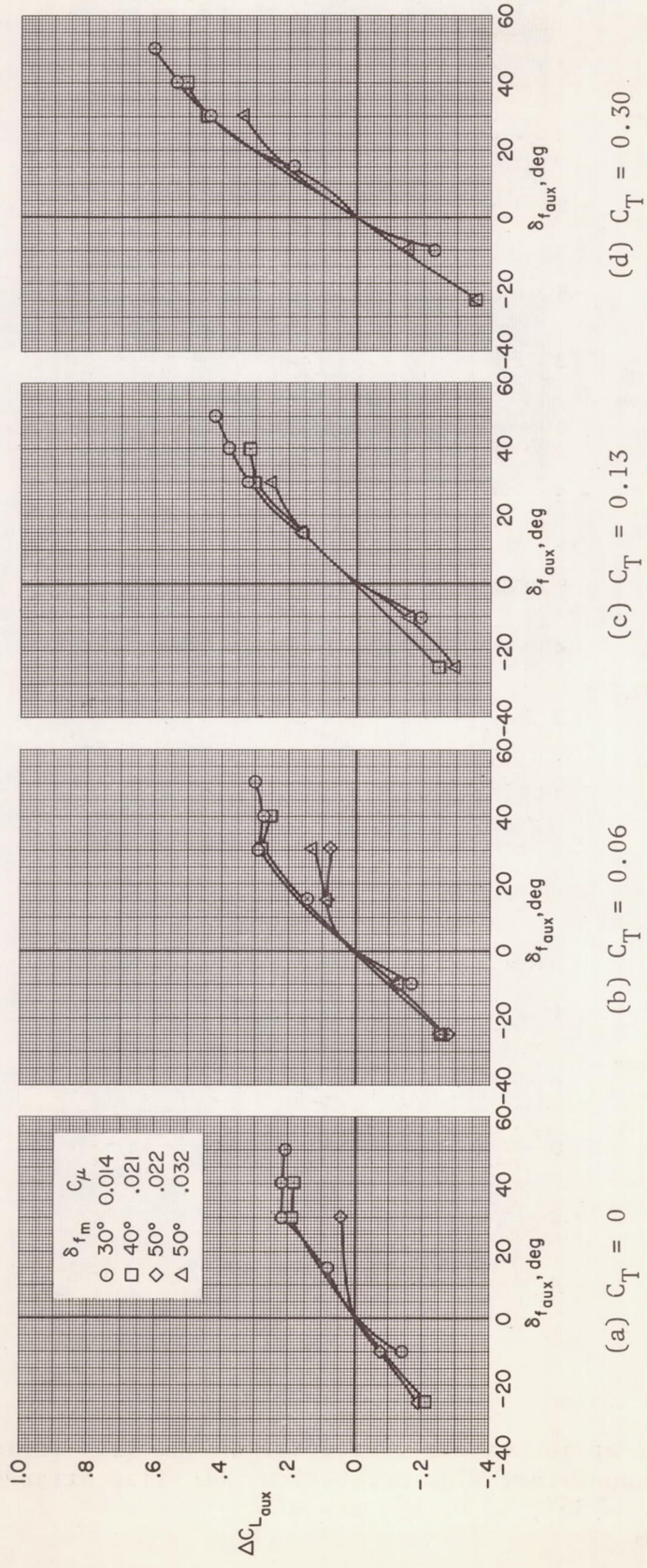


Figure 24.- Incremental lift due to extended chord auxiliary flap deflection; BLC flap arrangement A, $\delta_d = 15^\circ$, $\alpha = 0^\circ$.

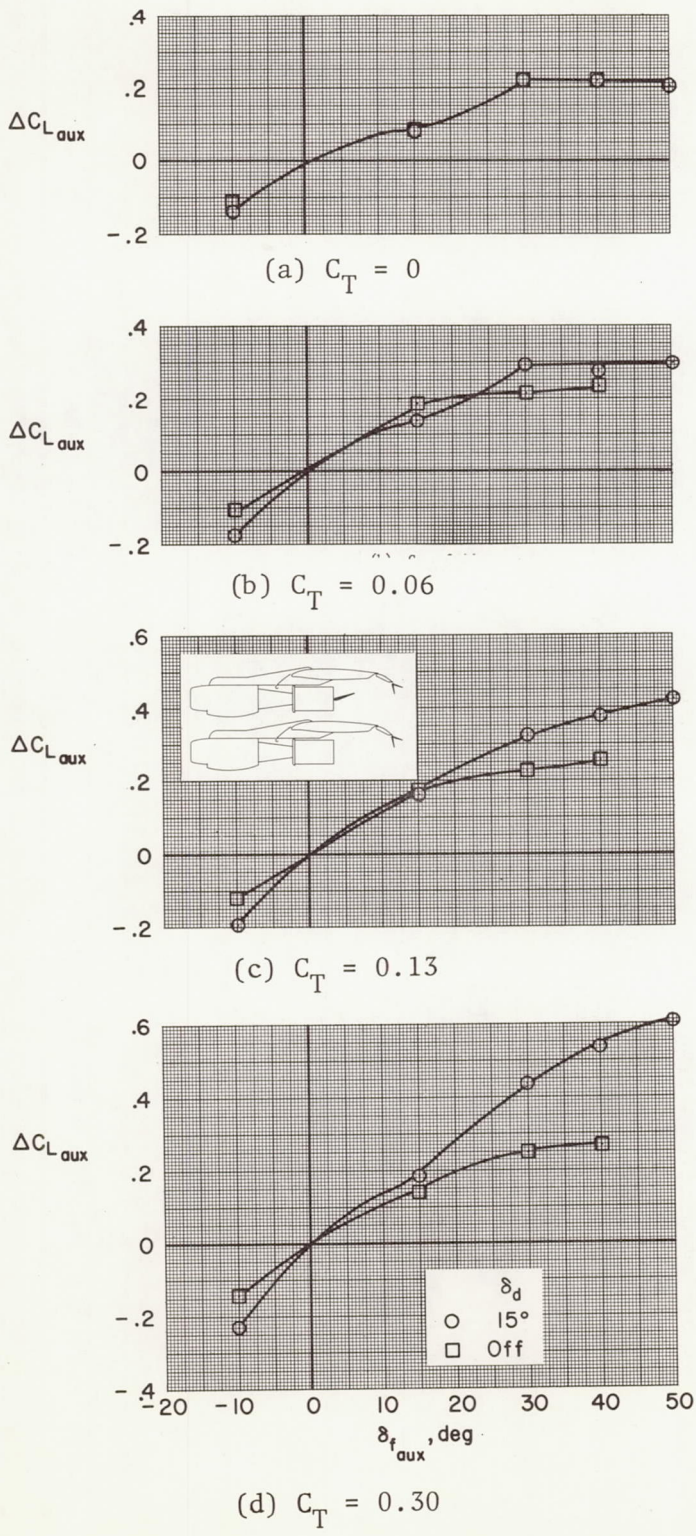


Figure 25.- Effect of jet exhaust deflector on the lift increment due to extended chord auxiliary flap deflection; BLC flap arrangement A, $C_\mu = 0.014$, $\delta_{f_m} = 30^\circ$, $\delta_d = 15^\circ$, $\alpha = 0^\circ$.

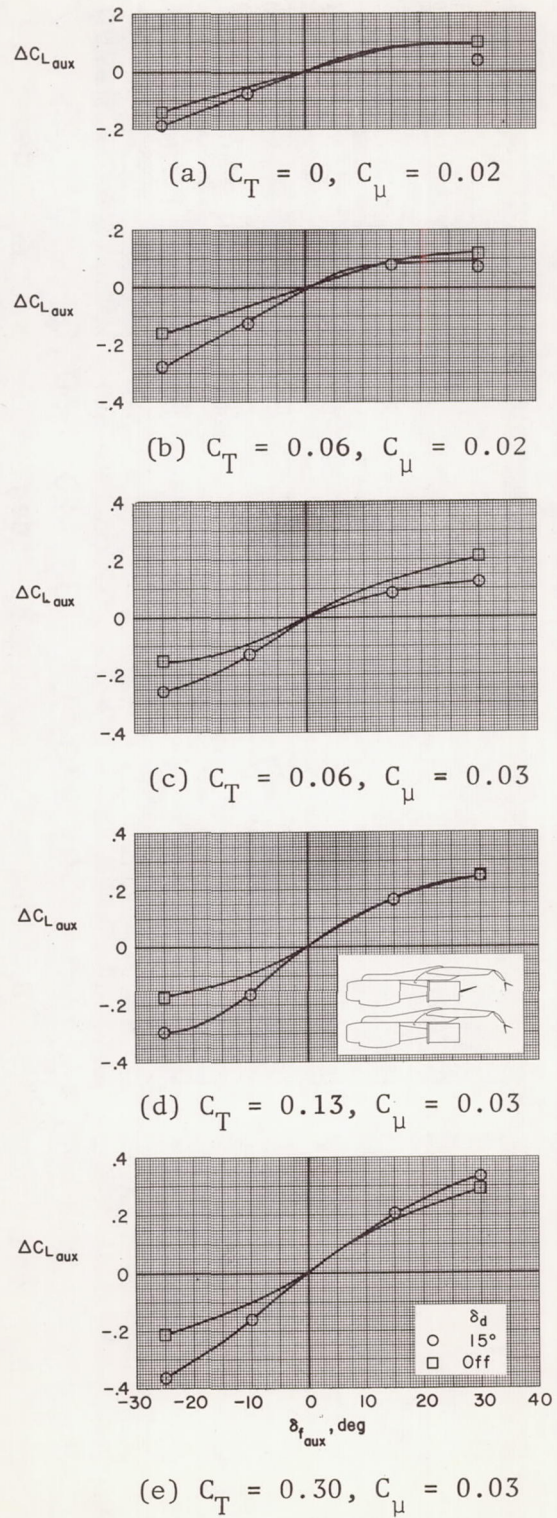


Figure 26.- Effect of jet exhaust deflector on the lift increment due to extended chord auxiliary flap deflection; BLC flap arrangement A, $\delta_{f_m} = 50^\circ$, $\delta_d = 15^\circ$, $\alpha = 0^\circ$.

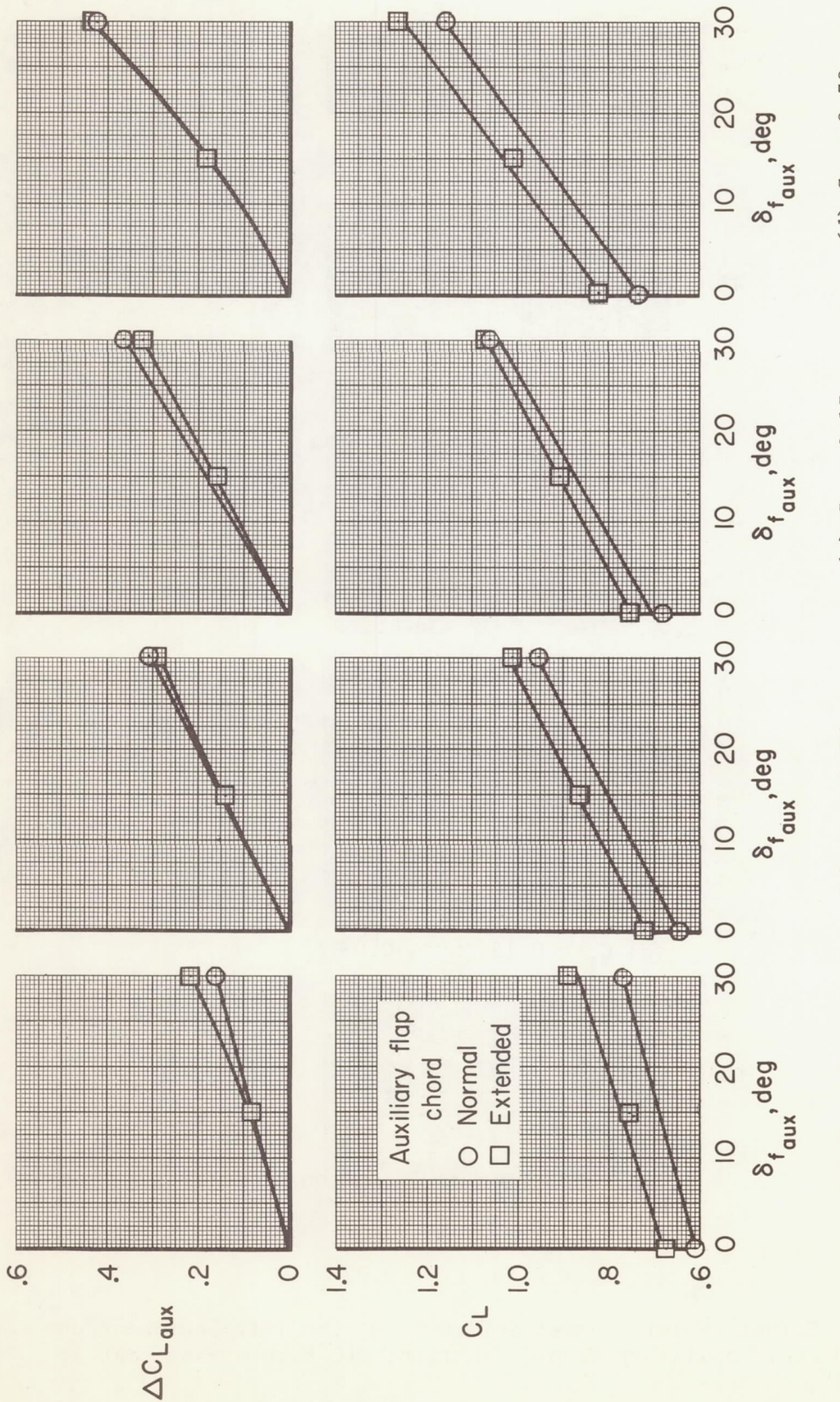


Figure 27.- Effect of auxiliary flap chord on lift coefficient and on lift increment due to auxiliary flap deflection; BLC flap arrangement A, $C_{\mu} = 0.014$, $\delta_f = 30^\circ$, $\delta_d = 15^\circ$, $\delta_s = 35^\circ$, $i_t = -5^\circ$, $\delta_e = 0^\circ$, $\alpha = 0^\circ$.

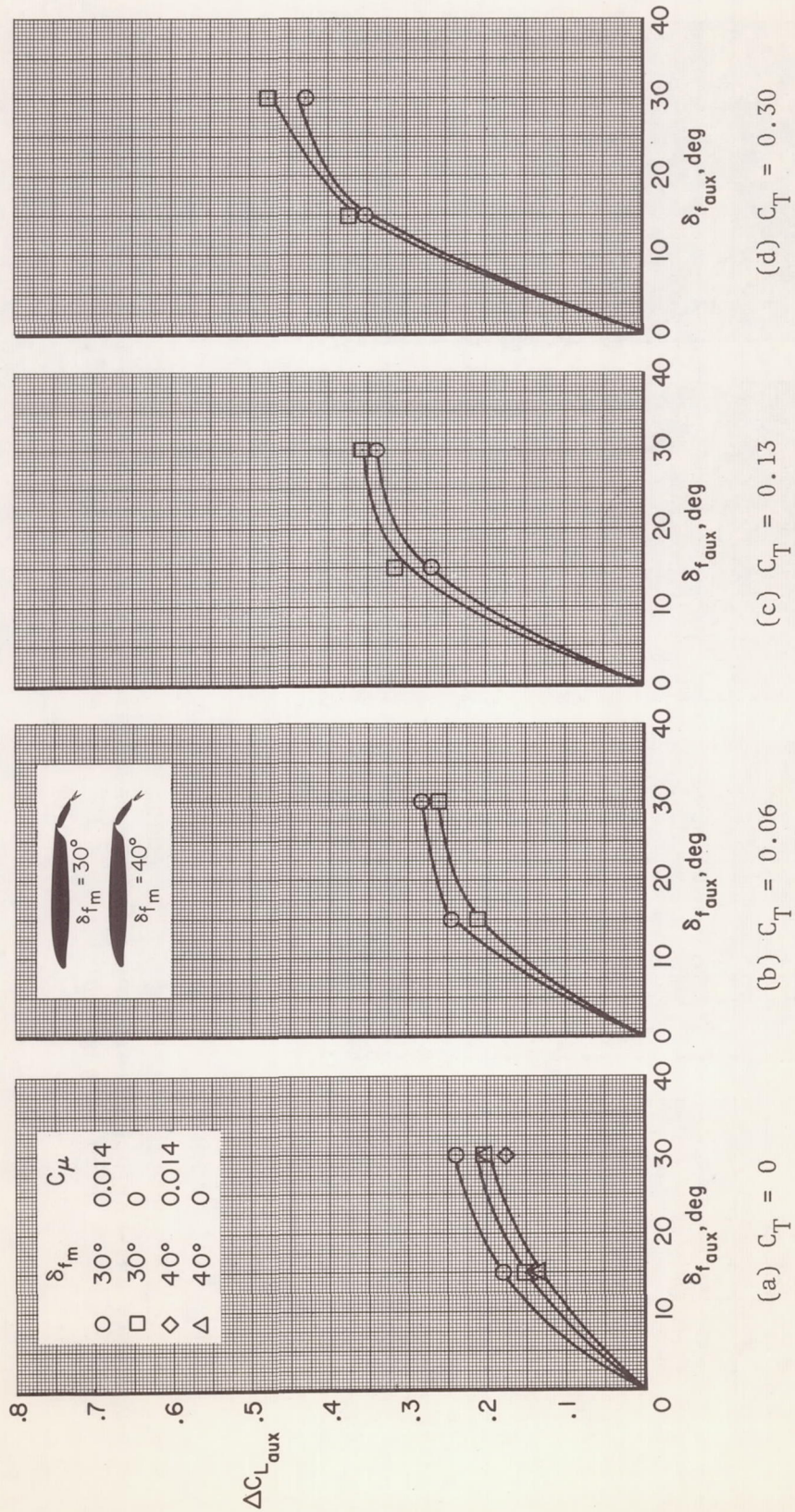


Figure 28.- Effect of blowing BLC over the trailing-edge main flap on the lift increment due to normal chord auxiliary flap deflection; BLC flap arrangement C, $\delta_d = 15^\circ$, $\alpha = 0^\circ$.

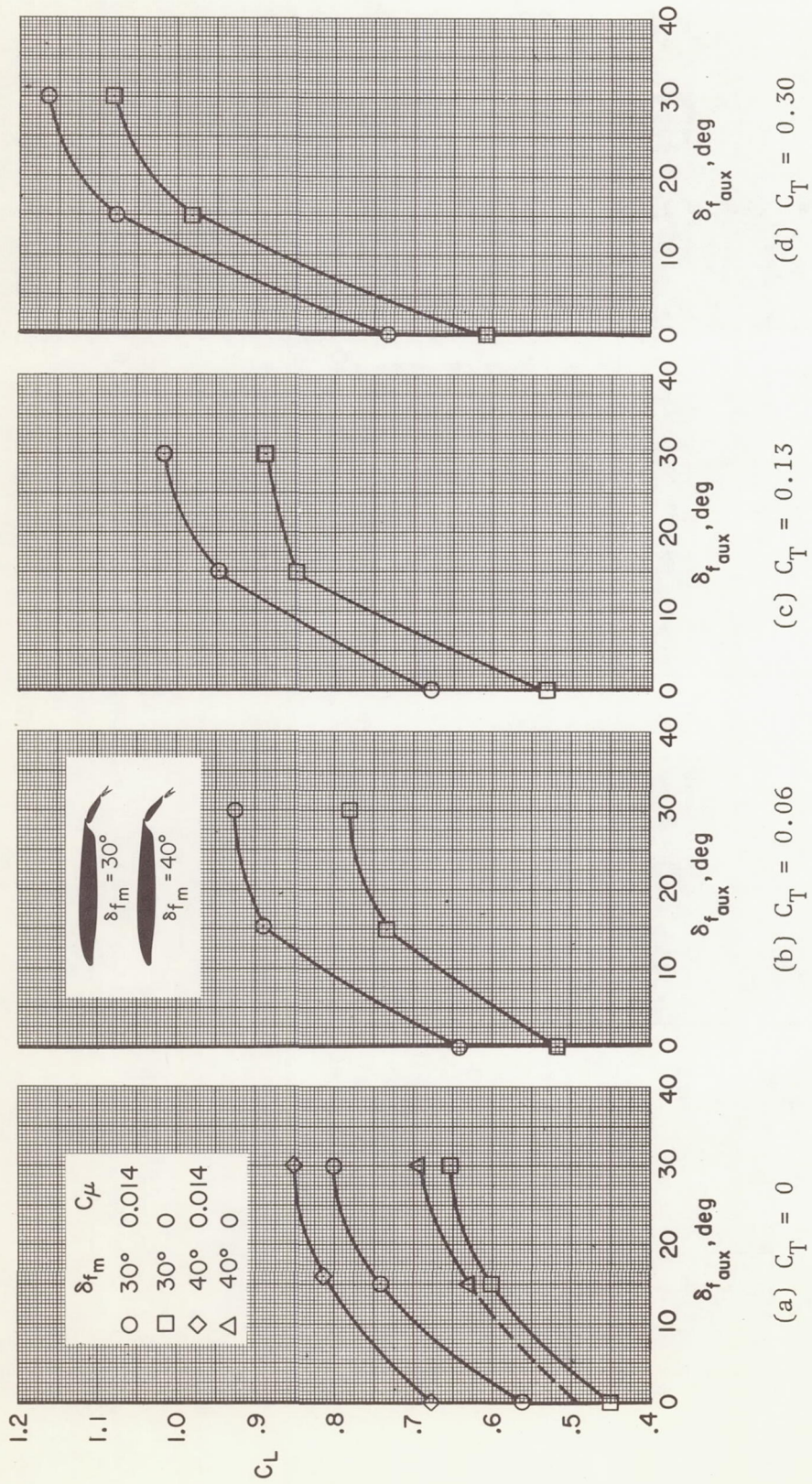
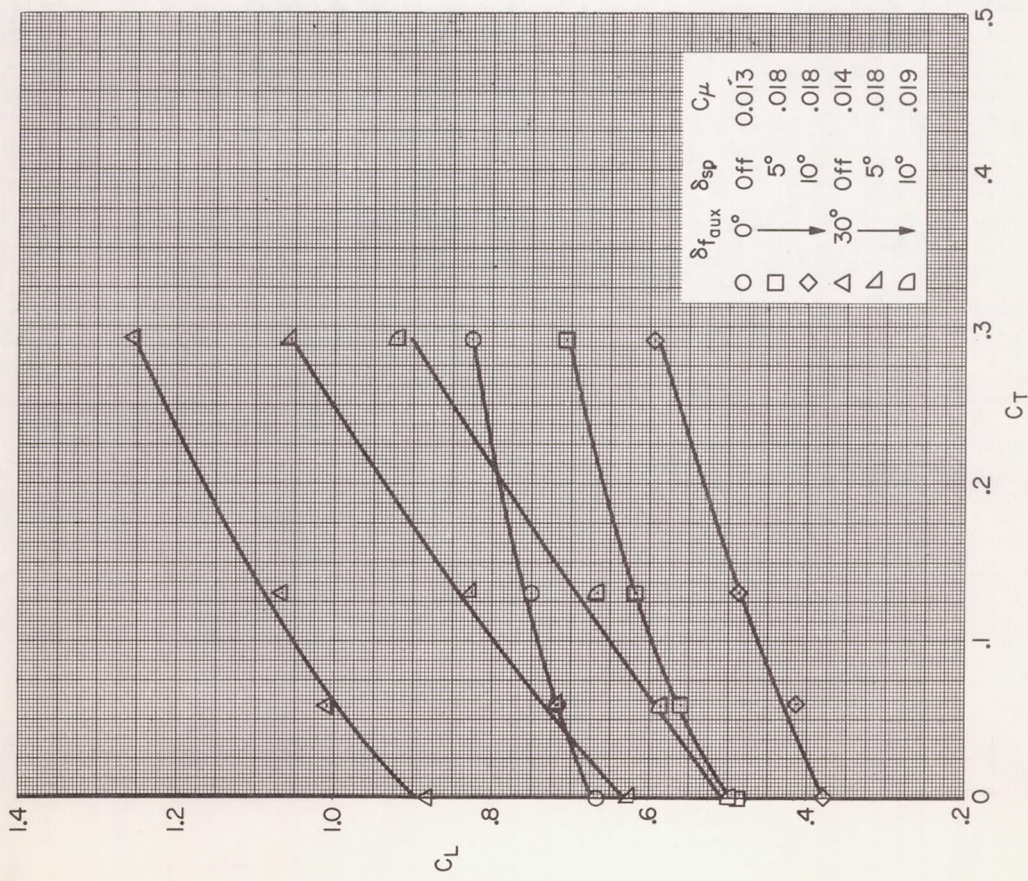
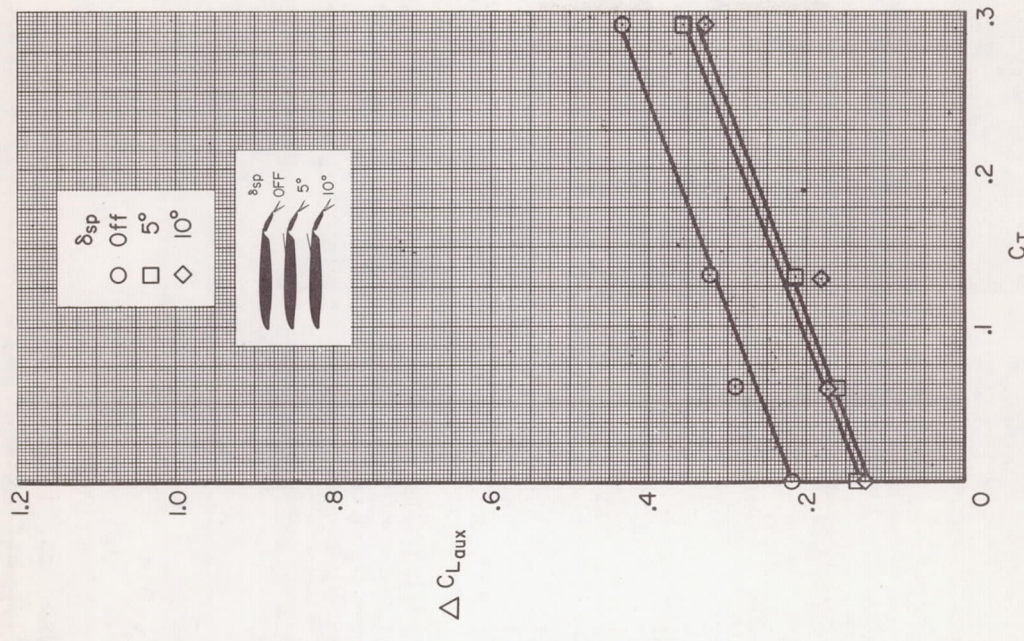


Figure 29.- Effect of blowing BLC over the trailing-edge main flap on lift coefficient; BLC flap arrangement C, $\delta_d = 15^\circ$, $\delta_s = 35^\circ$, $i_t = -5^\circ$, $\delta_e = 0^\circ$, $\alpha = 0^\circ$.

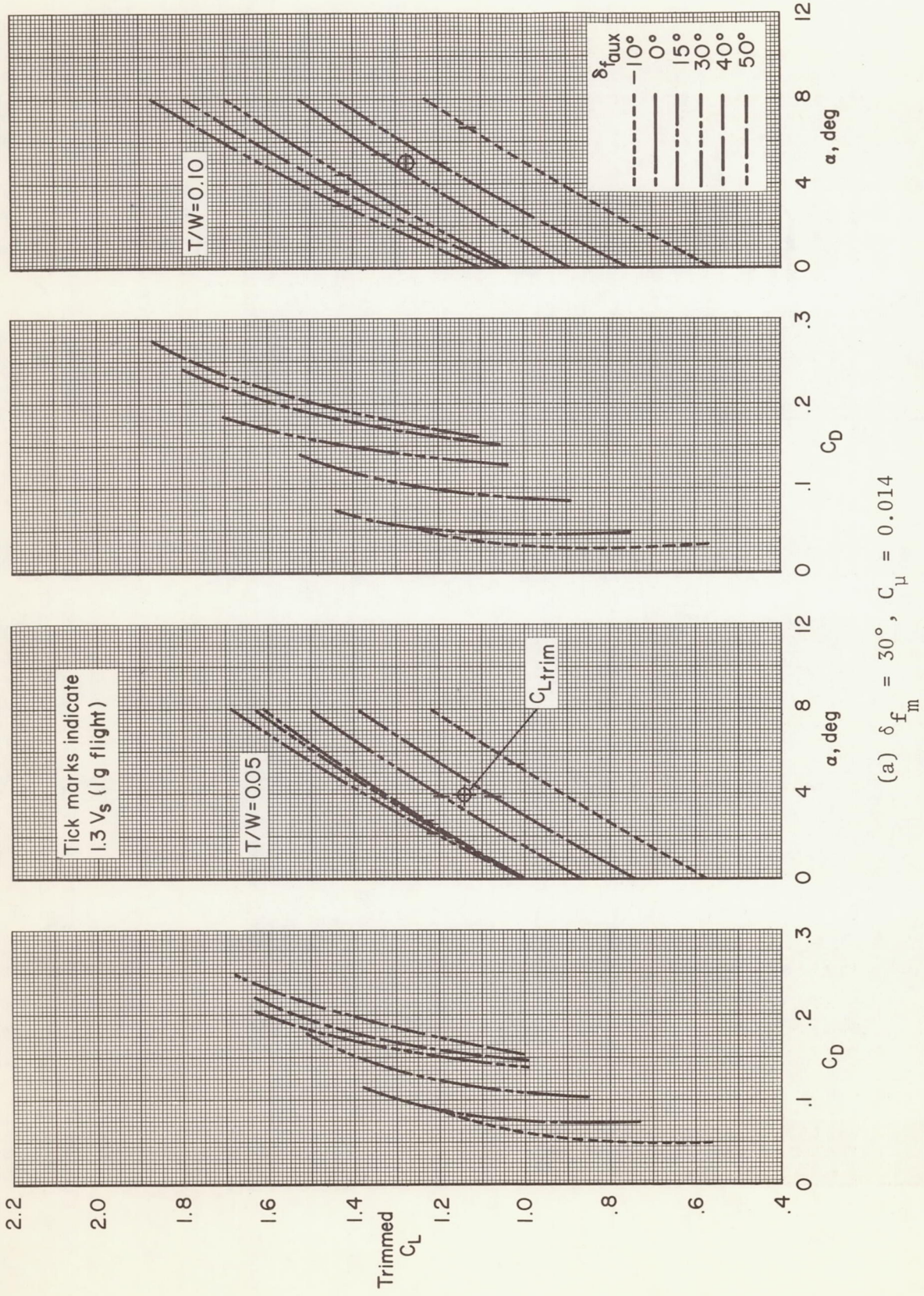


(a) Lift coefficient.



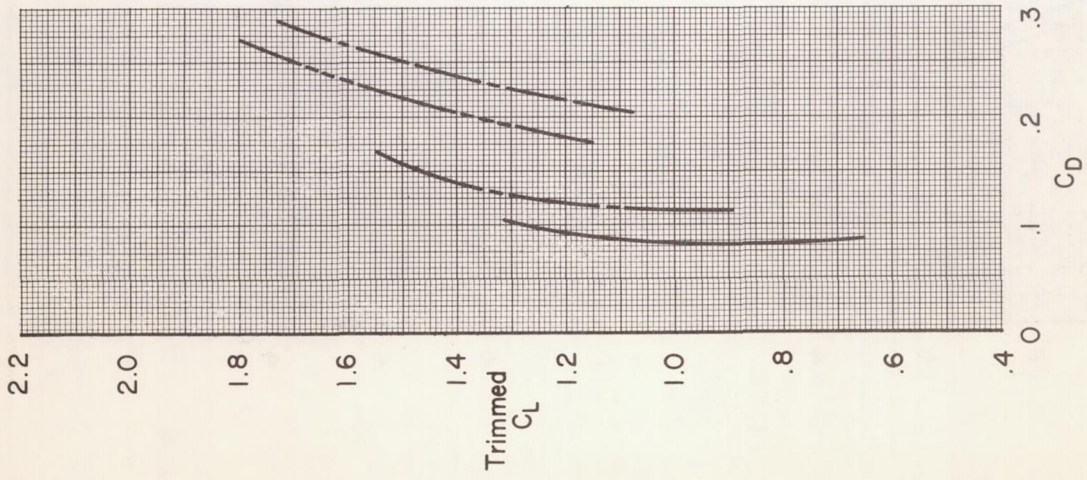
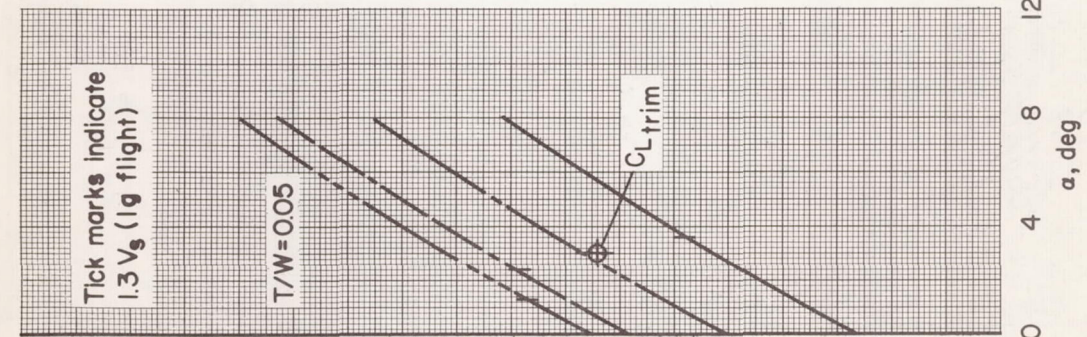
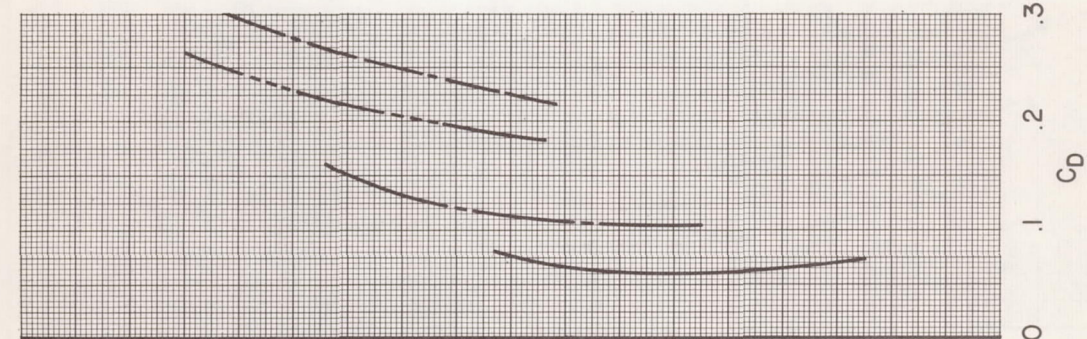
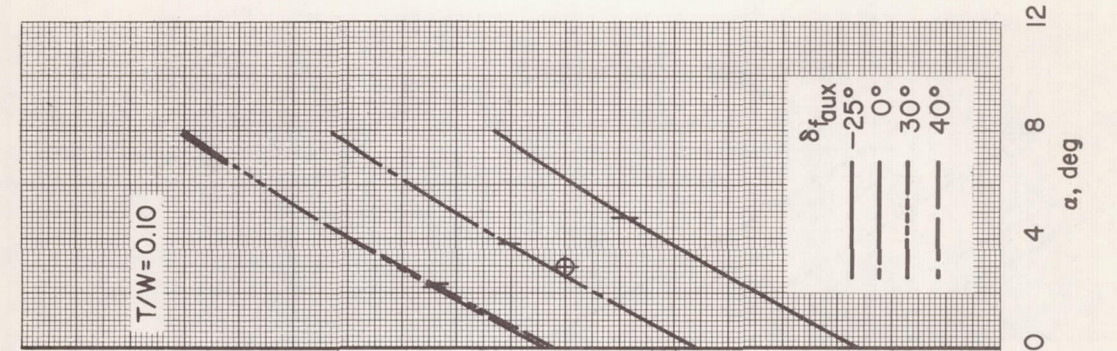
(b) Lift increment at $\delta_{f_{aux}} = 30^\circ$.

Figure 30.- Effect of symmetrically deflected spoilers on lift coefficient and lift increment due to extended chord auxiliary flap deflection; BLC flap arrangement A, $\delta_f = 30^\circ$, $\delta_d = 15^\circ$, $\delta_s = 35^\circ$, $i_t = -5^\circ$, $\delta_e = 0^\circ$, $\alpha = 0^\circ$.



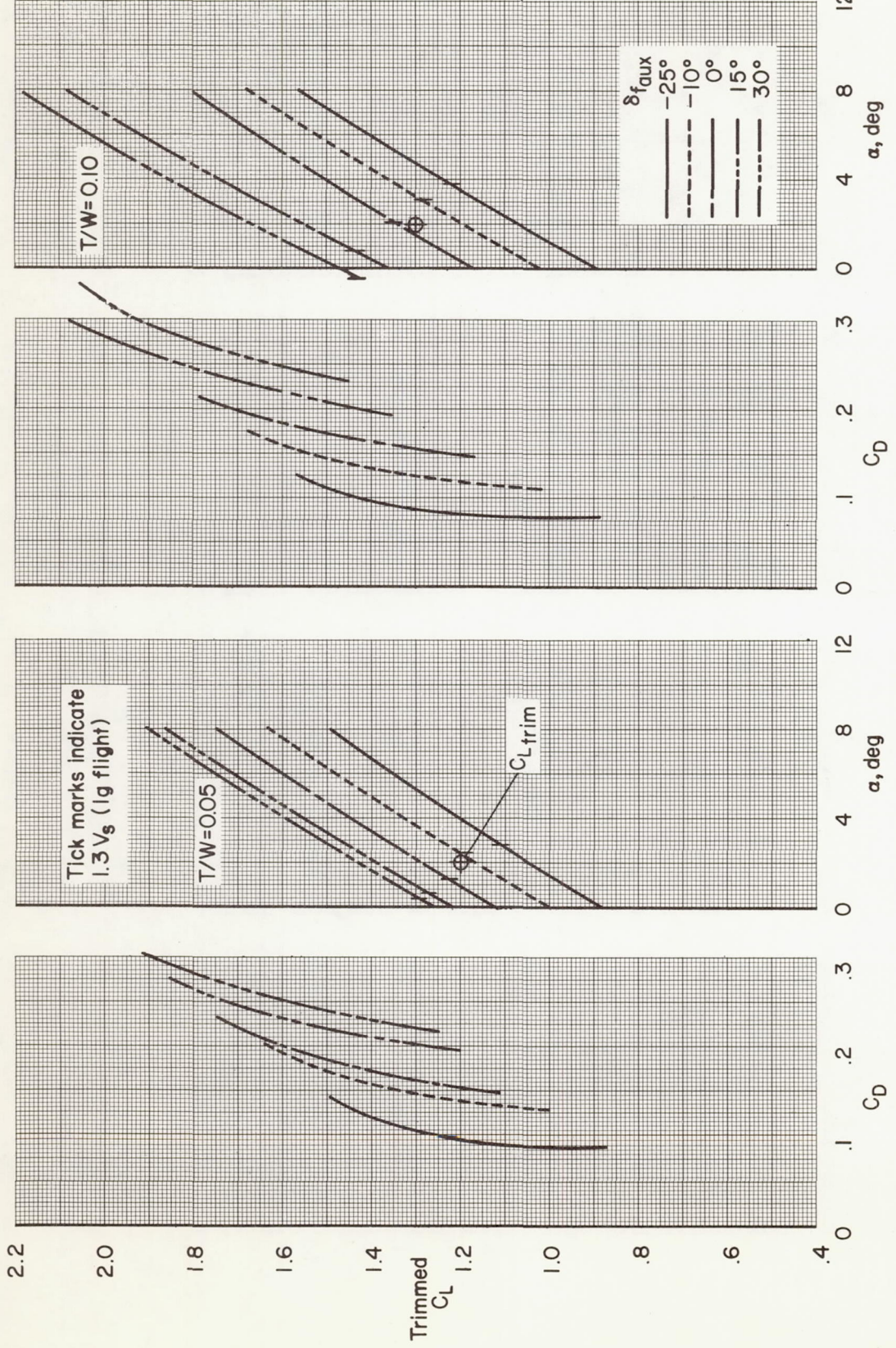
$$(a) \quad \delta_{f_m} = 30^\circ, \quad C_u = 0.014$$

Figure 31.- Longitudinal characteristics of the model used for flight-path control computations due to extended chord auxiliary flap deflection; BLC flap arrangement A, $\delta_d = 15^\circ$, $\delta_s = 35^\circ$.



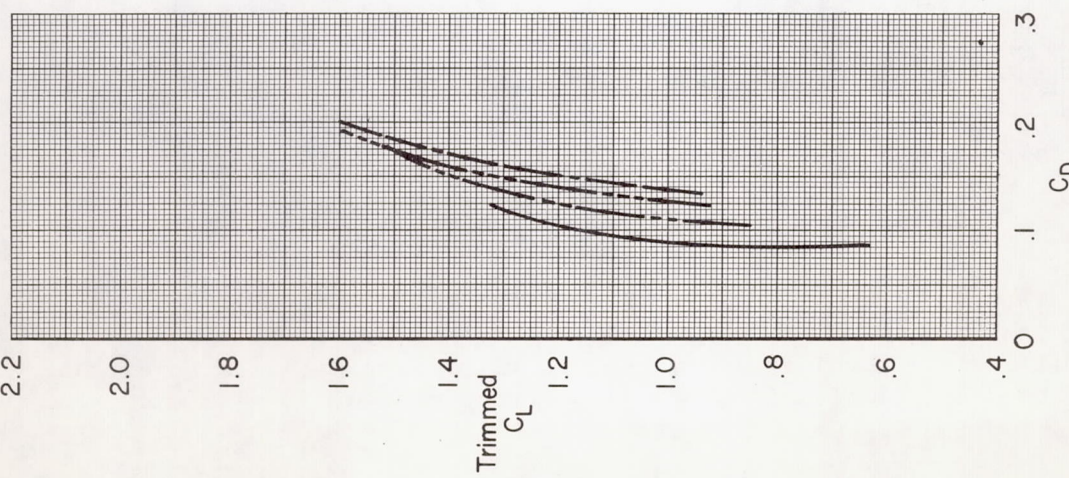
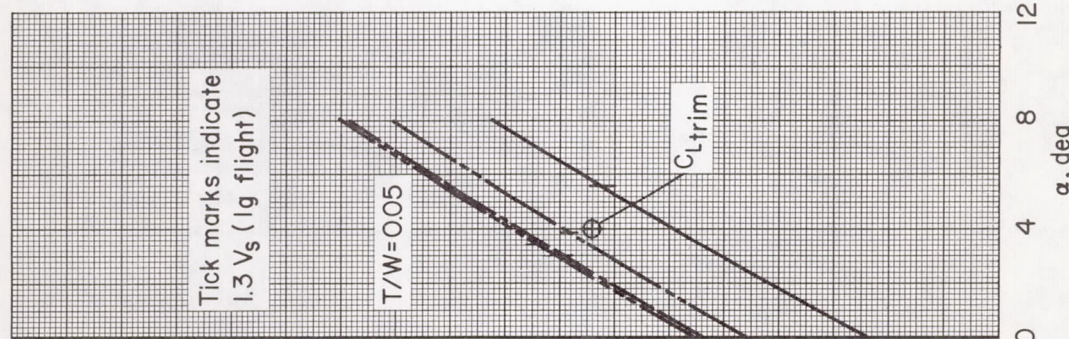
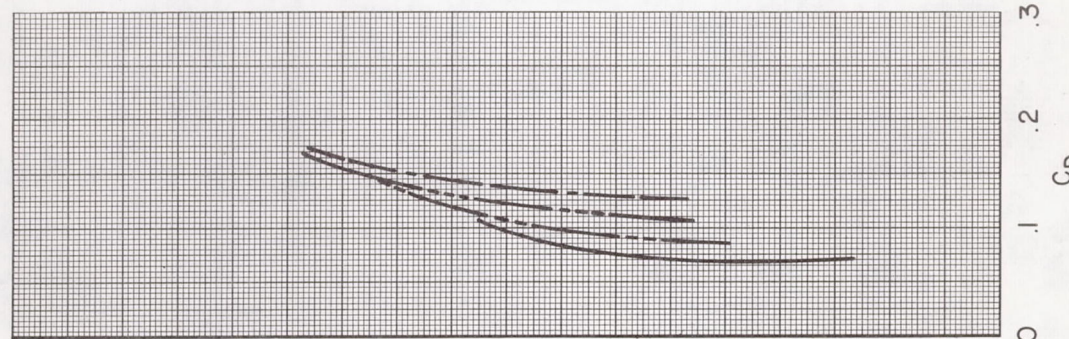
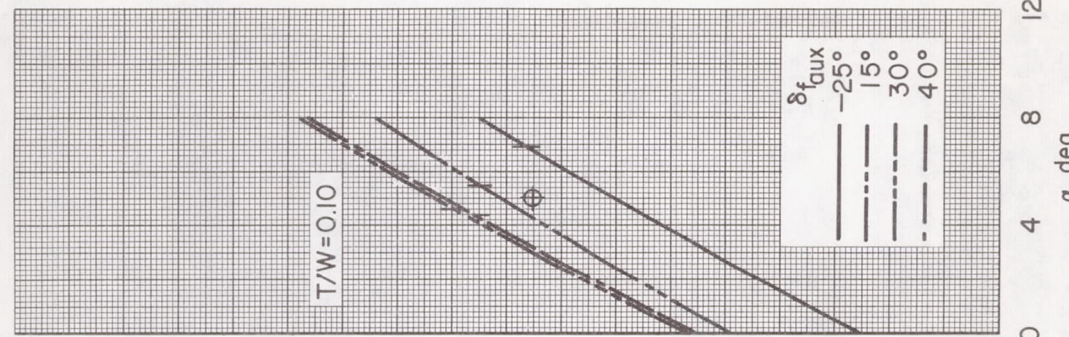
(b) $\delta_f = 40^\circ$, $C_{\mu} = 0.022$

Figure 31.- Continued.



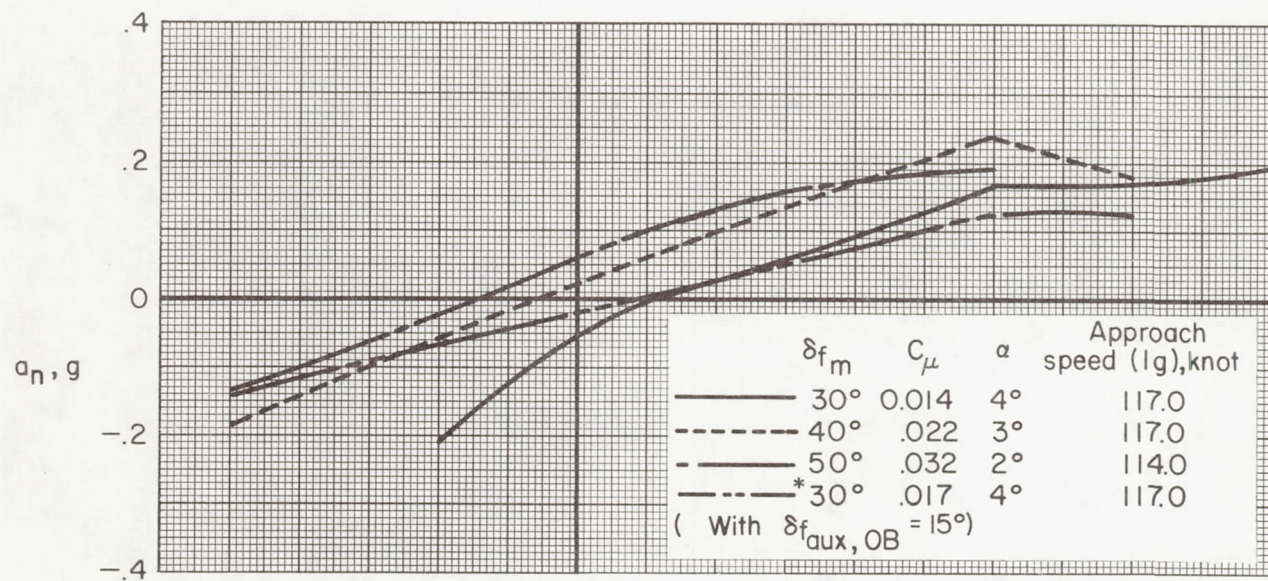
(c) $\delta_f = 50^\circ$, $C_\mu = 0.032$

Figure 31.- Continued.

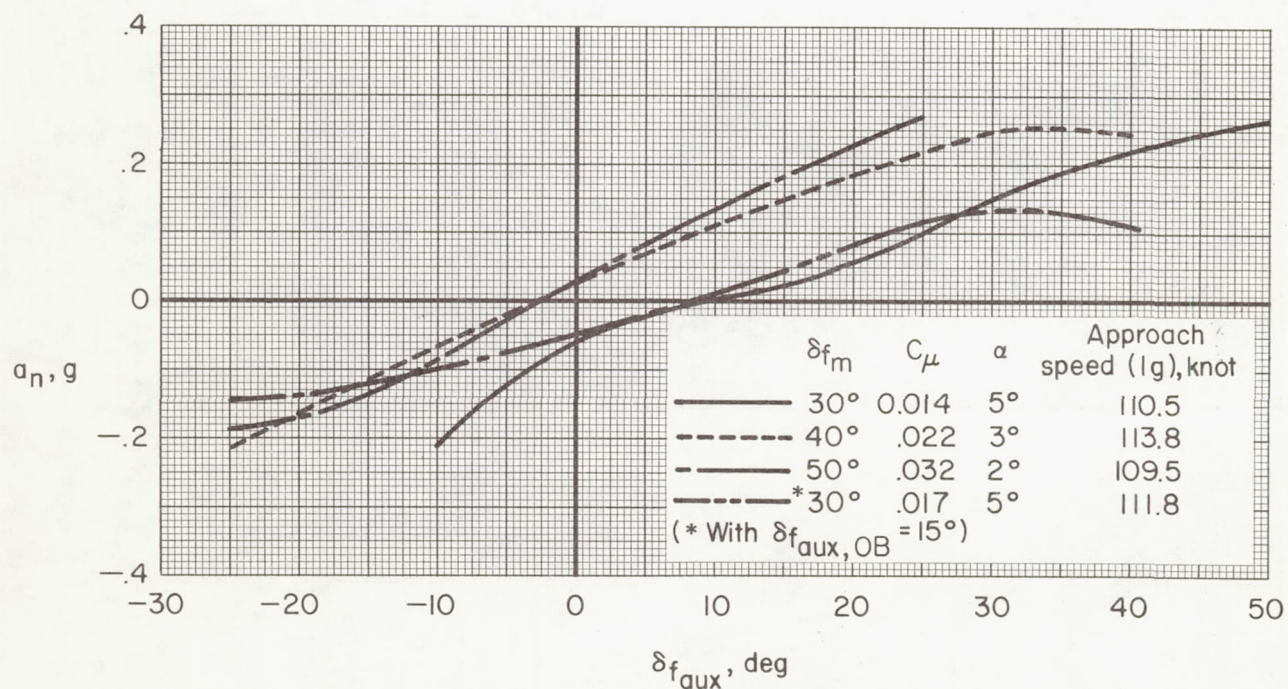


(d) $\delta_{f_m} = 30^\circ$, $\delta_{f_{aux,OB}} = 15^\circ$, $C_\mu = 0.017$

Figure 31.- Concluded.

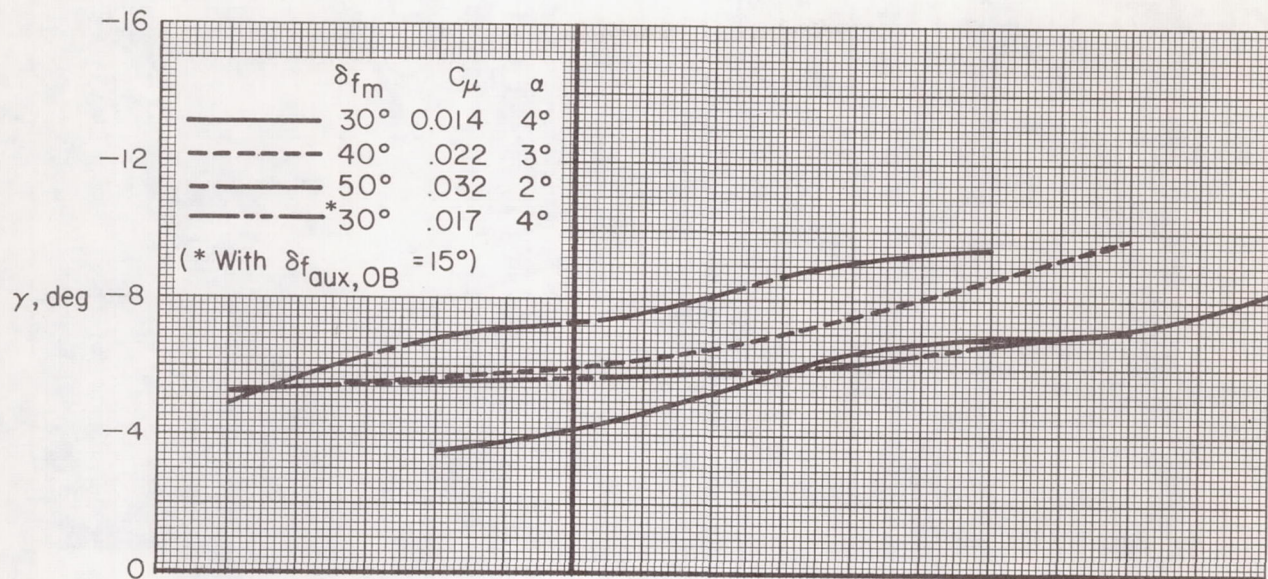


(a) $T/W = 0.05$

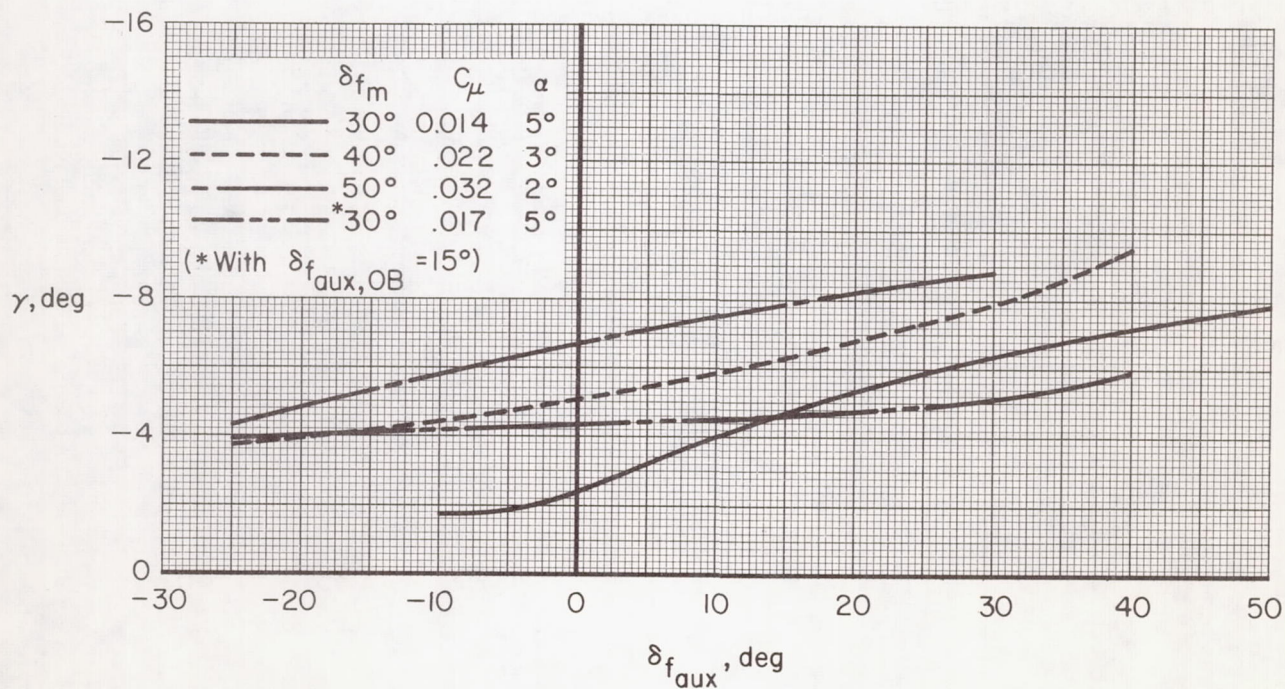


(b) $T/W = 0.10$

Figure 32.- Incremental acceleration normal to the flight path due to extended chord auxiliary flap deflection; BLC flap arrangement A, $\delta_d = 15^\circ$, $\delta_s = 35^\circ$, $W/S = 53$ psf.

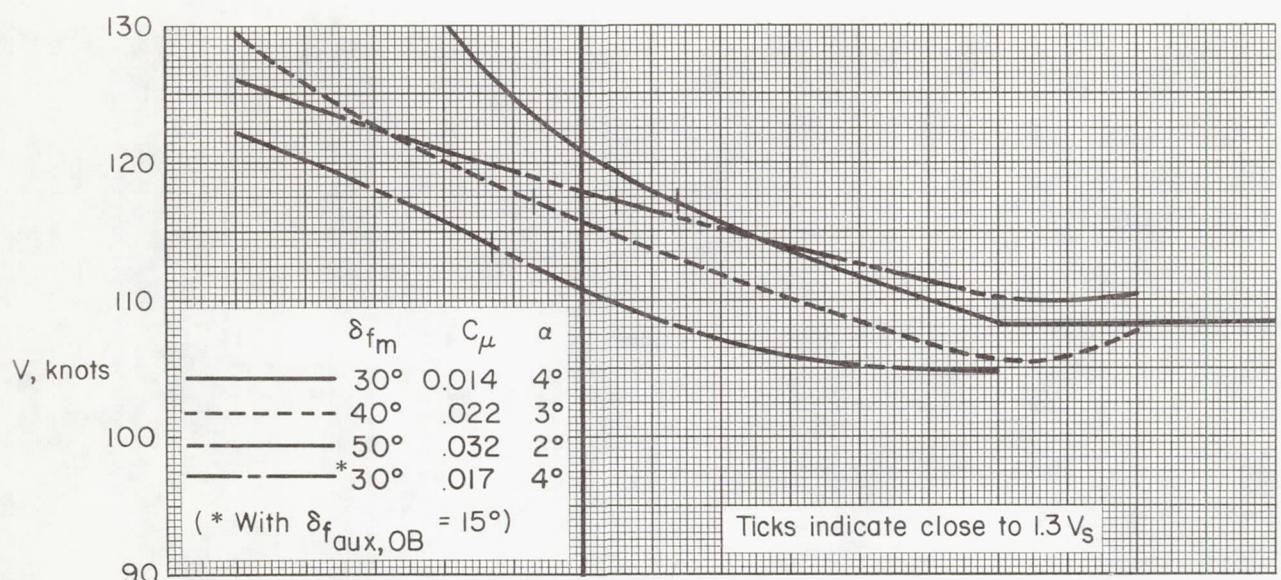


(a) $T/W = 0.05$

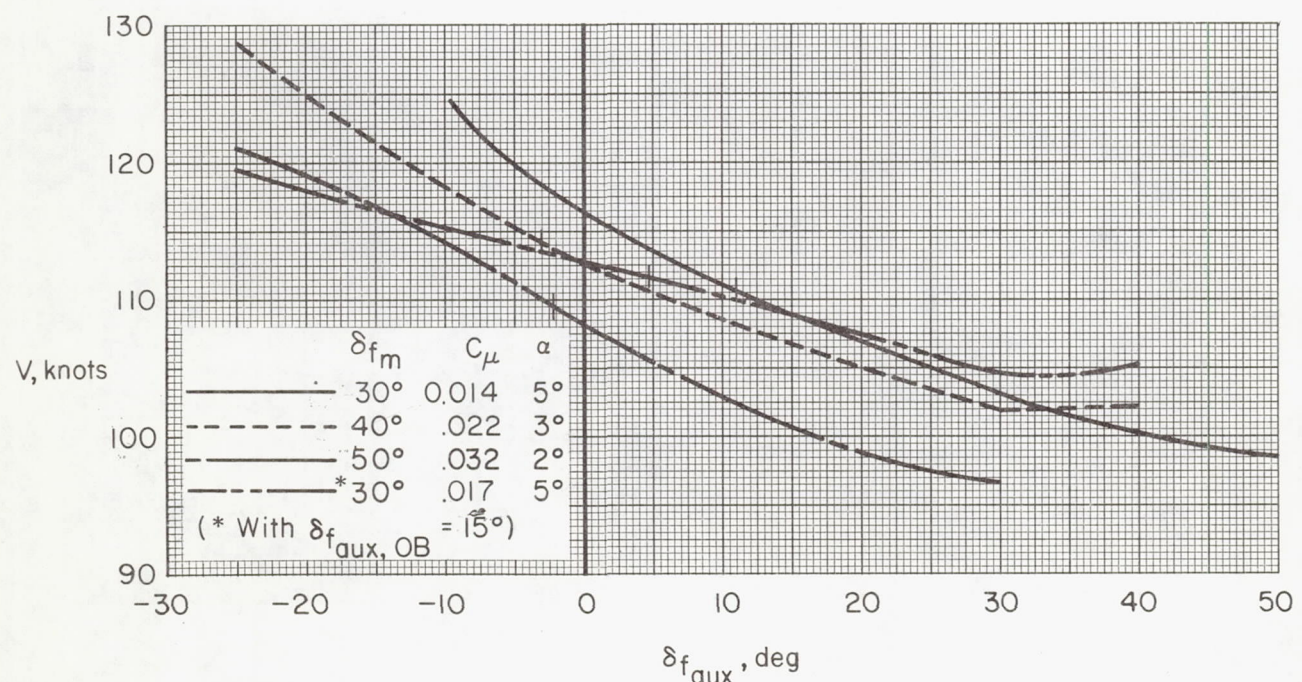


(b) $T/W = 0.10$

Figure 33.- Variation of flight-path angle during descent with extended chord auxiliary flap deflection; BLC flap arrangement A, $\delta_d = 15^\circ$, $\delta_s = 35^\circ$.



(a) $T/W = 0.05$



(b) $T/W = 0.10$

Figure 34.- Variation of approach speed for 1 g flight with extended chord auxiliary flap deflection; BLC flap arrangement A, $\delta_d = 15^\circ$, $\delta_s = 35^\circ$, W/S = 53 psf.